Production des états liés charmés dans les collisions d'ions lourds

Loïc Grandchamp-Desraux

N° d'ordre 151-2003 Année 2003

THESE

présentée

devant l'UNIVERSITE CLAUDE BERNARD - LYON 1

pour l'obtention

du DIPLOME DE DOCTORAT

(arrêté du 25 avril 2002)

présentée et soutenue publiquement le

26 Septembre 2003

par

M. Loïc GRANDCHAMP-DESRAUX

TITRE:

Charmonium production in heavy-ion collisions

Directeurs de thèse:

M. Guy CHANFRAY / M. Ralf RAPP

JURY: M. Aldo Deandrea, Président
M. Gerald E. Brown
M. Guy Chanfray
M. Jean-Yves Ollitrault
M. Ralf Rapp
M. Edward V. Shuryak

To my family and my wife

Acknowledgments

First and foremost, I would like to thank my principal advisor, Prof. Ralf Rapp, for his constant enthusiasm, dedication, criticism and guidance throughout my thesis. I am indebted to him for the education I received and I look forward to continued collaboration.

I am extremely grateful to Prof. Guy Chanfray who supervised this thesis. He has always shown keen interest in my research and offered very valuable insights.

I wish to express my sincere appreciation to Prof. Gerald E. Brown and Prof. Edward V. Shuryak for giving me the opportunity to prepare my thesis in the Nuclear Theory Group at Stony Brook. It has been a great pleasure to work and learn from them, and I am very thankful for all the advice and suggestions they provided me with.

I wish to deeply thanks the members of my thesis committee, and in particular Jean-Yves Ollitrault and Charles Gale who have kindly accepted to review my dissertation.

Many thanks go to the professors I met during my graduate studies, both at Stony Brook and in Lyon. As teachers and colleagues, they always have been very inspiring. I acknowledge fruitful discussions with Madappa Prakash, Jac Verbaarschot, Ismail Zahed, Aldo Deandrea and Claude Fayard. Various postdocs, graduate students and friends deserve my deepest thanks: Peter, Prasanth, Aziz and Pierre to name a few.

A penultimate thank-you goes to my parents and my family. For always being there when I needed them most, and never once complaining about how infrequently I visit, they deserve far more credit than I can ever give them.

My final, and most heartfelt, acknowledgment must go to my wife Soraya. Her support, encouragement, and companionship has turned my journey through graduate school into a pleasure. For all that, she has my everlasting love.

Contents

List of Figures

Chapter 1

Introduction

In this introductory Chapter, we first give an overview of the theory of strong interactions, Quantum Chromodynamics. We focus on the properties of QCD relevant for our studies, namely confinement and chiral symmetry. We then turn to the experimental heavy-ion program, and present a few observables related to the study of QCD at finite temperature and density. We conclude this chapter with charm spectroscopy and introduce the family of charmonium bounds states which play a central role in our thesis.

1.1 Quantum Chromodynamics

Nowadays, it is commonly believed that Quantum Chromodynamics (QCD) is the theory of strong interactions [1, 2]. In QCD, the matter particles are spin-1/2 colored quarks which interact through eight colored spin-1 gauge bosons, the gluons, associated with the color gauge symmetry $SU(3)_c$. Strong interactions are governed by the QCD Lagrangian

$$\mathcal{L}_{QCD} = \sum_{f}^{N_f} \bar{\psi}_f (i\gamma^\mu D_\mu - m_f)\psi_f - \frac{1}{4} F_a^{\mu\nu} F^a_{\mu\nu} \ , \tag{1}$$

where the gluon field strength tensor $F^a_{\mu\nu}$ reads

$$F^a_{\mu\nu} = \partial_\mu A^a_\nu - \partial_\nu A^a_\mu + ig f_{abc} A^b_\mu A^c_\nu \ , \tag{2}$$

in terms of the gluon gauge fields A^μ_a (a= $1 \cdots 8$). The colored quark fields ψ_f ($f = 1 \cdots N_f$) are coupled to the gluons through the gauge covariant derivative

$$D_\mu = \partial_\mu - ig \frac{\lambda_a}{2} A^a_\mu \ , \tag{3}$$

where λ_a are the Gell-Mann matrices generators of the $SU(3)_c$ group satisfying

$$[\lambda_a, \lambda_b] = f_{abc}\lambda_c \ , \tag{4}$$

f_{abc} being the structure constants of $SU(3)_c$.

1.1.1 Properties of QCD

Asymptotic freedom

The coupling constant g characterizing the strength of the strong interactions is a function of the momentum transfer scale Q, $g = g(Q)$. The gluons carry a color charge and are self-interacting due to the non-Abelian nature of the theory. This is at the origin of the *asymptotic freedom* [3, 4] property of QCD: the coupling constant g tends to zero as the inverse of the logarithm of the energy scale. Writing $\alpha_s = g^2/4\pi$, to one-loop, the coupling evaluated at the momentum transfer scale Q is related to the coupling at the scale Q_0 by

$$\alpha_s(Q) = \frac{\alpha_s(Q_0)}{1 + \alpha_s(Q_0)\frac{33-2N_f}{12\pi}\ln\left(\frac{Q^2}{Q_0^2}\right)} \ . \tag{5}$$

To obtain a parameterization of the Q dependence of α_s, one usually introduces the dimensional parameter Λ_{QCD} whose value is then determined by comparison with experiments. Although various definitions have been adopted (see [5] for a discussion), typically one has $\Lambda_{QCD} \sim 200$ MeV and

$$\alpha_s(Q) = \frac{4\pi}{(11 - \frac{2}{3}N_f)ln(Q^2/\Lambda_{QCD}^2)} \ . \tag{6}$$

The strength of the interaction decreases as the scale Q grows. It follows that for processes involving large momentum transfer Q, so-called *hard processes*, perturbation theory is applicable. The asymptotic freedom property of QCD has been widely tested experimentally, mostly in Deep Inelastic Scattering (DIS) and e^+e^- experiments, as shown in Fig. 1.1, from Ref. [6]. However, Fig. 1.1 also shows that towards typical hadronic energy scales, the coupling grows and becomes large so that non-perturbative methods are needed to study QCD at such scales.

Confinement

Another important property of QCD is the *confinement* of quarks. As one tries to separate two quarks from each other, the strong-interaction potential between them

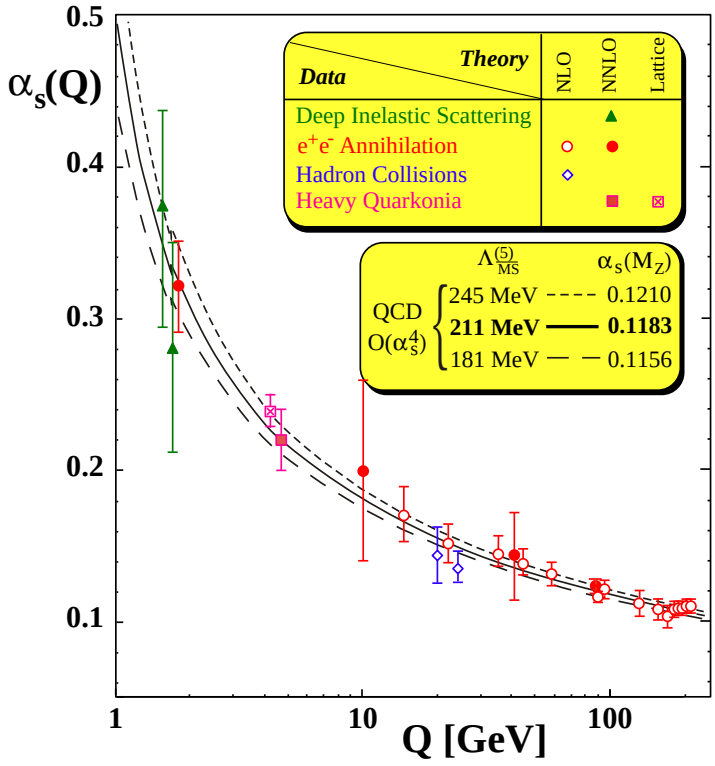

Figure 1.1: Strong coupling constant α_s as a function of the momentum transfer Q in a variety of experiments, compared to theoretical calculations (lines). Figure borrowed from Ref. [6].

increases so that it becomes energetically favorable to create a quark-antiquark pair from the vacuum to form two colorless mesons. Therefore, in nature, only colorless objects are observed, as opposed to free colored quarks and gluons. A characteristic energy scale for confinement is given by the typical size of a hadron ($\sim$ 1 fm) which corresponds to an energy scale of $\Lambda \sim 200$ MeV.

Although QCD is firmly established, its elementary degrees of freedom have never been directly observed. Evidence of the existence of quarks and gluons stems from DIS [7, 8, 9] and high energy e^+e^- collisions [10], among other types of experiments. In e^+e^- annihilations, a quark-antiquark pair is created and as the quarks move away from each other, $q\bar{q}$ pairs form along their trajectories to neutralize color. The original quark and antiquark are thus accompanied by large concentrations of hadrons along their direction of propagation, forming *jets*. Experimental events with three distinguishable jets indicate gluon production.

Chiral symmetry

Besides asymptotic freedom and confinement, another important aspect of QCD is *chiral symmetry*, see Ref. [11] for an introduction. Quarks come in six different flavors ($N_f = 6$), namely up(u), down (d), strange (s), charm (c), bottom (b) and top (t). The masses of these quarks differ by more than four orders of magnitude. The ordering is the following:

$$\begin{gathered} m_u \simeq m_d \simeq 5 \text{ MeV} < m_s \sim 100 \text{ MeV} \\ < \Lambda_{QCD} << \\ m_c \simeq 1.3 \text{ GeV}, \ m_b \simeq 4.5 \text{ GeV} << m_t \simeq 175 \text{ GeV} \ . \end{gathered}$$

This suggests a separation of the QCD matter particles into *light* flavors (u, d, s) and *heavy* flavors (c, b, t). In the limit of massless quarks in the light sector, the QCD Lagrangian $\mathcal{L}_{QCD}$ can be rewritten as

$$\mathcal{L}_{QCD} = \bar{\psi}_L i\gamma^\mu D_\mu \psi_L + \bar{\psi}_R i\gamma^\mu D_\mu \psi_R - \frac{1}{4} F_a^{\mu\nu} F^a_{\mu\nu} \ , \tag{7}$$

where

$$\psi_L = \frac{1}{2}(1-\gamma_5)\psi \qquad \text{and} \qquad \psi_R = \frac{1}{2}(1+\gamma_5)\psi \ , \tag{8}$$

which are respectively the left-handed and right-handed components of the fermion field (when working in a L+R, L-R basis, one recovers the vector and axial-vector symmetries). The Lagrangian (7) shows that left- and right-handed quarks do not mix. It is invariant under the transformations

$$SU(2)_L : \qquad \psi_L \ \rightarrow \ e^{-i\theta_L^a \tau_a/2} \psi_L \ , \qquad \psi_R \rightarrow \psi_R \tag{9}$$

$$SU(2)_R : \qquad \psi_R \ \rightarrow \ e^{-i\theta_R^a \tau_a/2} \psi_R \ , \qquad \psi_L \rightarrow \psi_L \tag{10}$$

which constitute the $SU(2)_L \otimes SU(2)_R$ chiral symmetry. Due to the larger mass of the strange quark (compared to u, d), chiral symmetry is usually considered only for two flavors, although sometimes the strange quark is included as well leading to a $SU(3)_L \otimes SU(3)_R$ chiral symmetry. Such symmetry seems to imply that chiral partners (hadronic states that transform into each other under chiral transormations) should be degenerate. However, as evidenced by the mass difference observed in the hadronic spectrum between chiral partners, (*e.g.* $\Delta m = m_{a1} - m_\rho \simeq 500$ MeV) chiral symmetry is spontaneously broken in the vacuum (*i.e.* the ground state does not possess the the

symmetry of the Lagrangian). The QCD vacuum breaks the chiral symmetry of the QCD Lagrangian by formation of a chiral condensate

$$\langle \bar{\psi}\psi \rangle = \langle 0|\bar{\psi}_R\psi_L + \bar{\psi}_L\psi_R|0\rangle \neq 0 \ . \tag{11}$$

1.1.2 QCD phases transitions

QCD at low temperatures and baryon chemical potentials is characterized by confinement and spontaneous breaking of chiral symmetry. In this regime, the effective degrees of freedom are hadrons, seen as excitation of the QCD vacuum. An interesting question to ask then is what happens to the QCD vacuum when external parameters T, μ_B increase and become comparable to the confinement scale $\Lambda_{QCD} \sim 200$ MeV ?

Intuitively, if hadronic matter is compressed highly enough so that hadrons start to overlap and loose their individual identity, one expects the relevant degrees of freedom describing the system to change from hadronic to partonic. This corresponds to the deconfinement phase transition of QCD [12]. Under very energetic conditions, one expects a new phase of matter, essentially a free gas of individual quarks and gluons, generically called the Quark-Gluon Plasma (QGP).

It must be pointed out that well before the advent of QCD, Hagedorn derived a limiting hadronic temperature [13]. He noted that the density $\rho(m)$ of hadronic states grows exponentially with the mass m of the hadronic states

$$\rho(m) \propto \frac{1}{m^\alpha} e^{m/T_H} \ . \tag{12}$$

From a fit to the known hadronic resonances, one obtains $T_H \sim 160$ MeV. In the narrow resonance approximation, this leads to a divergence in the partition function $\mathcal{Z}$ of the hadronic system

$$\mathcal{Z} \sim \int dm \ \rho(m) \ e^{-m/T} \ , \tag{13}$$

as T approaches T_H. Thus, T_H can be seen as a limiting hadronic temperature and is suggestive of a phase transition.

A different kind of estimate is obtained, making explicit reference to the underlying partonic QCD degrees of freedom. The following example also illustrates that the origin of the phase transition lies in the more abundant massless degrees of freedom in the deconfined phase than in the hadronic phase. At low temperatures, a hadron gas is primarily a pion gas whose pressure P_{HG}, assuming free massless pions is given by

$$P_{HG} = 3\frac{\pi^2}{90} T^4 \ , \tag{14}$$

where the factor 3 accounts for the three pionic degrees of freedom. Conversely, in a deconfined phase with two light flavors, one has

$$P_{QGP} = 37\frac{\pi^2}{90}T^4 - B \ , \tag{15}$$

where B is the MIT bag constant [14, 15], corresponding to the vacuum energy density which exerts a pressure on quarks and keeps them confined inside the bag. By equating the pressure in the two phases, one can deduce a critical temperature above which the Quark-Gluon Plasma phase is thermodynamically favored. Depending on the value chosen for B, the resulting critical temperature is $\sim 150 - 200$ MeV.

Also, chiral symmetry is expected to be restored at high temperatures/baryon chemical potentials. This has been suggested to be related to the disappearance of individual instantons (which are semi-classical configurations of the gluon fields in euclidean space and provide a mechanism of spontaneous chiral symmetry breaking) at large temperatures and densities [16]. This is also indicated by chiral perturbation theory calculations [17], which to leading order give the following result for the temperature dependence of the chiral condensate with two light flavors and f_π being the pion decay constant

$$\langle\bar{\psi}\psi\rangle_T = \langle 0|\bar{\psi}\psi|0\rangle \left(1 - \frac{T^2}{8f_\pi^2}\right) \ . \tag{16}$$

The chirally restored phase is then characterized by a vanishing value of the quark condensate $\langle\bar{\psi}\psi\rangle = 0$.

From the previous estimates, it seems that at the energy scales where the deconfinement and the restoration of chiral symmetry are expected, the strong coupling constant α_s is still large and perturbative QCD inapplicable. Therefore, to study the aforementioned QCD phase transitions, one has to invoke non-perturbative approaches. Besides phenomenological model building, another attempt to approach QCD problems in the non-perturbative limit is given by ab-initio calculations of QCD observables on the lattice.

1.1.3 Lattice gauge simulations of QCD

In the recent years, lattice gauge simulations of QCD − see [18] for an introduction − have contributed to the improved understanding of Quantum Chromodynamics. The main idea is to study a discretized version of QCD performing Monte-Carlo simulations [19, 20, 21].

The space-time discretization on a $N_\tau \times N_\sigma^3$ lattice provides a regularization of the ultra-violet divergences of the theory by introducing a cutoff scale $\Lambda = 1/a$ where a is the elementary lattice spacing. The QCD partition function $\mathcal{Z}(T, V)$ can be evaluated on the lattice (so far limited to small or zero values of the chemical potential) and provides a connection with statistical physics through thermal averages of observables

$$\langle \mathcal{O}(G, \bar{\psi}, \psi) \rangle = \frac{1}{\mathcal{Z}} \int [dG][d\bar{\psi}][d\psi] e^{-\int \mathcal{L} d^4x} \mathcal{O}(G, \bar{\psi}, \psi) \ , \tag{17}$$

as well as the usual thermodynamics quantities such as pressure, energy density, free energy, ... etc.

Fig. 1.2 provides two examples of such lattice QCD calculations, for the energy density as a function of temperature (left panel) and for the value of the quark condensate as a function of temperature (right panel). Fig. 1.2 is suggestive of the deconfinement

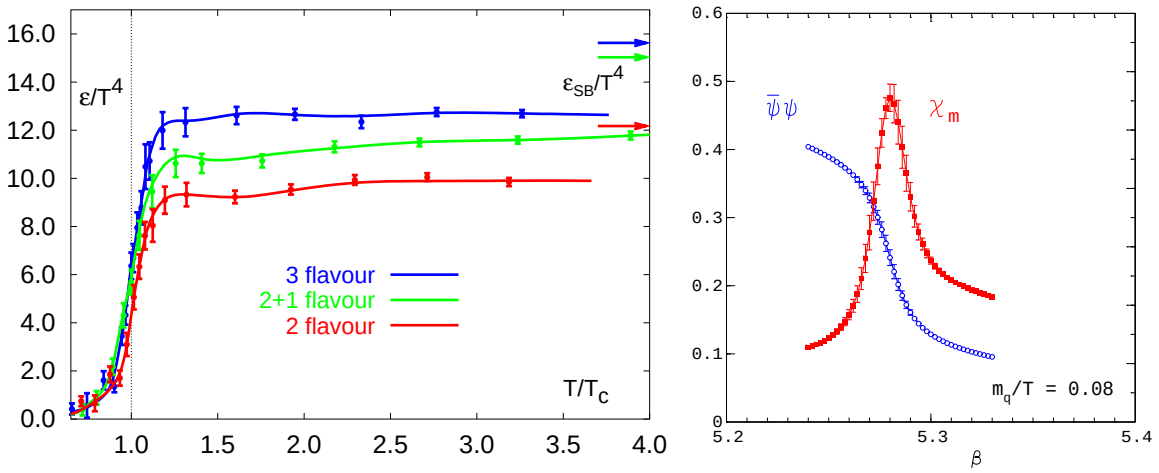

Figure 1.2: Left panel: Lattice calculation of the energy density of QCD matter as a function of temperature for different numbers of dynamical quark flavors. Right panel: Strength of the chiral condensate as a function of temperature. Both figures are reproduced from Ref. [18].

phase transition (rapid increase in the energy density) and chiral symmetry restoration (rapid decrease of the value of the quark condensate). The inferred critical temperatures are on the order of $\sim$ 200 MeV, and lattice QCD studies seem to imply that the two phase transitions occur at the same temperature. Further studies have investigated the order of the phase transition. They indicate that the non-zero light-quark masses as well as the precise value of the strange quark mass play an important role to discriminate between first order, second order or even a smooth cross-over.

The phase diagram of QCD is richer and more complex than suggested by these two brief accounts of the deconfinement and chiral restoration phase transitions. Important theoretical progresses have predicted new phases of QCD, in particular at large baryon chemical potential where a transition to a color superconducting phase of QCD matter is expected [22, 23, 24], most likely first order, inducing the existence of a tri-critical point [25, 26].

1.2 Heavy-ion collisions

The investigation of the QCD phase diagram is not merely an academic problem as QCD at finite temperature and density is very relevant to describe *(i)* the state of matter of the universe, a few microseconds after the Big-Bang and *(ii)* the core of compact astrophysical objects such as neutron stars. Since astrophysical signatures of new states of matter predicted by QCD are not easily obtained, experimentally, properties of QCD at finite temperatures/densities are assessed "in the laboratory" using (ultra-)relativistic heavy-ion collisions.

1.2.1 Experimental programs

The idea behind the heavy-ion program is that by colliding two heavy nuclei accelerated to ultra-relativistic energies, nuclear matter gets highly compressed and excited due to the conversion of the longitudinal energy of the beam into transverse energy. Provided that the conditions are energetic enough, one expects to recreate in the laboratory a deconfined and/or chirally symmetric state of matter [27]. Heavy-ion physics has been fastly growing from its birth two decades ago, with an increasing available energy in the center of mass of the collision.

Historically, the first nuclear collision experiments used fixed targets where only one ion beam is accelerated and hits the target. The heavy-ion experimental program started at the Lawrence Berkeley Laboratory (LBL) with the Bevalac particle accelerator. At the Alternating Gradient Synchrotron (AGS), experiments using O, Si and Au beams at energies around 10 GeV per projectile nucleon were conducted. At the Schwer-Ionen-Synchrotron (SIS), in the regime of a $1-2$ AGeV, data was taken, *e.g.*, for Au-Au and Ni-Ni collisions. In 1986, the CERN Super-Proton-Synchrotron started being used as a heavy-ion facility to carry out experiments with Oxygen and Sulfur beams

and was later on upgraded to study Pb(160 AGeV)-Pb collisions. This coincides with the beginning of the series of Quark Matter conferences devoted to heavy-ion physics. Despite a reduced beam time (compared to high-energy particle physics experiments), the experimental collaborations at CERN produced significant results summarized by a CERN press release in 2000 claiming the discovery of a new state of matter (but let us not enter these rather controversial matters). Nowadays, heavy-ion experiments have their own dedicated facility at the Brookhaven National Laboratory where the Relativistic Heavy-Ion Collider (RHIC) produces collisions between two gold beams at $\sqrt{s_{NN}} = 200$ GeV. The future lies in the Large Hadron Collider (LHC) now under construction at CERN with a designed cms energy of 5.5 TeV. According to model calculations, the initial temperatures reached at LHC should be on the order of 500 MeV, well above T_c. However, as the energy increases, the nuclei become more transparent and the baryonic densities achieved are smaller. Thus, to study density effects, smaller energies are preferable (the baryon stopping being larger). Such a program will be carried out at a new GSI facility (Gesellschaft für Schwer-Ionen Forschung), recently approved for funding [28].

Evolution of a heavy-ion collision

To understand how ion collisions can provide information about QCD, let us sketch the space-time evolution of a typical collision. Upon impact of the two colliding nuclei, provided that the conditions are energetic enough, we expect the quark and gluon degrees of freedom to be liberated. Following a pre-equilibrium partonic stage, the assumption is that the system thermalizes to form a plasma of quarks and gluons at an initial temperature T_0 above the critical temperature T_c of the deconfinement transition. The strong reinteractions in the plasma phase should lead to appreciable collective phenomena and an approach toward chemical equilibration in the light sector. The system continuously expands and cools down until it hadronizes when its temperature reaches T_c. Although lattice QCD results seem to disfavor a first order phase transition, for simplicity one can imagine that when the system reaches T_c, hadronic bubbles start to form. When hadronization is complete, hadrons continue to interact until the densities are so low that they decouple. This point in time where the elastic collisions cease is usually referred to as *thermal freeze-out*. From then on, the particles are free streaming to the detectors. It must be pointed out that so far, there is still a lack of understanding

of the pre-equilibrium partonic stage, as well as of the hadronization process. Since the final products of the collision observed in the detectors are hadrons, the study and proof of new state of matter formation necessitates the identification of clear probes (called signatures), which retain information about the initial hot and/or dense matter created in heavy-ion collisions, even after hadronization.

1.2.2 Experimental observables

We now review a few of the observables available from experiments and their connection with a putative Quark-Gluon Plasma formation. We articulate our discussion around a few recent experimental results. Our arbitrary selection of topics is guided by the desire to introduce a few concepts useful for our studies of charmonium production, and is influenced by the recent advent of RHIC results. We wish to give to the reader a feeling for the many facets of heavy-ion physics but this review is far from exhaustive.

Flow and other global observables

For sufficiently central collisions, the matter formed in collisions of heavy nuclei constitutes a strongly interacting system and the produced particles exhibit collective behaviors often referred to as flow phenomena. The collective expansion of the matter is reflected, *e.g.*, in the p_T-spectra hardening of hadrons.

We present here a specific type of collective phenomenon named *elliptic flow* [29, 30]. As a preliminary, we need to introduce the notion of centrality in heavy-ion experiments. Heavy ions cannot be treated as point-like particles and the characteristics of a collision of two such extended objects often depend upon the minimal distance of approach between the two centers of the colliding nuclei, called the impact parameter b. Assuming for a moment that the two nuclei can be approximated by two hard spheres of radius R, it is clear that the impact parameter ranges from $b = 0$ (for head-on collisions) to $b \simeq 2R$ (for the most peripheral collisions where the two nuclei barely touch each other). However, b is not directly accessible experimentally and we will present in Chapter 2 a simple model (the Glauber model) used to relate the impact parameter of the collision to experimentally accessible quantities such as, *e.g.* the transverse energy deposited in the calorimeters. Although one may, a priori, be more interested in central collisions, because more energetic, the varying centrality of a collision also gives rise to very interesting phenomena. For example, in semi-central to peripheral collisions,

the geometry of the initial interaction region has the shape of an ellipse (seen in the plane perpendicular to the beam axis: the transverse plane). This initial geometrical anisotropy translates into stronger pressure gradients in the direction of the smaller axis of the ellipse. In turn, this induces momentum correlations among particles which *flow* preferentially along the small axis of the ellipse. The corresponding "elliptic flow" is characterized by a quantity v_2 which is the second coefficient (associated with $\langle\cos(2\phi)\rangle$) in the Fourier expansion of the azimuthal particle distribution.

Fig. 1.3 shows the reconstructed $v_2(p_T)$ for different centrality bins at RHIC in *Au-Au* collisions, $\sqrt{s_{NN}} = 130$ GeV. v_2 smoothly increases as the collisions become more peripheral, due to an increase in the initial anisotropy of the initial interaction region. Fig. 1.3 demonstrates that the matter expands collectively, *i.e.* the system is the place of strong rescattering among the produced particles. Due to the faster expansion in the

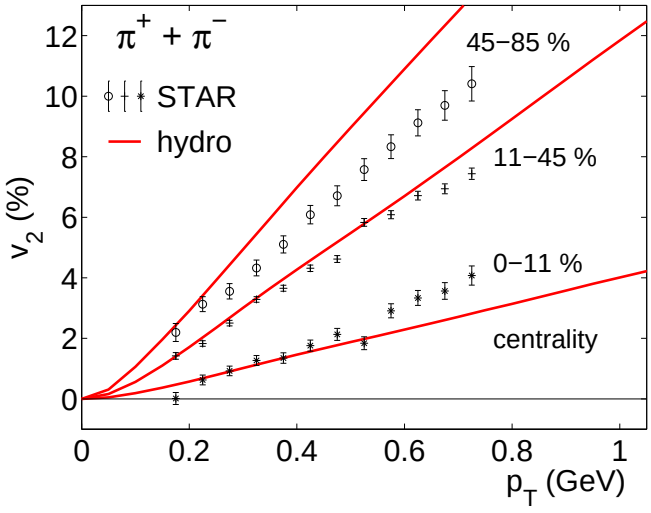

Figure 1.3: v_2 elliptic flow at RHIC. The data points are from the STAR collaboration [31], and the lines correspond to hydrodynamical calculations [32].

smaller direction of the initial interaction zone, the initial anisotropy tends to disappear. Therefore, elliptic flow is a good observable of the early times of the reaction. The connection between elliptic flow and Quark-Gluon Plasma formation is the following: the speed of sound being larger in a plasma phase than in the hadronic phase, we expect a stronger collective expansion (*i.e.* a larger v_2) if a plasma is formed [33]. The fact that the measured v_2 is substantially larger at RHIC than at SPS seems to indicate that the early stages at RHIC are dominated by a strong collective partonic expansion. This is further supported by comparison with hydrodynamic calculations [34, 32] assuming the initial formation of an equilibrated Quark-Gluon Plasma (see full lines in Fig. 1.3)

while conventional hadronic cascade models do not predict any significant increase in v_2 from SPS to RHIC.

Let us mention two other global observables which are commonly discussed to infer properties of the system created in heavy-ion collisions. The first one, is the HBT (Hanbury-Brown-Twiss) interferometry technique which attempts to determine the size of the system, based on Bose-Einstein correlations among particles [35]. It may be used to infer a delayed hadronization if the system goes through a plasma phase and then a mixed phase in which the expansion of the matter is very slow. However, so far it is still controversial and the fact that the characteristics of the emitting source seem to be the same at SPS and RHIC remains unexplained.

The second observable we wish to mention is the hadro-chemistry of the system. The relative chemical abundances of the particles in the fireball may hold some clue about the properties of the QCD matter encountered. As an example, consider strangeness production [36]: the lightest strange hadrons, the kaons, have a mass of nearly 500 MeV. Since strangeness is produced in pairs, strangeness production in a hadron gas has a threshold $\sim$ 1 GeV. If a plasma is formed, a nearly massless strange quark could be more easily produced in a deconfined phase, leading to a strangeness enhancement with respect to a superposition of individual p-p collisions. The latter was indeed observed at the SPS [37], going from peripheral to central collisions of Pb-Pb. The observed enhancement also increases with the strangeness content of the produced hadrons. This is at variance with predictions from hadronic rescattering since multi-strange hadrons have high-mass thresholds and small cross-sections. However, strangeness enhancement remains a questionable signature of QGP formation since the E910 experiment [38] reported a strangeness enhancement already in p-A collisions at AGS energies where no QGP is expected to be formed.

Observables of the early stages

We turn to a different kind of observables, more directly related to the very early times of the collision. Consider a particle with a very large p_T: it must have been produced very early in the collision, upon impact of the two colliding nuclei in hard N-N scattering. Later on during the evolution, typical exchanged momenta are too small to build up a particle momentum up to, *e.g.* 10 GeV. In addition, high-p_T particles are fast and may escape the interaction region early, carrying information about the

early phases. Fig. 1.4 displays the so-called R_{AA} ratio (left panel) and the back-to-back suppression of jets (right panel). For a given type of particles (π^0 in the left panel of

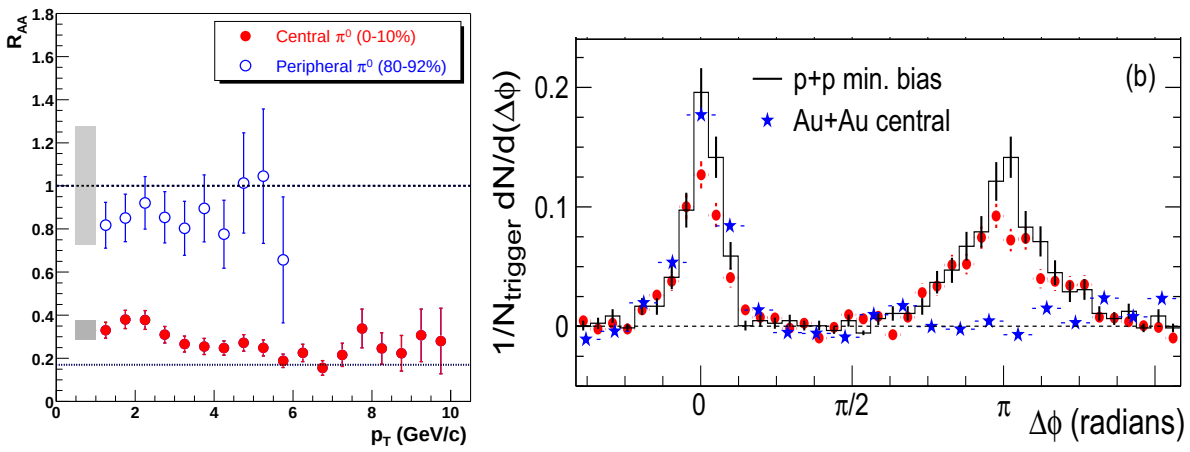

Figure 1.4: Left: $R_{AA}(p_T)$ ratio at RHIC for neutral pions [39]. Right panel: angular correlations of particles [40].

Fig. 1.4), R_{AA} is the ratio of the observed number of particles over what is expected if the heavy-ion system was a superposition of independent N-N collisions. This is a very general approach in heavy-ion physics. Many observables are compared to the same observable measured in p-p collisions and scaled by the number of binary collisions (*i.e.* the number of primordial N-N collisions from the two colliding nuclei). Such an approach allows to characterize how the system deviates from a superposition of elementary p-p collisions and thus gives information on the matter created in heavy-ion collisions (including initial nuclear effects). In Fig. 1.4, the R_{AA} ratio is given as a function of the transverse momentum of the detected particles. In central collisions (full dots), the particles with large p_T are very suppressed from what is expected with binary scaling, they seem absorbed by the system in contrast to peripheral collisions (where little matter, if any, is formed, as in p-p) where they freely escape the interaction region. This phenomenon, dubbed "quenching" [41] is monotonously increasing with the centrality of the collision. This is suggestive of the formation of a QGP where reinteractions of the particles with partonic degrees of freedom entails a larger energy loss – on average, reinteractions of high-p_T particles in the medium tend to *reduce* their transverse momentum, bringing the system closer to thermal equilibrium – than in the hadronic phase. Other interpretations of these experimental results in *Au-Au* collisions at RHIC have been proposed in terms of pre-equilibrium effects (initial state interactions as described in the Color Glass Condensate [42]) but they seem disfavored

by the recent results of the *d-Au* system which do not exhibit such quenching, implying that the underlying mechanism indeed corresponds to final state interactions (such as energy loss in the plasma [43]). The right panel of Fig. 1.4 displays a study of two-particle angular correlations. Usually, when a jet is produced it has its back-to-back counterpart in order to conserve momentum. Thus, when experiments identify a jet, they study the angular correlations of the other identified particle with respect to the direction of the jet. In *p-p* collisions, as indicated by the full line in the right panel of Fig. 1.4, particles are strongly correlated in the direction of the jet (this is the angular spread of the jet itself) and also for $\phi = 180$ degrees, demonstrating the presence of the back-to-back companion of the first identified jet. The stars correspond to the same observable in central *Au-Au* collisions at RHIC. The disappearance of the back-to-back jet is clearly visible. This again points toward a strong energy loss of the jet in the matter, which can be interpreted as a signal of QGP formation.

1.2.3 Electromagnetic probes

Another probe of the interaction region in the early times of the collision is given by thermal photons [44]. They are produced in quark-antiquark annihilation or Compton scattering in the plasma. The main advantage of photons is that they are insensitive to the strong interaction and they escape the hot and/or dense medium without further rescattering. Their p_T-spectra give then access to the temperature at which they were produced. One has to mention that many processes in a hadron gas lead to photon production. Detailed calculations [45, 46] have actually shown that around T_c, the Hadron Gas "shines" as bright as the QGP. In addition, one severe limitation of the photon signal is the huge secondary photon background arising from hadronic decays.

An interesting electromagnetic signal is also obtained by the detection of leptons, in particular lepton pairs (dileptons) which are experimentally accessible although their production rates are a factor α_{em}^2 smaller than strong particle production rates [27]. Their main advantage is the same one as for the photon, they are a direct signal of the medium in which they were produced since due to their leptonic nature they should escape the system with minimal rescattering. Fig. 1.5 shows an e^+e^- invariant mass spectrum from the NA50 collaboration [47], obtained at the CERN SPS in *Pb*(158 AGEV)-*Pb* collisions. A lot of information is present in such a spectrum so that it is usually divided into three regions: the low-mass region $M_{l^+l^-} < 1$ GeV, the intermediate-

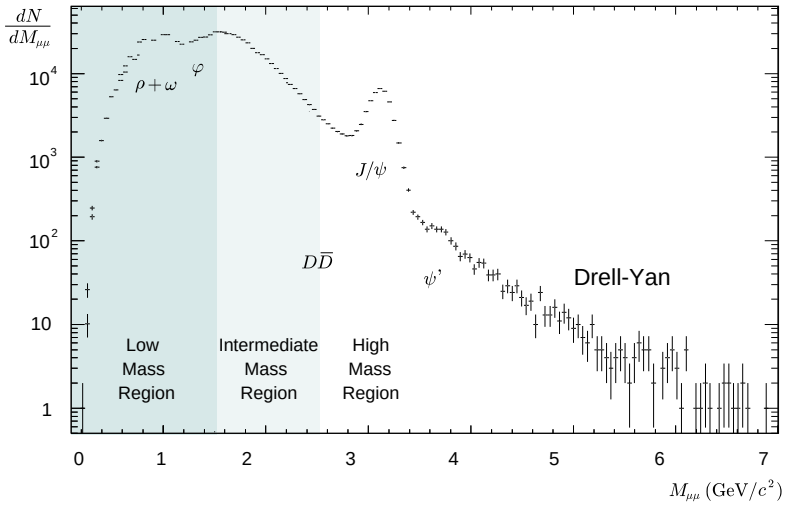

Figure 1.5: e^+e^- invariant mass spectrum in Pb(160 AGeV)-Pb collisions at SPS, adapted from [47].

mass region (IMR) for $1 < M_{l^+l^-} < 3$ GeV and the high-mass region, above 3 GeV. From the hadronic point of view, the low-mass region is the region of light vector mesons (ρ, ω, ϕ) and allows the study of the manifestation of chiral symmetry restoration [48]. The intermediate-mass region is the place of an important process for our studies, namely the semi-leptonic decay of D mesons, which we will return to later on. The high-mass region is dominated by the charmonium vector mesons, the study of which is the object of this thesis. In the low- and intermediate-mass region, another important source of dileptons is given by thermal radiation either from the plasma or the hadronic phase. Provided that all hadronic sources can be accurately evaluated, the hope is to identify the plasma contribution (coming from quark-antiquark annihilation). However, since around T_c, the plasma and hadronic rates of thermal dilepton radiation are comparable, rather high temperatures need to be achieved to isolate the plasma effect. Last but not least, the Drell-Yan process (hard process where two quarks from the incoming nucleons annihilate into a lepton pair [49]) must be precisely evaluated to extract the other signals. This is usually done by fitting the high-mass tail of the spectrum, saturated by the Drell-Yan. The study of dileptons in heavy-ion collisions offers a very rich physics involving both the confinement and chiral symmetry properties of QCD. The fact that the dilepton mass spectrum covers such a broad range of invariant mass gives an additional constraint to models which should describe dilepton production consistently over the full spectrum. We expect great results from the PHENIX experiment at RHIC whose detector is designed to detect dileptons and electromagnetic probes, among other

observables.

Heavy-ion collisions offer a broad range of observables to study in the laboratory the properties of QCD at finite temperature and density. Various model approaches indicate that the temperatures and densities achieved in central collisions of heavy nuclei, at cms energies comparable to SPS and above, should allow to observe the deconfinement phase transition and chiral symmetry restoration as predicted by lattice calculations. The systems produced seem large and strongly interacting enough to justify the use of macroscopic concepts such as thermal equilibrium and hydrodynamic descriptions. It seems fair to say that the hope for a *single* signal providing a clear signature of Quark-Gluon Plasma formation has been elusive. The evidence for a newly created state of matter will rather emerge from a scenario invoking many different observables accounted for within a common coherent picture.

1.3 Charm and charmonium in heavy-ion collisions

1.3.1 A brief history of charm

Before its experimental discovery, the existence of the charm quark had been postulated by Glashow-Iliopoulos-Maiani [50] to explain the absence of strangeness changing neutral currents. It was predicted to have the same charge $+2/3e$ as the lighter up quark, but a substantially larger mass to account for its absence in the known hadron spectrum in the early 70's.

One first experimental hint of the charm quark was given in 1972 from e^+e^- collisions [51] where the ratio

$$R = \frac{\sigma_{tot}(e^+e^- \rightarrow \text{ hadrons})}{\sigma(e^+e^- \rightarrow \mu^+\mu^-)} = N_c \sum_{f=1}^{N_f} q_f^2 \tag{18}$$

was measured for the first time at $\sqrt{s} > 3$ GeV and was found to be greater than two (its value if there would be only up, down and strange quarks).

Another strong evidence of the charm quark came in 1974 with the simultaneous observation of a narrow resonance at ~ 3.1 GeV in the e^+e^- spectrum, both at BNL [52] and SLAC [53]. At BNL, in p(30 GeV)-Be collisions, the observed width of 20 MeV was compatible with the experimental resolution of the detector, suggesting an narrower resonance. The newly found particle was called the "j". At the same time, at

the SLAC e^+e^- collider, the width of the "ψ" was measured to be 1.3 MeV. Due to its high mass, and its narrow width the J/ψ state was more suggestive of a bound state of heavy quarks rather than a high-lying light-quark excitation. Subsequently, similar higher mass resonances were identified at SLAC (hence, their name ψ', χ, ...).

1.3.2 Charm and charmonium spectroscopy

We give in Fig. 1.6 the full spectrum of known charmonium bound states [5]. Among

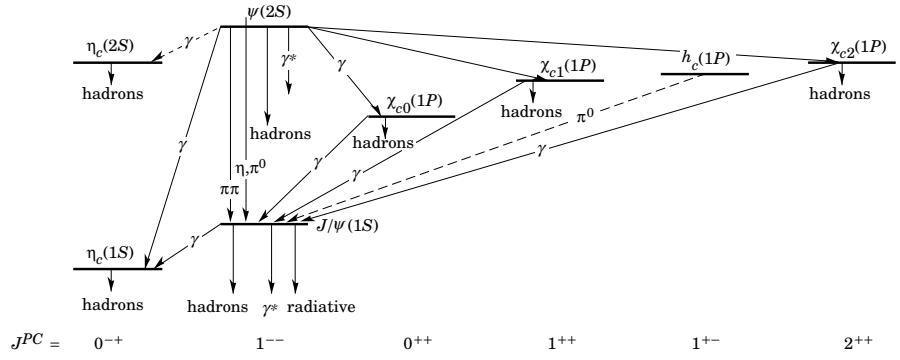

Figure 1.6: Charmonium spectrum from Ref. [5]. The arrows indicate strong and electromagnetic decays.

the states composing the charmonium mass spectrum of Fig. 1.6, we will consider only the J/ψ, ψ', χ_{c1} and χ_{c2} states and leave out the η_c, χ_0, ... for the following reason: experimentally, in heavy-ion collisions, charmonium states are observed in dilepton spectra (e^+e^- or $\mu^+\mu^-$ invariant mass spectrum), from the decays of vector mesons J/ψ, ψ'. On the contrary, the scalars η_c and χ_0 are not easily detected. There exists higher-lying states ($\psi(3770)$, $\psi(4030)$, ...) above the open-charm threshold which have broader widths due to their dominant decay into a $D\bar{D}$ pair. The charmonia of interest for our purposes have the following masses and widths:

$$\begin{aligned}
m_{J/\psi} &= 3096.87 \pm 0.04 \text{ MeV}, & \Gamma_{J/\psi} &= 87 \pm 5 \text{ keV}, \\
m_{\psi'} &= 3685.96 \pm 0.09 \text{ MeV}, & \Gamma_{\psi'} &= 300 \pm 25 \text{ keV}, \\
m_{\chi_{c1}} &= 3510.51 \pm 0.12 \text{ MeV}, & \Gamma_{\chi_{c1}} &= 0.92 \pm 0.13 \text{ MeV}, \\
m_{\chi_{c2}} &= 3556.18 \pm 0.13 \text{ MeV}, & \Gamma_{\chi_{c2}} &= 2.08 \pm 0.17 \text{ MeV}.
\end{aligned} \tag{19}$$

These states are characterized by widths much smaller than typical hadronic widths indicating that the mechanism for their strong decay is highly suppressed. This is a consequence of the OZI rules [54]. Since the J/ψ and the ψ' are below the open-charm

threshold, their strong decay must proceed through $c\bar{c}$ annihilation and disconnected quark diagrams which are OZI suppressed channels. The situation is different for the $\psi(3770)$ and higher states which can decay into a $D\bar{D}$ pair and have widths comparable to typical hadronic widths.

The ψ' and the χ states have hadronic and radiative decays into the J/ψ. This is of importance for the J/ψ yield observed in heavy-ion collisions since a large fraction of it arises from this feeddown. It has been experimentally determined that only $\sim 60\%$ of the total J/ψ yield comes from prompt J/ψ's. Approximately 32% of it comes from χ_{c1} and χ_{c2} radiative decays while about 8% are due to ψ' feeddown [55]. Since, a priori, J/ψ, ψ' and χ's evolutions in heavy-ion collisions may be different, this distinction has to be made when computing the J/ψ yield. We are aware that these fractions bear a substantial uncertainty when used in the heavy-ion context since they were determined in p-, π-p collisions.

Charmonium states carry zero net charm charge and are sometimes referred to as hidden charm. In contrast, since the discovery of the J/ψ, many open-charm hadrons have been identified, most importantly, the D mesons which are made of a charm quark and a light quark. The lowest-lying ones, the D^0, $\bar{D}^0$ ($m = 1864 \pm 0.5$ MeV) and $D^{\pm}$ ($m = 1869 \pm 0.5$ MeV) constitute the open-charm threshold at around ~ 3.74 GeV. Charmed strange mesons have also been identified as well as charmed baryons containing one charm quark. For completeness, let us mention that the recent discovery of new charmed-strange mesons by the BABAR [56] and CLEO [57, 58] experiments, identified as chiral partners of the D_s [59, 60], has attracted considerable interest and may influence the repartition of open charm among the different charmed particles in heavy-ion collisions.

We conclude this section by noting that the bottom quark offers a system in all points analogous to the charm family of states. Most of what can be said about charm and charmonium is directly applicable to bottom hadrons and bottomonium ($b\bar{b}$ bound states). The higher mass of the bottom quark ($m_b \sim 4.5$ GeV) improves the perturbative description of bottom production and the non-relativistic treatment of bottomonia. However, bottom has a high production threshold and significant bottom production is not expected until LHC energies are reached.

1.3.3 J/ψ suppression as a QGP signature

Although the J/ψ constitutes an interesting story by itself, so far we have not explained why it has attracted so much interest in the context of heavy-ion collisions. The originally proposed picture is (was) simple: since the J/ψ is made of (heavy) charm quarks, it was thought to be exclusively produced early in the collision through hard scattering of incoming nucleons. Therefore, the J/ψ could serve as a probe of the whole evolution of the heavy-ion collision system and by comparing with J/ψ production in p-p (or light systems) where matter is absent, the hope was to infer properties of the hot and/or dense phases of matter produced in central collisions of heavy nuclei.

More importantly, the J/ψ is a small and very tight bound state, lying ~ 640 MeV below the open-charm threshold. This rather robust state should, in principle, be only mildly affected in a hadronic environment. If on the contrary, J/ψ is destroyed by QGP formation, J/ψ and its suppression appears as a valuable probe of QGP formation.

J/ψ as a signature of the QGP was first suggested in 1986 by Matsui and Satz [61]. In their picture, if a QGP is formed, the attractive $c\bar{c}$ potential responsible for the J/ψ binding gets screened as the temperature of the medium increases, due to larger abundances of color charges screening the interaction between the c and $\bar{c}$ quarks. One then expects the existence of a critical temperature T_{diss}, above which J/ψ is no longer bound. If a QGP is formed (and is hot enough), the J/ψ is thus expected to dissolve into separate c and $\bar{c}$ quarks surrounded by their own Debye Cloud.

A similar phenomenon is expected for the ψ' and the χ states, although their lower binding energies imply smaller dissociation temperatures (not even necessarily above T_c). The resulting picture consists of a sequential dissolution (ψ', χ's and J/ψ in order of increasing T_{diss}) of the charmonium states in heavy-ion collisions. Experimentally, varying the collision energy, choosing different projectile/target combinations and studying the centrality dependence of the expected suppression, offers the possibility to study in detail the suggested suppression pattern.

However, recent developments have modified our understanding of J/ψ suppression as a QGP signature. These constitute the main part of this thesis.

1.3.4 Outline

In Chapter 2, we review existing models of primordial open-charm and charmonium production, going from p-p to p-A and A-A collisions. Theoretical frameworks have

been developed to explain charm production in p-p collisions, however extrapolations to the heavy-ion environment are not always straightforward. In particular, open-charm production uncertainties in the heavy-ion case are emphasized and we recall that J/ψ suppression already occurs in p-A collisions (where no plasma formation is expected) due to nuclear absorption.

Chapter 3 is devoted to static properties of charm in equilibrium matter. The aim of this chapter is two-fold: first, based on recent lattice QCD calculations, we discuss medium effects on the $c\bar{c}$ potential. We give our interpretation of the modified $c\bar{c}$ potential in terms of a reduced open-charm threshold, possibly associated with chiral symmetry restoration, the effects of which we assess within a NJL model. In addition, we discuss recent lattice studies of charmonium spectral functions which show that J/ψ states can survive in the plasma phase up to temperatures $\sim 1.5\ T_c$ (above previously inferred J/ψ dissociation temperatures). Second, we discuss a recently suggested mechanism of soft J/ψ production [62, 63], by coalescence of c and $\bar{c}$ quarks at the hadronization transition. We present how this additional source of J/ψ's complicates the simple picture of J/ψ suppression especially when the equilibrium abundances become comparable to the initial hard production. In addition, we show how the in-medium effects suggested by the lattice results influence statistical J/ψ production.

In order to make closer contact with heavy-ion collisions, we calculate in Chapter 4 the dissociation rates of charmonia in the plasma and hadronic phases of the reaction. In the QGP, we introduce a new calculation of J/ψ destruction by quarks and gluons using a "quasifree" mechanism [64]. In the hadronic phase, we discuss J/ψ hadronic interactions, based on a $SU(4)$ symmetric effective theory developed in [65, 66, 67]. This is a necessary step to distinguish between plasma and hadronic suppression. We also consider medium effects on open-charm states, which accelerates inelastic collisions in the hadronic phase and, in particular, allow for direct decay of higher charmonia (ψ') into $D\bar{D}$ pairs [68].

We present in Chapter 5 our model of the space-time evolution of a heavy-ion collision. To present a coherent picture of heavy-ion collisions, we use a thermal fireball model developed earlier for application to dilepton production in the low- [69] and intermediate-mass [70] region. This thermal evolution scenario is consistent with global observables such as the hadro-chemistry [71] or the observed flow velocities, and is also in line with the main features of hydrodynamic calculations. The simple thermal fireball model (which accounts for the bulk properties of the evolution) provides a convenient

framework to study J/ψ dynamics.

We present in Chapter 6 the main results of our model of charmonium production. We develop a two-component model [64, 72] including two sources to account for the observed J/ψ yield: *(i)* a direct component of primordially produced J/ψ's subjected to nuclear, plasma and hadronic suppression and *(ii)* a statistical component arising from coalescence of c and $\bar{c}$ at the hadronization transition. We first compare our approach to available data at SPS energies for S-U and Pb-Pb collisions. In addition to the J/ψ centrality dependence, we evaluate the ψ'/ψ ratio. At SPS, we find that the J/ψ yield is dominated by direct J/ψ's. We then turn to RHIC energies, where the statistical component is found to dominate over the direct one. This leads us to the conclusion that J/ψ suppression as to be reevaluated as a plasma signature at collider energies, and we suggest that the excitation function of J/ψ production (normalized to the open-charm production) would be valuable to study the transition from the regime of suppressed hard J/ψ production at SPS to mainly statistical (soft) J/ψ production at RHIC.

Chapter 7 presents improvements over our two-component model in two respects: First, we account for the in-medium effects inferred in Chapter 3 from lattice QCD studies. Specifically, this may help to resolve the discrepancy in the ψ'/ψ ratio that was identified in the two-component model of Chapter 6. Second, we adopt a more microscopic description of J/ψ regeneration by solving rate equations including the backward reaction in charmonium dissociation processes (thus allowing for J/ψ formation in the plasma, as suggested by lattice results).

We conclude in Chapter 8 and give a few directions along which we plan to expand the work undertaken in this thesis. The issue of charm quark thermalization, J/ψ transverse momentum spectra as well as comparable studies for the bottomonium systems should be addressed to develop a broader and consistent picture of heavy-quarkonia in heavy-ion collisions.

Bibliography

[1] F. Halzen and A. D. Martin, *Quarks and leptons: an introductory course in modern particle physics*, Wiley, New York, USA (1984).

[2] F. J. Yndurain, *The theory of quark and gluon interactions*, Springer, Berlin, Germany (1999).

[3] H. D. Politzer, Phys. Rev. Lett. **30**, 1346 (1973).

[4] D. J. Gross and F. Wilczek, Phys. Rev. Lett. **30**, 1343 (1973).

[5] K. Hagiwara *et al.*, Physical Review D **66**, 010001+ (2002).

[6] S. Bethke, (2002), hep-ex/0211012.

[7] J. I. Friedman, Rev. Mod. Phys. **63**, 615 (1991).

[8] H. W. Kendall, Rev. Mod. Phys. **63**, 597 (1991).

[9] R. E. Taylor, Rev. Mod. Phys. **63**, 573 (1991).

[10] G. Hanson *et al.*, Phys. Rev. Lett. **35**, 1609 (1975).

[11] V. Koch, Int. J. Mod. Phys. **E6**, 203 (1997), nucl-th/9706075.

[12] J. C. Collins and M. J. Perry, Phys. Rev. Lett. **34**, 1353 (1975).

[13] R. Hagedorn, Nuovo Cim. Suppl. **3**, 147 (1965).

[14] A. Chodos, R. L. Jaffe, K. Johnson, C. B. Thorn, and V. F. Weisskopf, Phys. Rev. **D9**, 3471 (1974).

[15] C. E. DeTar and J. F. Donoghue, Ann. Rev. Nucl. Part. Sci. **33**, 235 (1983).

[16] T. Schafer and E. V. Shuryak, Rev. Mod. Phys. **70**, 323 (1998), hep-ph/9610451.

[17] J. Gasser and H. Leutwyler, Ann. Phys. **158**, 142 (1984).

[18] F. Karsch, Lect. Notes Phys. **583**, 209 (2002), hep-lat/0106019.

[19] K. G. Wilson, Phys. Rev. **D10**, 2445 (1974).

[20] J. B. Kogut, Rev. Mod. Phys. **51**, 659 (1979).

[21] J. B. Kogut, Rev. Mod. Phys. **55**, 775 (1983).

[22] D. Bailin and A. Love, Phys. Rept. **107**, 325 (1984).

[23] R. Rapp, T. Schafer, E. V. Shuryak, and M. Velkovsky, Phys. Rev. Lett. **81**, 53 (1998), hep-ph/9711396.

[24] M. G. Alford, K. Rajagopal, and F. Wilczek, Phys. Lett. **B422**, 247 (1998), hep-ph/9711395.

[25] M. A. Halasz, A. D. Jackson, R. E. Shrock, M. A. Stephanov, and J. J. M. Verbaarschot, Phys. Rev. **D58**, 096007 (1998), hep-ph/9804290.

[26] M. A. Stephanov, K. Rajagopal, and E. V. Shuryak, Phys. Rev. Lett. **81**, 4816 (1998), hep-ph/9806219.

[27] E. V. Shuryak, Phys. Lett. **B78**, 150 (1978).

[28] For more information on the futur GSI project, see the GSI website: *http://www.gsi.de*.

[29] J.-Y. Ollitrault, Phys. Rev. **D46**, 229 (1992).

[30] J.-Y. Ollitrault, Phys. Rev. **D48**, 1132 (1993), hep-ph/9303247.

[31] STAR Collaboration, C. Adler *et al.*, Phys. Rev. Lett. **87**, 182301 (2001), nucl-ex/0107003.

[32] P. Huovinen, P. F. Kolb, U. W. Heinz, P. V. Ruuskanen, and S. A. Voloshin, Phys. Lett. **B503**, 58 (2001), hep-ph/0101136.

[33] H. Sorge, Phys. Lett. **B402**, 251 (1997), nucl-th/9701012.

[34] D. Teaney, J. Lauret, and E. V. Shuryak, Phys. Rev. Lett. **86**, 4783 (2001), nucl-th/0011058.

[35] S. Pratt, Phys. Rev. Lett. **53**, 1219 (1984).

[36] P. Koch, B. Müller, and J. Rafelski, Phys. Rept. **142**, 167 (1986).

[37] WA97 Collaboration, E. Andersen *et al.*, Phys. Lett. **B449**, 401 (1999).

[38] E910 Collaboration, R. Soltz *et al.*, J. Phys. **G27**, 319 (2001).

[39] PHENIX Collaboration, D. d'Enterria *et al.*, Nucl. Phys. **A715**, 749 (2003), hep-ex/0209051.

[40] STAR Collaboration, J. Adams *et al.*, (2003), nucl-ex/0306024.

[41] X.-N. Wang and M. Gyulassy, Phys. Rev. Lett. **68**, 1480 (1992).

[42] D. Kharzeev, E. Levin, and L. McLerran, Phys. Lett. **B561**, 93 (2003), hep-ph/0210332.

[43] X.-N. Wang, (2003), nucl-th/0307036.

[44] T. Peitzmann and M. H. Thoma, Phys. Rept. **364**, 175 (2002), hep-ph/0111114.

[45] J. Kapusta, P. Lichard, and D. Seibert, Phys. Rev. **D44**, 2774 (1991).

[46] S. Turbide, R. Rapp, and C. Gale, (2003), hep-ph/0308085.

[47] F. Bellaiche, Ph.D. Thesis (1997) , Université Claude Bernard Lyon-I, France.

[48] R. Rapp and J. Wambach, Adv. Nucl. Phys. **25**, 1 (2000), hep-ph/9909229.

[49] S. D. Drell and T.-M. Yan, Phys. Rev. Lett. **25**, 316 (1970).

[50] S. L. Glashow, J. Iliopoulos, and L. Maiani, Phys. Rev. **D2**, 1285 (1970).

[51] A. Litke *et al.*, Phys. Rev. Lett. **30**, 1189 (1973).

[52] J. J. Aubert *et al.*, Phys. Rev. Lett. **33**, 1404 (1974).

[53] J. E. Augustin *et al.*, Phys. Rev. Lett. **33**, 1406 (1974).

[54] G. H. Trilling, Phys. Rept. **75**, 57 (1981).

[55] E705 Collaboration, L. Antoniazzi *et al.*, Phys. Rev. **D46**, 4828 (1992).

[56] BABAR Collaboration, B. Aubert *et al.*, Phys. Rev. Lett. **90**, 242001 (2003), hep-ex/0304021.

[57] CLEO Collaboration, D. Besson *et al.*, (2003), hep-ex/0305017.

[58] CLEO Collaboration, D. Besson *et al.*, (2003), hep-ex/0305100.

[59] M. A. Nowak, M. Rho, and I. Zahed, Phys. Rev. **D48**, 4370 (1993), hep-ph/9209272.

[60] W. A. Bardeen and C. T. Hill, Phys. Rev. **D49**, 409 (1994), hep-ph/9304265.

[61] T. Matsui and H. Satz, Phys. Lett. **B178**, 416 (1986).

[62] P. Braun-Munzinger and J. Stachel, Phys. Lett. **B490**, 196 (2000), nucl-th/0007059.

[63] P. Braun-Munzinger and J. Stachel, Nucl. Phys. **A690**, 119 (2001), nucl-th/0012064.

[64] L. Grandchamp and R. Rapp, Phys. Lett. **B523**, 60 (2001), hep-ph/0103124.

[65] S. G. Matinian and B. Müller, Phys. Rev. **C58**, 2994 (1998), nucl-th/9806027.

[66] K. L. Haglin, Phys. Rev. **C61**, 031902 (2000), nucl-th/9907034.

[67] Z.-W. Lin and C. M. Ko, Phys. Rev. **C62**, 034903 (2000), nucl-th/9912046.

[68] L. Grandchamp, R. Rapp, and G. E. Brown, (2003), submitted to Phys. Rev. Lett., hep-ph/0306077.

[69] R. Rapp and J. Wambach, Eur. Phys. J. **A6**, 415 (1999), hep-ph/9907502.

[70] R. Rapp and E. V. Shuryak, Phys. Lett. **B473**, 13 (2000), hep-ph/9909348.

[71] P. Braun-Munzinger, I. Heppe, and J. Stachel, Phys. Lett. **B465**, 15 (1999), nucl-th/9903010.

[72] L. Grandchamp and R. Rapp, Nucl. Phys. **A709**, 415 (2002), hep-ph/0205305.

Chapter 2

Open-Charm and Charmonium Primordial Production

We start with a brief review of primordial open-charm and charmonium production from p-p to A-A collisions. "Primordial" (or hard) production refers to the production of charm in the very early stages of the collision ($\tau < 1$ fm/c) through hard N-N collisions, which due to the large mass m_c of the charm quark, $m_c \sim 1.3$ GeV/c^2, occurs on a natural time scale of

$$\tau \sim \frac{1}{m_c} \sim 0.2 \text{ fm/c} . \tag{20}$$

The importance of knowing the primordial production of open-charm and charmonium is clear: since we intend to use charmonium as a probe to characterize the hot and/or dense matter created in heavy-ion collisions, it is necessary to assess the amount of charm produced initially to estimate subsequent reinteractions of charm/charmonium in the medium.

We first describe open-charm production, going from p-p to p-A and A-A collisions. Due to the lack of theoretical accuracy to calculate charm production (although the charm quark is heavy, its mass is still rather moderate in regards to typical perturbative QCD scales and significant non-perturbative effects are involved in charm production), the emphasis will be on experimental results. We then give a short account of the different theoretical models of prompt charmonium production and show how they compare to experiments. Finally, we describe a simple model of early "pre-equilibrium" charmonium interactions (the so-called nuclear absorption) as it has been inferred from p-A and light A-A collisions.

2.1 Open-charm production

Heavy-quark production is a very interesting field of research by itself, because it constitutes a benchmark process to study perturbative QCD since m_Q defines the scale at which α_s is evaluated. Moreover, for charm, one expects to shed light on the non-perturbative effects which accompany charm production by comparing perturbative calculations to data. It is also a flag for very specific production mechanisms (*e.g.* W + *charm* hadro-production which probes the strange content of the proton) and has been under intense investigations, see [1] for a review.

2.1.1 Open-charm production in p-p collisions

In perturbative QCD, charm production occurs through gluon fusion which dominates at high energies, and quark annihilation

$$g + g \to c + \bar{c}, \qquad q + \bar{q} \to c + \bar{c}\,, \tag{21}$$

whose corresponding Feynman diagrams at leading order are shown in Fig. 2.1. Such

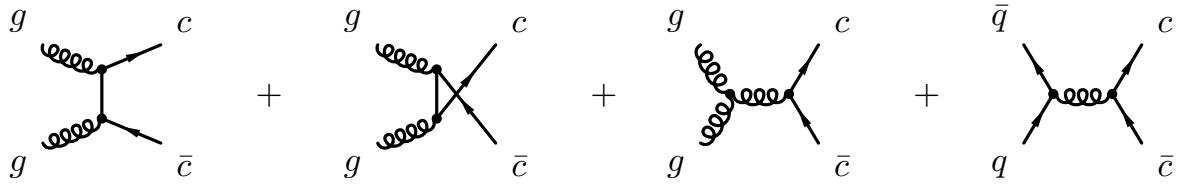

Figure 2.1: Feynman graphs of charm production in leading order perturbative QCD.

processes have been calculated to leading order (LO) and next-to-leading order (NLO) perturbative QCD, see *e.g.* [2]. Due to the "not so heavy" mass of the charm quark, NLO corrections are large as characterized by the theoretical K-factors

$$\frac{\sigma^{LO} + \sigma^{NLO}}{\sigma^{LO}} \sim 3\,. \tag{22}$$

The hadro-production of charm is then obtained by convolution of the partonic cross-sections with the parton distribution functions inside the nucleons. The differential charm production cross-section is then given by:

$$\frac{d\sigma}{dy_c dy_{\bar{c}} dp_t^2} = \frac{1}{16\pi s} \sum_{i,j} x_1 f_i(x_1,\mu) x_2 f_j(x_2,\mu) \overline{\sum} |\mathcal{M}_{ij}|^2 \tag{23}$$

where the $\mathcal{M}_{ij}$ correspond to the matrix elements of the graphs shown in Fig. 2.1. y_c ($y_{\bar{c}}$) is the rapidity of the outgoing c ($\bar{c}$) and the $f_{i,j}$'s are the parton distribution functions of the incoming i, j partons. s is the center of mass energy, and $x_{1,2}$ are given by

$$x_1 = \frac{m_T}{\sqrt{s}} \left(e^{y_c} + e^{-y_{\bar{c}}}\right), \qquad x_2 = \frac{m_T}{\sqrt{s}} \left(e^{y_c} - e^{-y_{\bar{c}}}\right) , \tag{24}$$

where $m_T = \sqrt{m_c^2 + p_T^2}$ is the transverse mass of the heavy quarks. The produced heavy quarks are close in rapidity and have typical momenta of the order of m_Q. The factorization scale μ in Eq. (23) and the uncertainty on the charm quark mass induce strong dependencies in the total charm cross section. Nevertheless, NLO pQCD and a simple phenomenology of non-perturbative effects such as *(i)* the use of universal fragmentation functions to describe hadronization and *(ii)* the inclusion of an intrinsic k_T broadening (to account for pre-scattering and/or the Fermi motion of partons inside the nucleons) give a coherent picture of charm (and bottom) production which reproduces experimental data on the cms energy dependence, the transverse momentum and the azimuthal distributions of $\sigma_{c\bar{c}}$ ($\sigma_{b\bar{b}}$). Calculations using event generators such as PYTHIA (LO pQCD) upscaled by experimental K-factors ($K \sim 4 - 5$) also describe reasonably well the main features of $\sigma_{c\bar{c}}$ [3].

2.1.2 Open-charm in p-A collisions

Charm production being a hard process, one expects the following scaling from p-p to p-A collisions for the charm production cross-section

$$\sigma(pA \to c\bar{c}) = A\sigma(pp \to c\bar{c}) , \tag{25}$$

or equivalently for the charm multiplicities

$$N_{c\bar{c}}^{pA} = A^{1/3} N_{c\bar{c}}^{pp} . \tag{26}$$

This has been experimentally verified [4, 5] as shown in Fig. 2.2. After background subtraction, the contributions of charm decays to the dimuon invariant mass spectrum (thick dashed line, scaled according to Eq. (25)), in addition to small J/ψ and Drell-Yan yields (thin dashed lines) account very well for the data in the intermediate mass region (full line) for a wide range of targets with different A numbers.

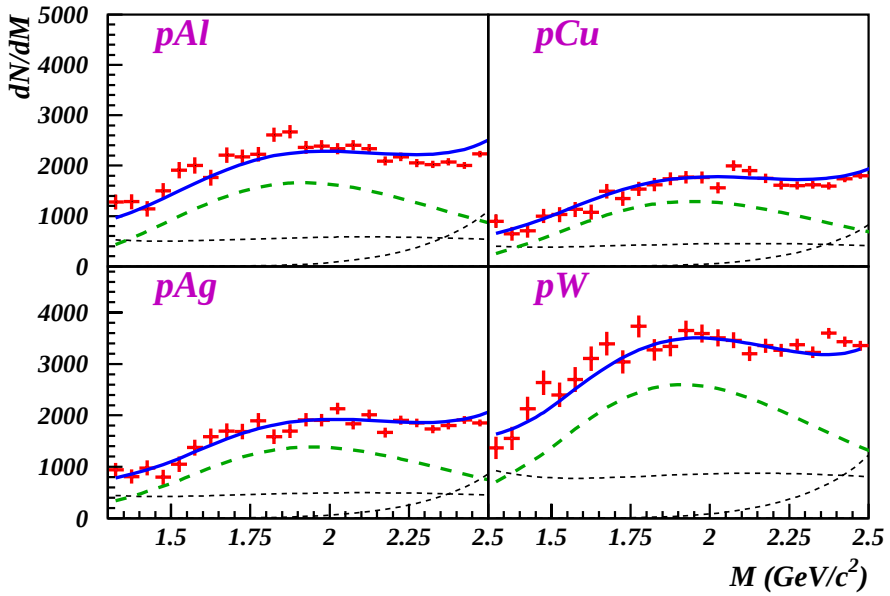

Figure 2.2: Open-charm contributions to the dilepton invariant mass spectrum in the intermediate mass region for p-Al, p-Cu, p-Ag and p-W collisions at the CERN-SPS, from [5]. The full line is the sum of the $D\bar{D}$ contribution (thick dashed line) extrapolated according to Eq. (25) with the J/ψ and Drell-Yan contributions (thin dashed lines).

2.1.3 Open-charm production in A-A collisions

In heavy-ion collisions, the production of $c\bar{c}$ pairs is also expected to behave as a hard process, *i.e.* to scale with the number of primordial N-N collisions or equivalently,

$$\sigma(AB \to c\bar{c}) = AB\sigma(NN \to c\bar{c}) \; . \tag{27}$$

However, for heavy-ion reactions, only indirect measurements via semi-leptonic decays are available so far (hopefully, the STAR experiment at RHIC will be able to reconstruct D-mesons in the $K\pi$ invariant mass spectrum). The semi-leptonic decay of D-mesons

$$D^- D^+ \to \begin{cases} \mu^+ \nu_\mu X \\ \mu^- \nu_{\bar{\mu}} Y \end{cases}$$

allows to infer the charm production cross-sections by studying dilepton spectra (NA50 at SPS) or single lepton spectra (PHENIX at RHIC) provided that all other known sources of leptons are under control.

In Pb-Pb at SPS energy, $\sqrt{s_{NN}}$=17.3 GeV, the NA38/NA50 collaborations [5] found an enhancement of intermediate-mass (*IM*, $M_{\mu\mu}$=1.5-2.5 GeV) dimuon pairs over the expected Drell-Yan and open charm sources, gradually increasing with centrality up to a factor of ∼2.5 in the most central events. This excess is well reproduced if an

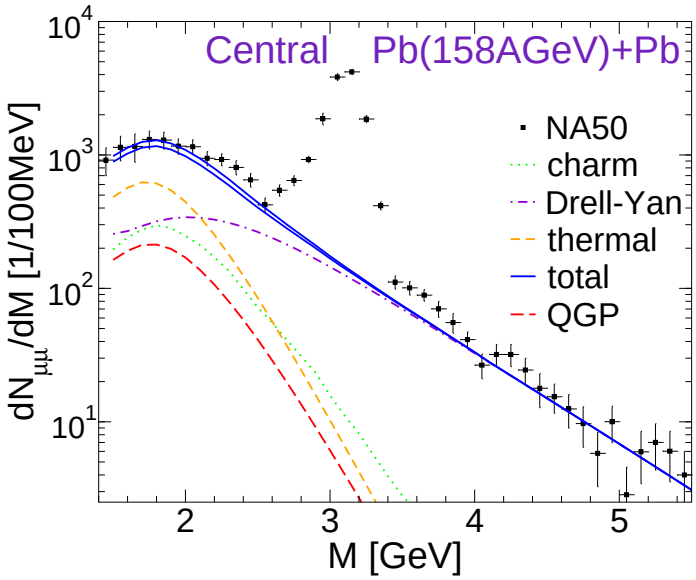

Figure 2.3: Description of the dilepton excess in the intermediate mass region of the dilepton spectrum observed by the NA50 collaboration at SPS [5] described in term of thermal radiation from an equilibrated fireball [6].

increase in open charm production by a factor of ∼3.5 is postulated. However, underlying mechanisms for such an increase are not easily conceivable. In fact, it has been found [6, 7, 8] that *thermal* dimuon radiation from a fireball with reasonable initial temperatures, T_i=200-250 MeV, can, maybe more naturally, account for the *IM* dimuon excess, as shown in Fig. 2.3. In the intermediate mass region, the thermal dimuon radiation (short-dashed line) including a QGP contribution (long-dashed line) dominates over Drell-Yan (dot-dashed) and charm (dotted) contributions, and successfully explains the observed dilepton excess (difference between the full lines). The definitive experimental resolution of this problem is expected from the NA60 experiment [9].

In *Au-Au* at RHIC energy, $\sqrt{s_{NN}}$=130,200 GeV, single-electron ($e^{\pm}$) transverse-momentum (p_t) spectra have been measured at various centralities [10, 11]. After subtraction of light-hadron decay sources, the remaining spectra can be accounted for by "standard" charm-production extrapolated from *N-N* event generators, as shown in Fig. 2.4. For all four classes of centrality, the electron signals expected from charm decays (data points) are well described by binary scaling of $\sigma_{c\bar{c}}^{pp}$. On the one hand, this limits the possibility for an appreciable charm enhancement. On the other hand, it is somewhat surprising that even for central collisions the spectral shape is reasonably well reproduced without any reinteractions, as one would naively expect a softening if charm quarks (partially) thermalize. However, thermalization also implies that *c*-quarks partic-

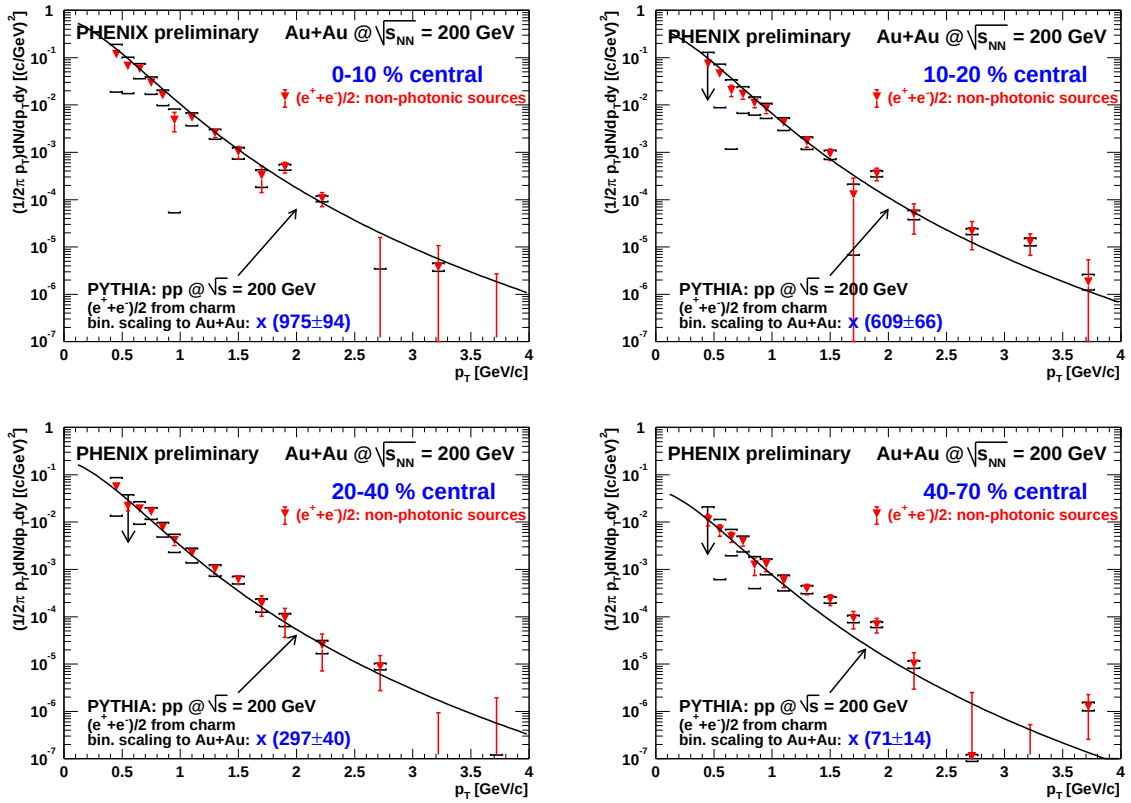

Figure 2.4: Single electrons spectra at RHIC for four classes of centrality [11], after background subtraction. The full lines correspond to LO pQCD calculations (upscaled by a K-factor $\sim 4-5$) scaled with the number of binary collisions at a given centrality.

ipate in the collective matter expansion. In Ref. [12] it has been shown that the current PHENIX data [10, 11] for "charm-like" $e^{\pm}$ are also consistent with the assumption of complete c-quark thermalization *and* collective flow. As discussed in the next chapter, c-quark reinteractions have important consequences for charmonium production; the obvious observable to disentangle the two extremes is the c-quark *elliptic* flow [12].

Overall, it seems that in heavy-ion collisions, charm production indeed scales like a hard process. Fig. 2.5, taken from Ref. [10] shows the total charm cross-section divided by the number of binary collisions over a wide range of cms energies. The $\sigma_{c\bar{c}}$ excitation function is well reproduced by a PYTHIA calculation which indicates the hard process nature of charm production in A-A collisions. The preliminary PHENIX experimental point ($\sqrt{s} = 200$ AGeV at RHIC [11], not shown on Fig. 2.5) is also well in line with standard extrapolation. Therefore, throughout this work, we will assume that charm production is given by hard scaling from p-p and we will not consider any further the open-charm enhancement at SPS energies advocated in [13, 14, 15]. We

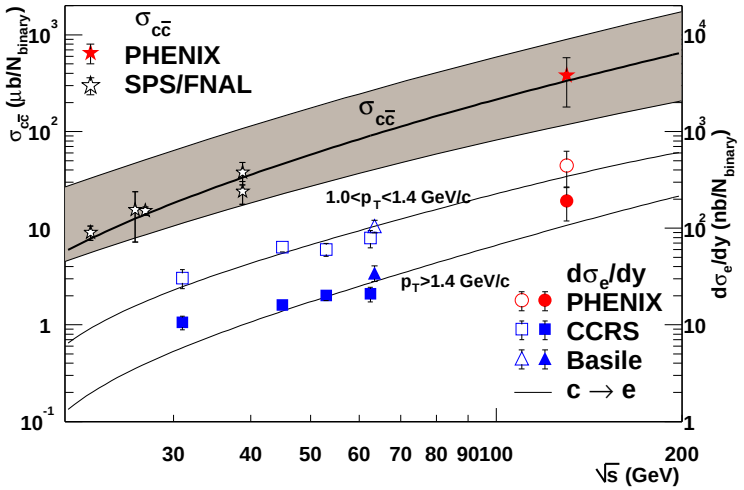

Figure 2.5: Excitation function of the charm production cross-section per binary collision [10]. The data follow the trend of $\sigma_{c\bar{c}}^{pp}$ (LO pQCD, thick line) indicating the hard process nature of charm production.

rely on extrapolations from the experimental data, similar to Fig. 2.5, to input $N_{c\bar{c}}$ in our models. Typically, in the SPS regime ($\sqrt{s_{NN}} \simeq 20$ GeV) $\sigma_{c\bar{c}}^{pp} \simeq 5\mu$b, while at full RHIC energy, $\sigma_{c\bar{c}}^{pp} \simeq 600\mu$b. When extrapolated to central collisions of heavy nuclei, one expects roughly 0.2 $N_{c\bar{c}}$ per central collision at SPS to be compared to $N_{c\bar{c}} \simeq 10-20$ at RHIC. As we will see, this two order of magnitude increase in the charm abundance is very important for the dynamics of charmonium formation, going from SPS to RHIC.

2.2 Hidden-charm production in p-p collisions

In p-p collisions, only a small fraction $f \sim 1-2\%$ of the total charm production develops into a charmonium state. Intuitively, this may be understood in terms of the azimuthal distributions of $c\bar{c}$ production, which are strongly peaked at $\phi = \pi$, ϕ being the angle between the c and the $\bar{c}$ quarks. Namely, c and $\bar{c}$ quarks are produced most of the time back-to-back and fly away from each other. The case of two comoving c and $\bar{c}$ quarks, which seems more likely to lead to the formation of a charm bound state occurs only in a small fraction of events, entailing a small abundance of charmonia with respect to open-charm abundances.

We review in this section the different theoretical models of charmonium production in p-p collisions, which have been under intense investigation both theoretically and

experimentally, and have significantly improved over the course of the last decade, see Ref. [16] for a review..

2.2.1 The Color Evaporation Model

We start with the simplest, yet phenomenologically rather successful, model of charmonium production, namely the Color Evaporation Model (CEM) [17, 18, 19]. The $c\bar{c}$ pair, whose production mechanism within the framework of pQCD has been detailed in Sec. 2.1.1, is usually produced in a colored state ($q\bar{q}$ annihilation always leads to a colored $c\bar{c}$ pair while gluon fusion leads to a mix of singlet and octet states). Therefore, to form a fully developed charmonium state, the $c\bar{c}$ pair needs to neutralize color with the surrounding color field.

The underlying assumption of the CEM is that color quantum numbers are adjusted at no cost in rate and with no dynamical effects. Hence, in this model, the production cross-section σ_Ψ of a charmonium state Ψ is given by:

$$\sigma_\Psi = f_\Psi \int_{2m_c}^{2m_D} dm_{c\bar{c}} \frac{d\sigma_{c\bar{c}}}{dm_{c\bar{c}}} \tag{28}$$

where f_Ψ is a constant associated to the charmonium Ψ, usually obtained by fit to the data. One immediate prediction of the Color Evaporation Model is that ratios of different charmonium states are energy independent. Being rather successful at describing x_f distributions and the energy dependence of charmonium production, the CEM model has recently attracted renewed interest [19, 18].

2.2.2 The Color Singlet Model

Before 1993, charmonium production was usually calculated within the Color Singlet Model (CSM) [20, 21, 22, 23, 24]. This model relies on the assertion that charmonium production involves two distinct length scales: the first scale $1/m_c$ concerns the short distance part of the amplitude corresponding to the production of a $c\bar{c}$ pair and is much smaller than the typical length scale associated with the charmonium wavefunction. The $c\bar{c}$ pair is created point-like (calculated within pQCD) and subsequently develops into a charmonium state through non-perturbative effects encoded in the charmonium wavefunction.

The production cross-section for a $^{2S+1}L_j$ charmonium state is then factorized as

$$d\sigma(pp \rightarrow {}^{2S+1}L_j + X) = d\sigma(pp \rightarrow c\bar{c}(\underline{1}, {}^{2S+1}L_j) + X) \left| \frac{d^l}{dr^l} R_{nl}(0) \right|^2 , \qquad (29)$$

where $\underline{1}$ indicates a $c\bar{c}$ pair in a color singlet state. The first factor in the product of the right-hand-side (rhs) is the short distance part of the amplitude calculated perturbatively. It takes into account the number of gluons needed to arrive at a color singlet state and therefore, the expansion of the different graphs for a given process is organized in powers of α_s (see Fig. 2.6). The second factor in the rhs product is the wavefunction at the origin of the charmonium state under consideration and encodes all non-perturbative effects. This factorization scheme confers a big predictive power to the color singlet model since only the wavefunction at the origin is needed, a quantity which is obtainable from the study of decay widths.

In the CSM model, selection rules are imposed by quantum numbers as shown in Fig. 2.6 which compares the production of (η_c, χ_0, χ_2) to that of (J/ψ, χ_1, ψ'). In this

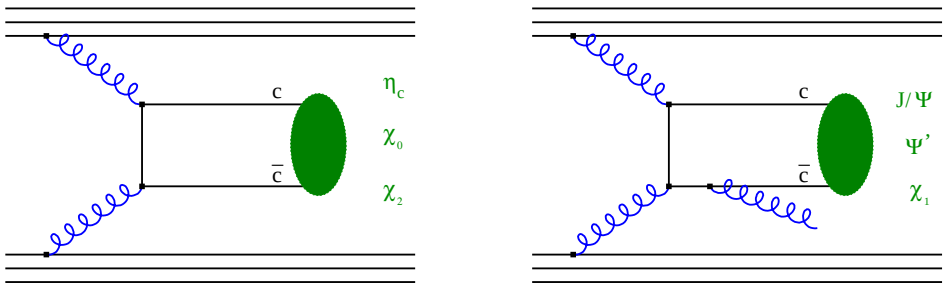

Figure 2.6: Graphs of charmonium production within the factorization scheme of the CSM model. The ellipses represent the wavefunction at the origin of the different charmonia.

model, the J/ψ and ψ' production mechanism is of higher order in α_s than χ_2 production which is not seen in the data. Actually, the CSM underpredicts the J/ψ and ψ' yield observed at the Tevatron by the CDF collaboration [25, 26] by a factor 50. It also fails at describing charmonium production at large transverse momenta, predicting spectra much softer than the ones observed at the Tevatron. This points toward the limitations of the CSM model which among others include: *(i)* the relative velocity (whose average value is roughly $v^2 \sim 1/3$ for charmonium systems) between the c and the $\bar{c}$ quarks is neglected and *(ii)* color-octet processes which can make a non-perturbative transition to a color-singlet state by radiating a soft gluon are simply absent.

2.2.3 NRQCD and the Color Octet Model

Since 1993, the major shortcomings of the CSM model, corrections due to the relative velocity v between c and $\bar{c}$ and absence of color octet processes have been successfully addressed and have led to the Color Octet Model (COM) [27, 16, 28] based on Non-Relativistic QCD (NRQCD). The latter is an effective field theory developed in Ref. [29] in which the heavy quarks are treated non-relativistically, approaches that have proven to be successful to describe heavy quarkonium physics (*e.g.* potential models for charmonium spectroscopy). In NRQCD, the heavy quarks are described by a Schrödinger field theory while the gluons and light quarks are modelled by the usual relativistic Lagrangian of QCD. NRQCD and the COM improve on the Color Singlet Model with progress made on the factorization between the short distance physics of heavy-quark creation and the long distance physics of bound state formation. Essentially, two scales of charmonium physics are identified as shown below:

m_c	$m_c v$
1.5 GeV	750 MeV
$c\bar{c}$ formation $\sim \frac{1}{m_c}$	$c\bar{c}$ size $\sim \frac{1}{m_c v}$

If these two scales are well separated, the formation of the bound state should be insensitive to the details of the heavy-quark creation process, which is essentially local on the scale of the quarkonium size.

The power counting is done in terms of the small parameter v^2 and allows to separate the scales m_c and $m_c v$ so that all effects of the scale $m_c v$ are isolated in a $c\bar{c}$ subdiagram which is reproduced by NRQCD. The parts of the diagram involving the scale m_c are included in the hard scattering subdiagram and are dealt with within pQCD. Thus the formation of a charmonium state Ψ is factorized as

$$d\sigma(\Psi + X) = \sum_{n=\underline{1},\underline{8}} d\sigma\left(c\bar{c}[n] + X\right) \langle \mathcal{O}^{\Psi}[n] \rangle \tag{30}$$

where the sum runs over all color and angular momentum states of the $c\bar{c}$ pair. The short distance coefficients $d\sigma((c\bar{c}[n] + X)$ are given by pQCD and the long distance matrix elements $\langle \mathcal{O}^{\Psi}[n] \rangle$ are calculated as matrix elements of the NRQCD operators. An example of power counting is shown in Fig. 2.7.

The organization of charmonium production processes in powers of α_s, m_c, p_T and v shows that color octet processes induce small corrections as long as the hard scattering subparts of the diagrams, given by $d\sigma((c\bar{c}[n] + X)$, have same magnitude for singlet and octet mechanisms. However, when extra suppression by powers of α_s and/or kinematical

(a) leading-order colour-singlet: $g + g \to c\bar{c}[^3S_1^{(1)}] + g$

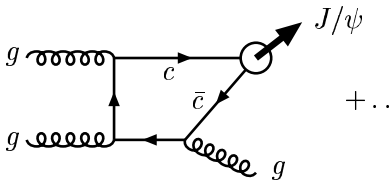

$+\ldots \qquad \sim \alpha_s^3 \frac{(2m_c)^4}{p_t^8}$

(b) colour-singlet fragmentation: $g + g \to [c\bar{c}[^3S_1^{(1)}] + gg] + g$

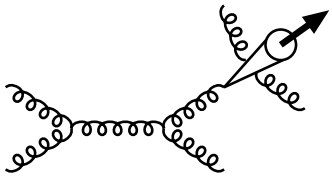

$+\ldots \qquad \sim \alpha_s^5 \frac{1}{p_t^4}$

(c) colour-octet fragmentation: $g + g \to c\bar{c}[^3S_1^{(8)}] + g$

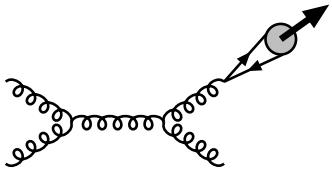

$+\ldots \qquad \sim \alpha_s^3 \frac{1}{p_t^4} v^4$

(d) colour-octet t-channel gluon exchange: $g + g \to c\bar{c}[^1S_0^{(8)}, {}^3P_J^{(8)}] + g$

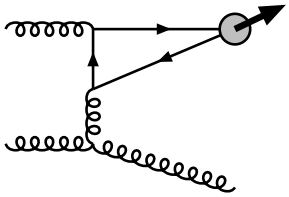

$+\ldots \qquad \sim \alpha_s^3 \frac{(2m_c)^2}{p_t^6} v^4$

Figure 2.7: Power counting in the Color Octet Model, taken from Ref. [30].

factors, octet processes can dominate. This is especially relevant at high p_T where octet graphs give a harder spectrum (falling as $1/p_T^4$, see graph (c) in Fig. 2.7) and dominate over the leading order color singlet term (graph (a)) which falls steeply as $1/p_T^8$.

Within the COM, NRQCD matrix elements are obtained from decay widths or by fits to experimental data (such as charmonium transverse momentum distributions). This model gives a solid theoretical framework to hidden charm production in p-p collisions. It describes well the CDF data [25, 26] on J/ψ production at large p_T and also accounts for the recent PHENIX experimental results obtained in p-p collisions at RHIC, $\sqrt{s} =$ 200 AGeV [31]. Both the p_T distributions, the rapidity distribution and the center of mass energy dependence can be described using the COM with a reasonable choice of parameters.

In the future, the PHENIX experiment at RHIC will, in addition, further address the remaining issue of the J/ψ polarization. The Color Octet Model predicts that the J/ψ should be polarized at very large p_T since the dominant process (the color octet fragmentation, see graph (c) of Fig. 2.7) preserves spin. This is however at variance with the CDF data on J/ψ polarization [32].

2.2.4 Total J/ψ cross-section in p-p collisions

For our purposes, *i.e.* the study of the J/ψ yield observed in heavy-ion collisions, we rely on experimental measurements and consider $\sigma_{J/\psi}^{pp}$ as an input of our models. Fig. 2.8 shows the excitation function of the J/ψ production cross-section in p-p collisions for 5 GeV $\leq \sqrt{s} \leq$ 200 GeV. The amount of J/ψ initially produced in p-A and A-A collisions is then inferred from the p-p cross-section using standard extrapolation (*i.e.* scaling with the number of binary collisions).

2.3 Nuclear absorption of charmonia in p-A and A-A collisions

From experimental studies of J/ψ production in p-A, it was realized that for such systems, J/ψ production deviates from scaling with the number of binary collisions (as expected for a hard process). Experiments at SPS [33, 34, 35, 36] and Fermilab [37, 38]

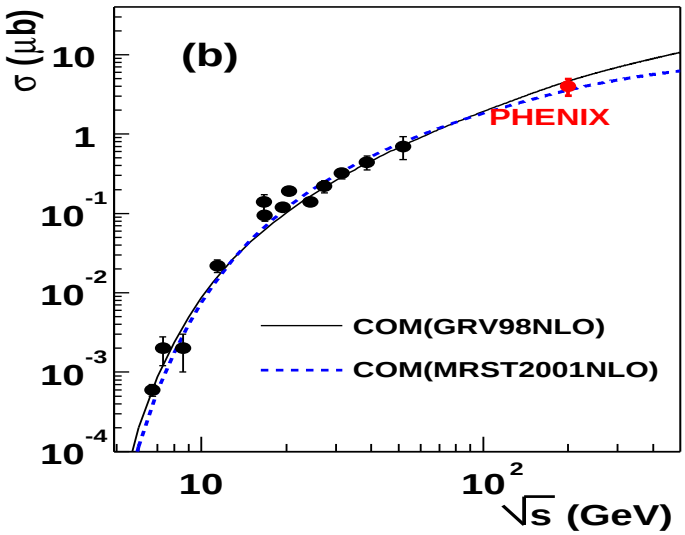

Figure 2.8: J/ψ total cross-section at $\sqrt{s_{NN}} = 200$ GeV obtained by the PHENIX collaboration [31] and compared with previous measurements at other values of $\sqrt{s}$. The curves correspond to COM calculations.

found

$$\sigma\left(AB \to J/\psi, \psi'\right) = (AB)^{\alpha}\, \sigma\left(pp \to J/\psi, \psi'\right) \ , \qquad \alpha = 0.92 \pm 0.02 \ . \tag{31}$$

In p-A collisions at cms energies around $\sqrt{s} \sim 20$ GeV, one does not expect significant reinteractions with secondaries. In addition, the fact that such suppression is quantitatively similar for J/ψ and ψ' which are very different charmonium states in size and binding energies, makes it difficult to explain by means of conventional hadronic physics. Following extensive experimental studies of charmonium suppression in p-A and light A-A reactions, it is now a well established fact such a suppression can be understood as the absorption of a pre-resonance state $c\bar{c} - g$ in nuclear matter. As seen in the previous sections, charmonium production occurs mostly through a $c\bar{c}$ pair in a colored state which couples to a gluon to neutralize color. In this picture, the actual physical charmonium state forms outside the nucleus, and charmonium suppression in p-A and light-ion collisions is interpreted as the absorption of a the $c\bar{c} - g$ state in nuclear matter. This picture accounts for the fact that very different charmonia such as J/ψ and ψ' suffer similar absorption. In A-A, we use the framework of the Glauber model to introduce the geometry of nucleus-nucleus collisions in the calculation of nuclear absorption as a function of the centrality of the collision.

2.3.1 Glauber calculation of nuclear absorption

In the Glauber model of A-B collisions, the probability for the pre-resonance $c\bar{c}-g$ state to be absorbed on its way through the nucleus, at fixed impact parameter $b = \|\vec{b}\|$, is

$$\begin{aligned} \mathcal{S}_{nuc}(b,\sigma_{nuc}) &= \int d^2s\; dz\; dz'\; \rho_A(\vec{s},z)\; \rho_B(\vec{b}-\vec{s},z') \\ &\times \exp\left\{-(A-1)\int_z^\infty dz_A \rho_A(\vec{s},z_A)\sigma_{nuc}\right\} \\ &\times \exp\left\{-(B-1)\int_{z'}^\infty dz_B \rho_B(\vec{b}-\vec{s},z_B)\sigma_{nuc}\right\}\ , \end{aligned} \tag{32}$$

where $\rho_A(\vec{s},z)$ is the nuclear density profile of the corresponding nucleus taken from [39], $\vec{s}$ the position of the production point in the transverse plane (with respect to the beam axis), and z (resp. z') is the position within nucleus A (resp. B) along the axis of the collision. The above formula has a single parameter σ_{nuc}, corresponding to the dissociation cross-section of the charmonium precursor with nucleons, which is adjusted phenomenologically to reproduce the experimental data. $\mathcal{S}_{nuc}(b,\sigma_{nuc}=0)$ corresponds to the usual nuclear overlap function of the two colliding nuclei, often referred to as $T_{AB}(b)$. Note that the nuclear density profile and the overlap function are normalized such that

$$\int d^2s\; dz\; \rho_A(\vec{s},z) = 1 \quad \text{and} \quad \int d^2b T_{AB}(b) = 1\ . \tag{33}$$

To compare the Glauber calculation to available experimental data and infer σ_{nuc}, we have to relate the impact parameter $\vec{b}$ which is a geometrical quantity to the centrality of the collision. The experiments NA50 and NA38 determine the centrality of a collision measuring the transverse energy deposited in their calorimeter, which can be related to the centrality of the collision using the wounded nucleon picture [40]. A wounded nucleon (or participant) is a nucleon from either the projectile or the target which suffers at least one inelastic collision and fragments to produce the observed secondary hadrons. Under the assumption that each participant produces on average N_h secondary hadrons with an average energy ϵ_h, one has

$$E_T(b) = \epsilon_h N_h = q N_{part}(b)\ , \tag{34}$$

where the number of wounded nucleons N_{part} is given within the Glauber theory by

$$N_{part}(b) = A \int d^2s\, T_A(\vec{s}) \left\{ 1 - [1 - \sigma_{in} T_B(\vec{s} - \vec{b})]^B \right\} \tag{35}$$

$$+ \; B \int d^2s\, T_B(\vec{s} - \vec{b}) \left\{ 1 - [1 - \sigma_{in} T_A(\vec{s})]^A \right\} \; ,$$

and $T_{A,B}(\vec{s})$ are the so called thickness functions defined by

$$T_A(\vec{s}) = \int dz\; \rho_A(\vec{s}, z) \; . \tag{36}$$

In addition, to account for fluctuations of transverse energy E_T at fixed impact parameter $\vec{b}$, we use a $E_T - b$ distribution function given by

$$\mathcal{P}_{AB}(E_T, b) = \frac{1}{\sqrt{2\pi q^2 a N_{part}^{AB}(b)}} \exp\left\{ -\frac{[E_T - q N_{part}^{AB}(b)]^2}{2q^2 a N_{part}^{AB}(b)} \right\} \; , \tag{37}$$

where q is the proportionality factor between the transverse energy and the number of participant

$$E_T(b) = q N_{part} \; , \tag{38}$$

which depends on the specific experiment settings and a is a phenomenological parameter which characterizes the size of the fluctuations in the relation between E_T and b. Values of q and a are determined either with data on minimum bias distribution or with Drell-Yan data versus centrality. The suppression of charmonium in nuclear matter as a function of E_T follows as

$$\frac{B_{\mu\mu}\sigma_{J/\Psi}}{\sigma_{DY}} = \frac{B_{\mu\mu}\sigma_{J/\Psi}^{pp}}{\sigma_{DY}^{pp}} \frac{\int d^2b\, \mathcal{P}_{AB}(E_T, b) \mathcal{S}_{nuc}(b, \sigma_{nuc})}{\int d^2b\, \mathcal{P}_{AB}(E_T, b) \mathcal{S}_{nuc}(b, \sigma_{nuc} = 0)} \; , \tag{39}$$

where $B_{\mu\mu}$ is the branching ratio for J/ψ decaying into a muon pair. The pre-factor $B_{\mu\mu}\sigma_{J/\Psi}^{pp}/\sigma_{DY}^{pp}$ has not been measured accurately experimentally and depends on the energy of the collision. Therefore, we will leave it as a free normalization parameter adjusted to the available data.

2.3.2 Normalization and comparison with experiments at SPS

Pre-resonance charmonium absorption in nuclear matter as seen in p-A and light-ion reaction constitute a baseline reference, the so-called "normal" J/ψ suppression.

Therefore, it is important for any model to reproduce this effect in order to characterize any additional source of J/ψ suppression. We concentrate on two different systems: S(200 AGeV)-U studied by the NA38 collaboration and Pb(158 AGeV)-Pb studied by the NA50 collaboration. For these two different systems, we use the values of q and a reported by the experiments, *i.e.* $q = 0.275$ and $a = 1.27$ for Pb-Pb (resp. $q = 0.72$ and $a = 1.56$ for S-U). We found that a value of $\sigma_{nuc} = 6.4$ mb reproduces the data (prior to 2002) very well. To compare with NA50 and NA38, we used normalization factors of 52.8 for Pb-Pb and 48.2 for S-U. Our description of nuclear absorption are shown Fig. 2.9 and coincides with the studies of NA50 and NA38 [41, 42, 43]. NA50 data have been

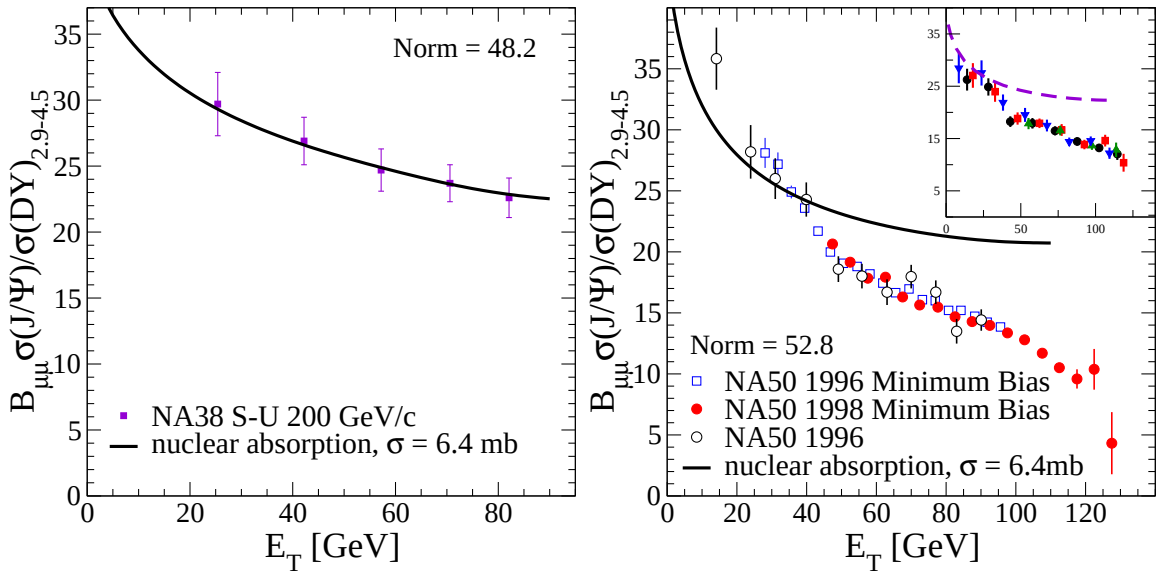

Figure 2.9: Nuclear absorption calculations for the S(200 AGeV)-U (left panel) and Pb(158 AGeV)-Pb (right panel) systems at the CERN-SPS, compared to data from , respectively, NA38 [44] and NA50 [42] using $\sigma_{nuc} = 6.4$ mb (full lines). The normalization factor $B_{\mu\mu}\sigma_{pp}^{J/\Psi}/\sigma_{pp}^{DY}$ has been fixed at 48.2 (52.8) for the S-U (Pb-Pb) system. The right panel also includes reanalyzed data by the NA50 experiment [43] together with a nuclear absorption calculation using $\sigma_{nuc} = 4.4$ mb (dashed line).

reanalyzed in 2002 [43] and the resulting updated data are also shown in the right panel of Fig. 2.9. They are described by a Glauber calculation using the updated $\sigma_{nuc} = 4.4$ mb (dashed line) together with a normalization of 43.6.

Nuclear absorption alone seems to describe the data on S-U very well. However, let us recall that such nuclear absorption calculations correspond to two-parameter fits which renders questionable the interpretation of the S-U data in terms of nuclear absorption alone. It would certainly be preferable to determine σ_{nuc} and the corresponding normalization using only p-A data. For the Pb-Pb system, the data depart from nu-

clear absorption at $E_T \sim 40$ GeV. This deviation from standard nuclear absorption was reported by the NA50 collaboration [45] as "anomalous" J/ψ suppression and was suggested as an evidence for Quark-Gluon Plasma formation [46].

2.3.3 Nuclear absorption at RHIC

There is no available data on nuclear absorption at RHIC yet. Hopefully, the *d-Au* run at $\sqrt{s_{NN}} = 200$ AGeV will allow to shed light on nuclear absorption at RHIC since extrapolations to RHIC energies differ vastly. It is not very clear how the mechanism of nuclear absorption is modified at higher energies. Some authors expect a stronger suppression, mostly due to most energetic conditions. Others [47], using field theoretical methods to infer nuclear absorption at RHIC find that one should expect the same magnitude as at SPS. Finally, it has also been predicted [48], that for charmonia at mid-rapidity, nuclear absorption at RHIC may be weaker than at SPS based on the fact that the time scale over which the two nuclei pass through eachother ($\tau \sim 2R/\gamma$, R: radius of the nuclei; γ: Lorentz factor) is shorter at RHIC and consequently, the charmonia form outside the nuclei. We show in Fig. 2.10 two curves of nuclear absorption at RHIC for different values of $\sigma_{nuc} = 6.4$ mb (dashed) and $\sigma_{nuc} = 4.4$ mb (solid) normalized to the *p-p* point.

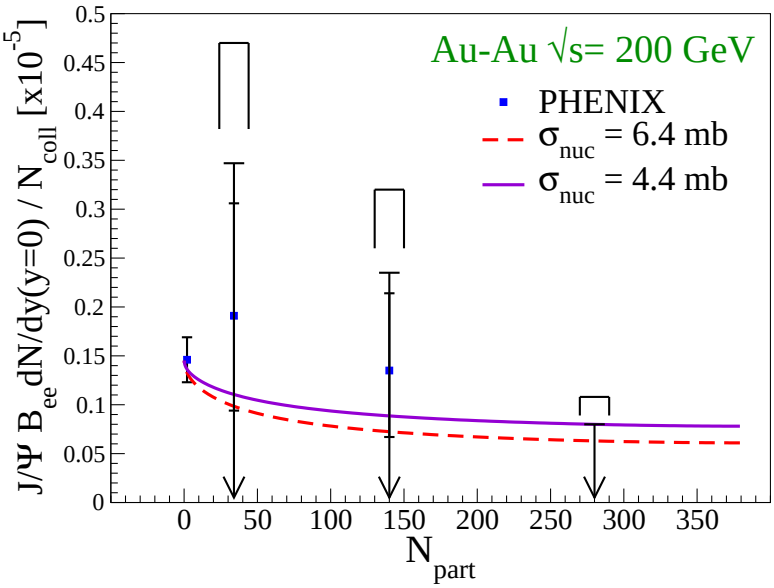

Figure 2.10: Study of nuclear absorption at RHIC for $\sigma_{nuc} = 6.4$ mb (dashed line) and $\sigma_{nuc} = 4.4$ mb (solid line), normalized to the *p-p* value from PHENIX data [49].

The precise magnitude of nuclear absorption has important consequences if one wants

to characterize additional effects. This reinforces the need for a detailed analysis of J/ψ suppression in *d-Au* collisions at RHIC together with the reference *p-p* cross-section already obtained. In this work, we have been using the same values of σ_{nuc} at RHIC and SPS energies. In early predictions (see Chapter 6), we used the previously reported value of $\sigma_{abs} = 6.4$ mb by the NA50 collaboration, while for more recent work (see Chapter 7), the latter was updated to $\sigma_{abs} = 4.4$ mb to reflect the latest analysis of the NA50 experiment [43].

Bibliography

[1] S. Frixione, M. L. Mangano, P. Nason, and G. Ridolfi, Adv. Ser. Direct. High Energy Phys. **15**, 609 (1998), hep-ph/9702287.

[2] R. V. Gavai *et al.*, Int. J. Mod. Phys. **A10**, 2999 (1995), hep-ph/9411438.

[3] P. Braun-Munzinger, D. Miskowiec, A. Drees, and C. Lourenco, Eur. Phys. J. **C1**, 123 (1998), nucl-ex/9704011.

[4] E789 Collaboration, M. J. Leitch *et al.*, Phys. Rev. Lett. **72**, 2542 (1994).

[5] NA38 Collaboration, M. C. Abreu *et al.*, Eur. Phys. J. **C14**, 443 (2000).

[6] R. Rapp and E. V. Shuryak, Phys. Lett. **B473**, 13 (2000), hep-ph/9909348.

[7] K. Gallmeister, B. Kampfer, and O. P. Pavlenko, Phys. Lett. **B473**, 20 (2000), hep-ph/9908269.

[8] I. Kvasnikova, C. Gale, and D. K. Srivastava, Phys. Rev. **C65**, 064903 (2002), hep-ph/0112139.

[9] NA60 Collaboration, B. Lenkeit *et al.*, (2001), nucl-ex/0108015.

[10] PHENIX Collaboration, K. Adcox *et al.*, Phys. Rev. Lett. **88**, 192303 (2002), nucl-ex/0202002.

[11] PHENIX Collaboration, R. Averbeck *et al.*, Nucl. Phys. **A715**, 695 (2003), nucl-ex/0209016.

[12] S. Batsouli, S. Kelly, M. Gyulassy, and J. L. Nagle, Phys. Lett. **B557**, 26 (2003), nucl-th/0212068.

[13] P. Braun-Munzinger and J. Stachel, Phys. Lett. **B490**, 196 (2000), nucl-th/0007059.

[14] P. Braun-Munzinger and J. Stachel, Nucl. Phys. **A690**, 119 (2001), nucl-th/0012064.

[15] M. I. Gorenstein, A. P. Kostyuk, H. Stöcker, and W. Greiner, Phys. Lett. **B509**, 277 (2001), hep-ph/0010148.

[16] E. Braaten, S. Fleming, and T. C. Yuan, Ann. Rev. Nucl. Part. Sci. **46**, 197 (1996), hep-ph/9602374.

[17] M. B. Einhorn and S. D. Ellis, Phys. Rev. **D12**, 2007 (1975).

[18] J. F. Amundson, O. J. P. Eboli, E. M. Gregores, and F. Halzen, Phys. Lett. **B390**, 323 (1997), hep-ph/9605295.

[19] R. Gavai *et al.*, Int. J. Mod. Phys. **A10**, 3043 (1995), hep-ph/9502270.

[20] C.-H. Chang, Nucl. Phys. **B172**, 425 (1980).

[21] E. L. Berger and D. L. Jones, Phys. Rev. **D23**, 1521 (1981).

[22] R. Baier and R. Ruckl, Phys. Lett. **B102**, 364 (1981).

[23] R. Baier and R. Ruckl, Z. Phys. **C19**, 251 (1983).

[24] G. A. Schuler, (1994), hep-ph/9403387.

[25] CDF Collaboration, F. Abe *et al.*, Phys. Rev. Lett. **79**, 572 (1997).

[26] CDF Collaboration, F. Abe *et al.*, Phys. Rev. Lett. **79**, 578 (1997).

[27] G. T. Bodwin, E. Braaten, and G. P. Lepage, Phys. Rev. **D51**, 1125 (1995), hep-ph/9407339.

[28] M. Beneke, (1997), hep-ph/9703429.

[29] W. E. Caswell and G. P. Lepage, Phys. Lett. **B167**, 437 (1986).

[30] M. Kramer, Prog. Part. Nucl. Phys. **47**, 141 (2001), hep-ph/0106120.

[31] PHENIX Collaboration, S. S. Adler *et al.*, (2003), hep-ex/0307019.

[32] CDF Collaboration, T. Affolder *et al.*, Phys. Rev. Lett. **85**, 2886 (2000), hep-ex/0004027.

[33] NA38 Collaboration, C. Baglin *et al.*, Phys. Lett. **B255**, 459 (1991).

[34] NA51 Collaboration, M. C. Abreu *et al.*, Phys. Lett. **B438**, 35 (1998).

[35] NA38 Collaboration, M. C. Abreu *et al.*, Phys. Lett. **B444**, 516 (1998).

[36] M. C. Abreu *et al.*, Phys. Lett. **B466**, 408 (1999).

[37] D. M. Alde *et al.*, Phys. Rev. Lett. **66**, 133 (1991).

[38] FNAL E866/NuSea Collaboration, M. J. Leitch *et al.*, Phys. Rev. Lett. **84**, 3256 (2000), nucl-ex/9909007.

[39] C. W. D. Jager, H. De Vries, and C. De Vries, Atom. Data Nucl. Data Tabl. **14**, 479 (1974).

[40] A. Bialas, M. Bleszynski, and W. Czyz, Nucl. Phys. **B111**, 461 (1976).

[41] NA50 Collaboration, M. C. Abreu *et al.*, Nucl. Phys. **A661**, 93 (1999).

[42] NA50 Collaboration, M. C. Abreu *et al.*, Nucl. Phys. **A698**, 127 (2002).

[43] NA50 Collaboration, B. Alessandro *et al.*, Nucl. Phys. **A715**, 243c (2003).

[44] NA38 Collaboration, M. C. Abreu *et al.*, Phys. Lett. **B449**, 128 (1999).

[45] NA50 Collaboration, M. C. Abreu *et al.*, Phys. Lett. **B410**, 337 (1997).

[46] NA50 Collaboration, M. C. Abreu *et al.*, Phys. Lett. **B477**, 28 (2000).

[47] M. A. Braun, C. Pajares, C. A. Salgado, N. Armesto, and A. Capella, Nucl. Phys. **B509**, 357 (1998), hep-ph/9707424.

[48] A. Capella and D. Sousa, (2003), nucl-th/0303055.

[49] PHENIX Collaboration, S. S. Adler *et al.*, (2003), nucl-ex/0305030.

Chapter 3

Equilibrium Properties of Charm in Matter

In this chapter, we study the properties of open charm and charmonium in matter, both in the plasma and in the hadronic phases. Since there is no direct experimental access to medium effects on charmed hadrons, we rely on static Lattice QCD studies of charmed systems to infer the possible medium modifications occurring at finite density and temperature. We first present some recent lattice gauge simulations of the heavy-quark potential at finite temperature as well as spectral functions of charmonia. We then show how one can model the medium modifications which affect the charm quark and the charmed mesons from a phenomenological point of view, and we further study the consequences of the medium modifications on J/ψ thermal equilibrium abundances.

3.1 Lattice QCD Results

The free energy of a heavy-quark pair at finite temperature

$$F_{Q\bar{Q}}(r,T) = V_{Q\bar{Q}}(r,T) - TS_{Q\bar{Q}}(r,T) \tag{40}$$

has been recently studied on the Lattice (see *e.g.* [1] for a review), in both quenched and unquenched situations. Such a calculation, including dynamical fermions, is shown in Fig. [2], where the free energy of a heavy-quark pair is plotted as a function of the distance r between the two quarks, for a set of different temperatures ranging from 0.58 T_c to 1.15 T_c. The full lines indicate the Cornell potential, *i.e.* a parameterization of the heavy-quark potential at $T = 0$, showing the characteristic Coulomb behavior

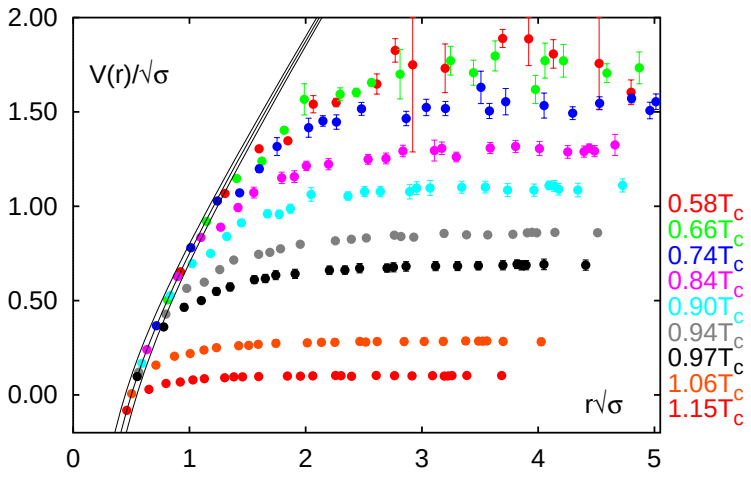

Figure 3.1: Heavy-quark free energy from the unquenched lattice gauge calculations of [2] as a function of the distance r separating the two heavy-quarks. The different sets of points correspond to different temperatures as labeled on the right of the plot.

at short distances ($r < 1$ fm) and the rising linear confining term at larger distances. For $T \neq 0$, the heavy-quark free energy is strongly modified. Starting below T_c, the free energy exhibits a plateau at large distances. At large distances, the interaction between the two quarks is completely screened and the free energy reaches its plateau value, naively corresponding to two independent charmed particles in the medium (the lowest-lying ones), that is two charm quarks above T_c and two D-mesons below T_c. The fact that the free energy reaches its plateau value for smaller and smaller distances as the temperature increases illustrates how the screening increases with temperature.

An important feature of Fig. 3.1 is that the asymptotic value of the free energy decreases as the temperature increases. Since, as mentioned previously, this plateau may reflect the open-charm threshold, lattice QCD results seem to point toward an in-medium reduction of the open-charm threshold. This important result may find its origin in (partial) chiral symmetry restoration, which is expected to occur at the same temperature as the the deconfinement phase transition from lattice gauge simulations [1]. As chiral symmetry gets restored, the constituent light-quark mass is expected to drop (as it is linked to the chiral condensate $\langle \bar{q}q \rangle$) possibly entailing a reduction of the D-meson masses[1]. Fig. 3.2 shows the decrease of the plateau value as a function of the temperature. If one takes the lattice results on a quantitative level, the potential drops

[1]Other authors [3] find that the main effect is an increased width of the D-meson. The drop in the constituent light-quark mass may be compensated by an increase in the light-quark kinetic energy and more detailed studies are needed to assess the bound state mass.

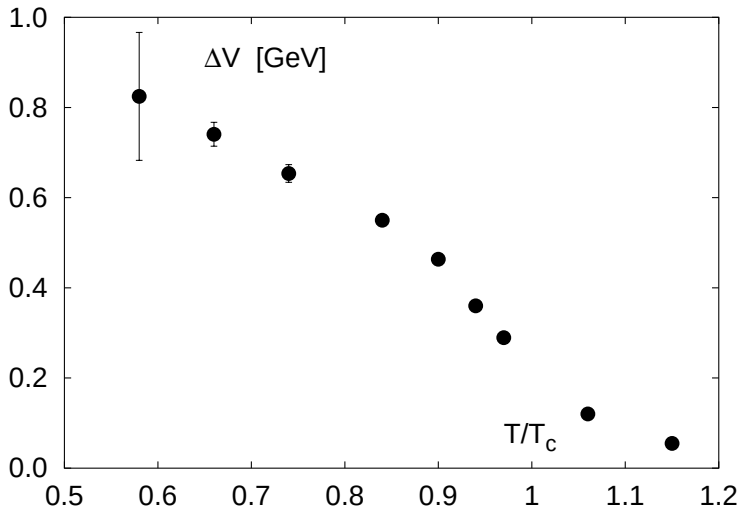

Figure 3.2: Evolution of the asymptotic value ($r \to \infty$) of the heavy-quark free energy as a function of temperature, taken from [1]. The two last points on the right correspond to temperatures above T_c.

from $T = 0$ to $T \sim T_c$ by roughly $\Delta V \sim 600$ MeV, quite reminiscent to twice the mass of a constituent light quark.

Another interesting feature revealed by lattice calculations of the heavy-quark potential is that the temperature dependence of the plateau value is remarkably smooth, even across T_c. The open-charm threshold does not exhibit any jump through the phase transition. This is suggestive of a continuity of the open-charm states across the phase transition which we identify to an in-medium charm quark mass $m_c \sim 1.6$ GeV. The difference to the bare charm quark mass ($m_c \sim 1.3$ GeV) is naturally attributed to a thermal correlation energy of heavy quarks in the QGP, see Sec. 3.2.1. This has interesting implications on the charmonium yield in heavy-ion collisions, which we will return to in Chapter 7.

This finite-T heavy-quark potential has been used to infer charmonium "dissociation" temperatures T_{diss} [4, 5], upon solving the Schrödinger equation for the bound state problem. The resulting dissociation temperatures are smaller than T_c for the ψ' and χ states and lead to $T_{diss} \sim 1.1T_c$ for J/ψ. However, such calculations suffer from the fact that the heavy-quark interaction potential ($V_{Q\bar{Q}}(r,T)$ in Eq. (40)) is hard to extrapolate from the free energy $F_{Q\bar{Q}}(r,T)$ due to the distance dependent entropy term in Eq. (40). In addition, even if a bound state moves above its threshold for spontaneous decay, this does not necessarily mean that the state disappears from the spectrum, but it can rather

survive as a resonance. This is indeed found in two recent (quenched) lattice calculations [6, 7], where reconstructed η_c and J/ψ spectral functions exhibit well-defined states up to $T \sim 1.5\ T_c$. Such a spectral function is shown in Fig. 3.3 for two temperatures, $T = 0.9\ T_c$ and $T = 1.2\ T_c$. Below T_c, the charmonium peak is very well defined with a

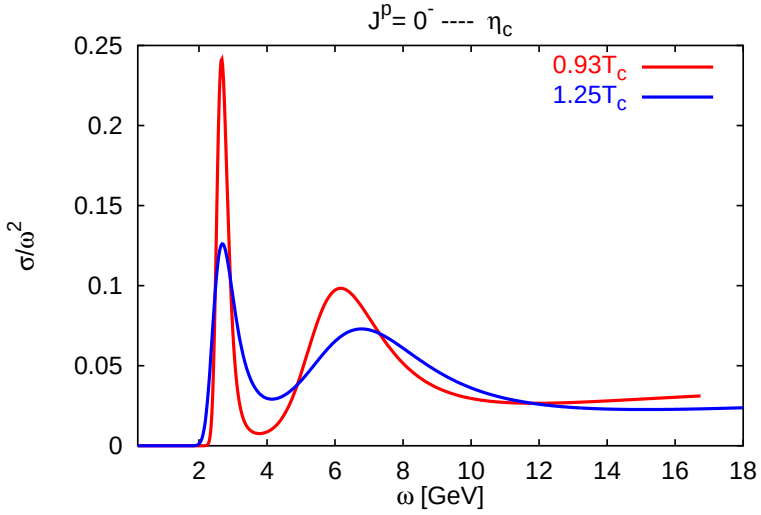

Figure 3.3: η_c spectral function on the lattice, below and above T_c from [7]. The J/ψ spectra function exhibits a very similar behavior.

very small width. However, contrary to the dissolution scenario of [5], the charmonium state still persists above T_c, as indicated by the remaining peak in the spectral function. Note that the study of spectral functions is a very valuable tool since they include all information (mass and width) on the charmonium system in the medium. In particular, such spectral functions incorporate both (static) screening and (dynamical) dissociation mechanisms. The masses appear to be essentially T-independent (as opposed to the open-charm states) whereas the widths increase significantly, to about $0.2 \sim 0.5$ GeV slightly above T_c [6, 7].

3.2 In-medium properties of charm

Based on the lattice QCD results discussed in the previous section, medium effects on charmed particles may manifest themselves by a reduction of the D-meson masses in the hadronic phase and by an increased effective charm quark mass in the plasma phase. Let us now present model calculations of such effects.

3.2.1 QGP phase: Thermal correlation energies of charm

In the plasma, the charm quark acquires an effective mass associated with a thermal correlation energy. The latter is the result of the interaction of a static charge (the charm quark) with its Debye cloud. The correlation energy can be estimated classically [8] by writing the screened Coulomb potential and expanding at small distances

$$4\pi V(r) = -\frac{4}{3}\frac{g e^{-m u_D r}}{r} \sim -\frac{4}{3}\frac{g}{r} + \frac{4}{3} g \mu_D + \cdots \tag{41}$$

The correlation energy is then given by (Δ being the Laplacian operator)

$$E_{corr} = -\frac{1}{8\pi}\int V \Delta V d^3 r \ , \tag{42}$$

leading to

$$E_{corr} = -\frac{4}{3}\alpha_s \mu_D \sim g^3 T \ . \tag{43}$$

In practice, due to the remarkable continuity of the heavy-quark potential (at large distances) through T_c, we make the hypothesis of a continuity in the open-charm states across the phase transition. Thus, the charm quark mass is obtained such that the open-charm abundances on the plasma side (calculated using Eqs. (72)- (73)) smoothly match the open-charm abundances approaching T_c from the hadronic side according to Eq. (62) with in-medium charmed meson masses. A D-meson mass drop of $\Delta_m(T_c) \sim 140$ MeV (see next section) entails an effective charm quark mass

$$m_c^* \sim 1.6 \text{ GeV} \tag{44}$$

to be compared to the bare charm quark mass $m_c \sim 1.3$ GeV.

3.2.2 Hadronic phase: reduction of the D-meson masses within a NJL calculation.

Although QCD is widely believed to be the theory of strong interactions, it has been mostly tested in the kinematic range of large momentum transfer, when the strong coupling constant α_s becomes small and allows for a perturbative expansion. However, at moderate temperatures (around T_c), one expects the relevant physical processes to be dominated by non-perturbative effects. One then has to look for simpler models, incorporating the most relevant features of QCD one wishes to study, characterized by a more "tractable" Lagrangian. Since the reduction of the D-meson mass draws its natural explanation from the restoration of chiral symmetry, one model of choice is certainly the Nambu-Jona-Lasinio (NJL) model.

The Nambu-Jona-Lasinio model at finite temperature and density

Historically, the Nambu-Jona-Lasinio model [9, 10] was introduced as a pre-QCD theory of nucleons interacting through an effective two-body interaction. Since then it has been reinterpreted as a theory with quarks degrees of freedom, reviewed in [11]. The main features of the NJL model are that it respects chiral symmetry (which is present in the QCD Lagrangian in the limit of massless quarks) and it implements the complicated gluon exchange process between quarks and antiquarks by means of a simple 4-point pointlike interaction characterized by the strength of the coupling constant G. We start from the following NJL Lagrangian [12]

$$\mathcal{L} = \overline{\psi}(i\partial\!\!\!/ - m)\psi + G\left[\left(\overline{\psi}\psi\right)^2 + \left(\overline{\psi}i\tau\gamma_5\psi\right)^2\right], \qquad \psi = \begin{pmatrix} u \\ d \end{pmatrix} \tag{45}$$

where ψ is a $SU(2)$ spinor, m the current quark mass (we work in the approximation $m_u \simeq m_d$), τ are the isospin Pauli matrices and $\gamma_5 = i\gamma^0\gamma^1\gamma^2\gamma^3$ is a standard Dirac matrix. The Lagrangian Eq. (45) is invariant under chiral symmetry, see Sec. 1.1.1. One shortcoming of the NJL model resides in the point-like character of the interaction between quarks (which necessitates the introduction of a regularization scheme) and in the fact that the model does not confine. However, a simple phenomenological way to overcome the first difficulty is to introduce a cutoff scale Λ which renders finite the momentum integrals appearing in the theory.

To study the effect of temperature and density on the quark condensate and on the constituent light-quark mass, we follow the work of [12] who calculate the quark self-energy Σ entering the propagator S

$$S^{-1}(k) = k\!\!\!/ - \Sigma(k) - m + i\epsilon \ , \tag{46}$$

in the Hartree-Fock approximation using the formalism of imaginary time Green's function. Upon decomposing the self-energy Σ as

$$\Sigma = \sigma_1 - \gamma^0\sigma_0 \ , \tag{47}$$

one obtains the following set of coupled gap-equations (see Appendix A for details)

$$\sigma_1 = \frac{G}{2\pi^2}(2n_f n_c + 1)(\sigma_1 + m) \int_0^\Lambda \frac{k^2}{\omega_k}\left[\tanh\left(\frac{\beta\omega_k^-}{2}\right) + \tanh\left(\frac{\beta\omega_k^+}{2}\right)\right] dk \ , \tag{48}$$

$$\sigma_0 = \frac{2G}{\pi^2}\int_0^\Lambda k^2\left(n_k^+ - n_k^-\right) dk \ , \tag{49}$$

where

$$\omega_k^2 = \vec{k}^2 + (\sigma_1 + m)^2 \ , \tag{50}$$

$$\omega_k^\pm = \omega_k \pm (\mu + \sigma_0) \ , \tag{51}$$

$$n_k^\pm = \left(1 + e^{\beta\omega_k^\pm}\right)^{-1} \ , \tag{52}$$

with $\beta = 1/T$ being the inverse temperature and μ the quark chemical potential. In the limit of zero temperature and density, $\sigma_0 = 0$ and we recover the well-known NJL gap-equation

$$\sigma_1 = \frac{G}{2\pi^2}(2n_f n_c + 1)(\sigma_1 + m)\int_0^\Lambda \frac{k^2}{\omega_k} dk \ . \tag{53}$$

For $T, \mu \neq 0$, we solved numerically Eqs. (48, 49) for σ_0 and σ_1 which characterize the propagation of light quarks in the medium. In particular the effective constituent light-quark mass M^* is given by

$$M^* = \sigma_1 + m \ . \tag{54}$$

Our results for the constituent light-quark mass M^* as a function of temperature and chemical potential are shown in Fig. 3.4 with our choice of parameters

$$\Lambda = 700 \text{ MeV} \tag{55}$$

$$G\Lambda^2 = 1.9 \tag{56}$$

which give a reasonable account of vacuum physics (*i.e.* $T = \mu = 0$) for the pion decay constant $f_\pi = 97$ MeV and the quark condensate $-\langle\bar{q}q\rangle^{1/3} = 280$ MeV. Note also that in the chiral limit, we obtain a phase transition temperature T_c of the order of $T_c \simeq 170$ MeV. We have used a current quark mass $m = 5.5$ MeV which breaks explicitly chiral symmetry and delays the restoration of chiral symmetry to higher temperatures and

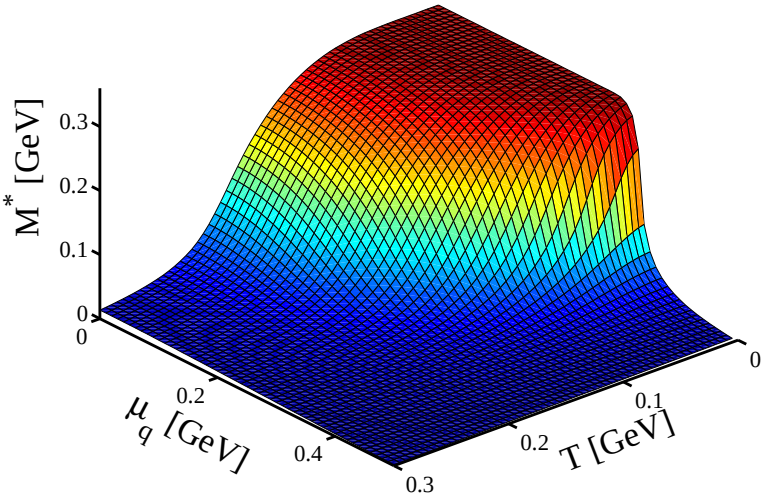

Figure 3.4: Effective light-quark mass as a function of quark chemical potential and temperature in the NJL model.

chemical potential than in the chiral limit. However, approaching $T_c \simeq 170$ MeV from below, we see that temperature and density effects significantly reduce the effective mass of the light quarks.

In-medium D-meson masses

We proceed to calculate the masses of the D-mesons in the medium, as relevant to heavy-ion collisions. We work in the simplest (and very crude) approximation where the D-meson mass is simply given by the sum of the charm quark mass and the light quark mass. Since we do not expect the charm quark mass to be significantly altered below T_c, the D-meson mass reduction at finite temperature and density amounts to the drop in the light quark mass obtained from our previous NJL calculations. To make contact with heavy-ion collisions, we used phenomenological parameterizations of the baryon chemical potential $\mu_B = 3\mu_q$ as a function of temperature as the system cools down from hadronization to thermal freezeout. The corresponding in-medium D-meson masses are shown in Fig. 3.5 as a function of temperature for SPS and RHIC collisions. With our current set of parameters, the D-meson mass drop at the transition temperature is roughly $\Delta_m(T_c) = 140$ MeV (SPS: $T_c = 170$ MeV, RHIC: $T_c = 180$ MeV). Since the reduction of the D-meson mass follows from a simple approximation and is not accurately known, we also considered the cases of $\Delta_m(T_c) = 80$ MeV and $\Delta_m(T_c) = 250$ MeV (as indicated by the band enclosed between the dotted lines in Fig. 3.5) in latter calculations.

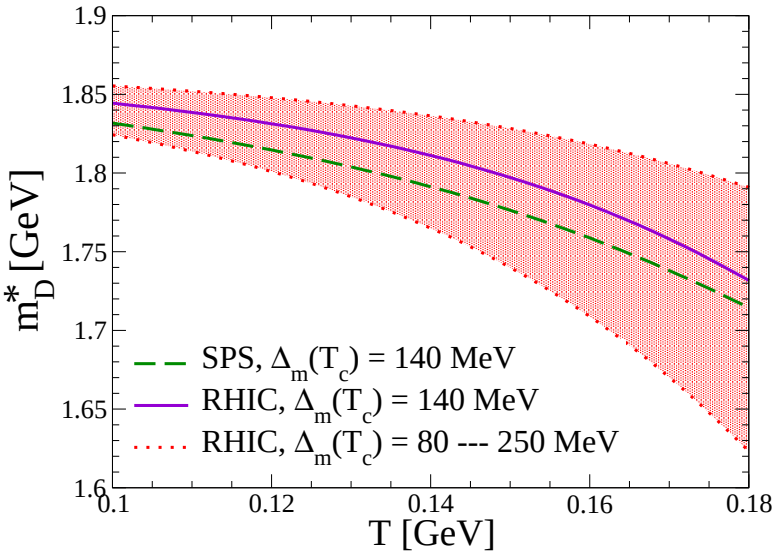

Figure 3.5: In-medium D-meson masses as a function of temperature including density profiles expected at SPS (dashed line) and RHIC (full line). The dotted curves defining the band correspond to weaker ($\Delta_m(T_c) = 80$ MeV) and stronger ($\Delta_m(T_c) = 250$ MeV) medium effects.

The reduction of the D-meson masses has important consequences on different aspects of charm physics in heavy-ion physics to which we shall return throughout this work: it impacts the equilibrium abundances of open-charm and charmonium (see Sec. 3.3), it increases charmonium inelastic reactions (Sec. 4.4.1) and also renders direct decays of higher charmonia, such as $\psi' \to D\bar{D}$ possible as discussed in Sec. 4.4.2.

3.3 Charmonium equilibrium abundances and in-medium effects

Recently, besides hard J/ψ production as described in Chapter 2, another source of charmonium in heavy-ion collisions has been attributed to statistical production either at the hadronization transition [13, 14, 15] or throughout the course of the QGP evolution [16]. The underlying mechanism of this soft charmonium production is the coalescence of c and $\bar{c}$ quarks (or the interaction between to D mesons in the hadronic phase). In this section, we describe this soft production mechanism (also referred to as regeneration since it occurs after the initial hard production and recreates charmonia from open-charm states). We first review briefly the statistical models of particle production as they have been successfully employed before to describe particle abundances in the light

and strange sectors [17]. We then turn to their application to calculate charmonium production by statistical coalescence and we finally consider the consequences of the reduction of the open-charm threshold in the medium on the charmonium abundances given by such models.

3.3.1 Statistical models of light particle production

Statistical models have been put forward to explain the observed abundances of light and strange particles in heavy-ion reactions over a wide range of cms energies from SIS to RHIC, see [18] for a recent review. With the exception of strange particles, they even give a satisfactory description of particle ratios in p-p and e^+e^- [19, 20] collisions, although their validity for such small systems is rather questionable or at least not really understood. In such models, upon the assumption of thermal equilibrium, hadron production occurs in a narrow interval of temperature near the chemical freezeout temperature T_{ch} (when the relative abundances of the different flavors are frozen) according to the available phase space. Statistical models that use a grand canonical ensemble to formulate the partition function and hadron thermal multiplicities of species i are then given by

$$N_i = V_H \frac{di}{2\pi^2} \int_0^\infty p^2 dp \left[\exp\left(\frac{\sqrt{p^2 + m_i^2} - \mu_i}{T_{ch}} \right) \pm 1 \right]^{-1} , \tag{57}$$

where d_i is the spin-isospin degeneracy of a particle i with mass m_i. V_H and T_{ch} are the volume and the temperature of the system. The pertinent particle chemical potential μ_i,

$$\mu_i = b_i \mu_B + s_i \mu_s + \dots \tag{58}$$

encodes all conserved charges such as net baryon and strangeness numbers. If one considers ratio of particle abundances, the volume dependence drops out and the model has only two parameters, assumed to be common for all particle species, namely the temperature T_{ch} of chemical freezeout and the baryon chemical potential μ_B which regulates the net baryonic density of the hadron gas system. In addition, such models include the contributions from resonance decays so that the total measured multiplicity for a given specie i is

$$N_i^{tot} = N_i + \sum_{res} \mathcal{BR}(res \to i) N_{res} \ . \tag{59}$$

The freezeout temperature and baryon chemical potential are then fitted using particle abundances ratios and can be used to predict any other ratio of particle abundances.

The results of such a model are shown in Fig. 3.6 for particle ratios observed at RHIC, $\sqrt{s_{NN}} = 130$ GeV. The agreement with the observed ratio is impressive. In the strange

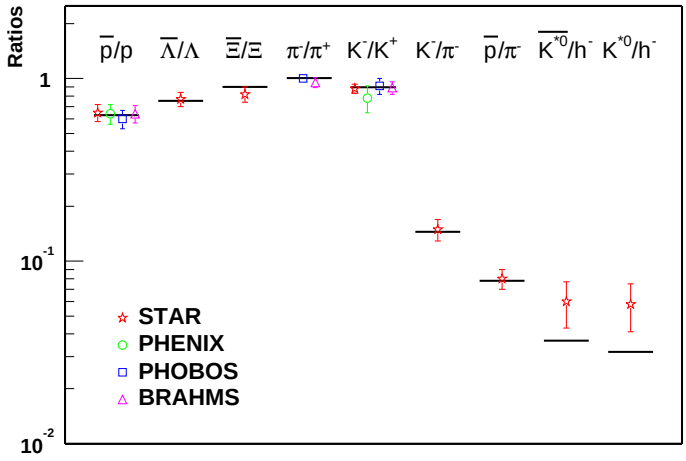

Figure 3.6: Two parameter fit to ratios of particle abundances at RHIC, $\sqrt{s_{NN}} = 130$ GeV, from the statistical model of [21]. The two parameters of the model extracted from the fit are $T_{ch} = 174 \pm 4$ MeV and $\mu_B = 46$ MeV.

sector, strangeness appears equilibrated, a feature not found in p-p and e^+e^- collisions and not easily understood within hadronic event generators, which has been put forward as a signature for QGP formation. Equally good fits are obtained at SIS energies [22, 23], AGS [24, 18], SPS [25, 17, 26]. Fig. 3.7, taken from Ref. [18], summarizes the extracted chemical freezeout temperatures and baryon chemical potentials for different collision systems at various cms energies. These chemical freezeout parameters define a line in the phase diagram (the T-μ_B plane) which is well described by a constant energy per particle $\langle E\rangle/\langle N\rangle \sim 1$ GeV of the system [27] or a constant baryon density $n_B \sim 0.12$ fm^{-3} [28]. At SPS and RHIC, the chemical freezeout temperature is very close to the expected phase transition temperature, suggesting a possible chemical equilibration in the partonic stage. Even though statistical models have been proven to be very successful at describing ratios of particles abundances, they have raised serious issues, including:

- Their success in p-p and e^+e^- collisions remains unexplained. If in heavy-ion collisions, one expects to create systems large enough to justify the macroscopic concept of thermal equilibrium, the picture of p-p or e^+e^- collisions is counterintuitive in that respect.

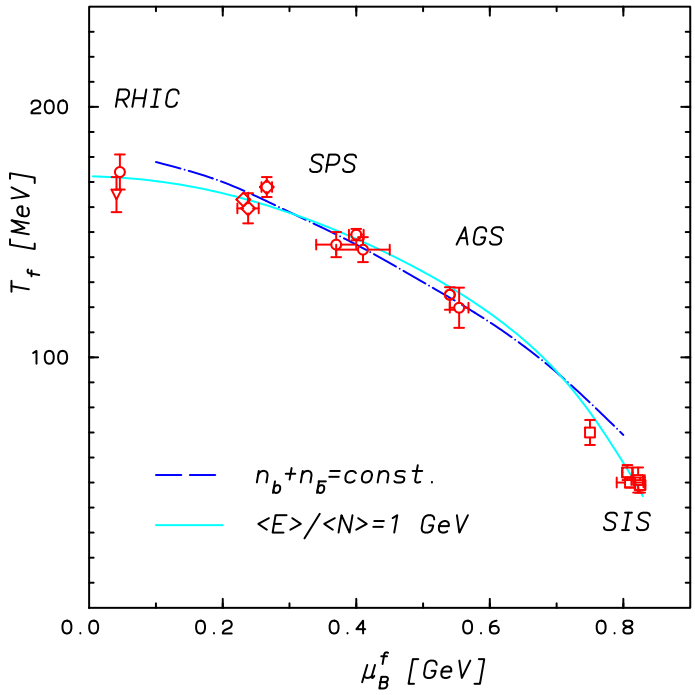

Figure 3.7: Compilation of the different chemical freezeout parameters extracted from thermal models fit from SIS to RHIC energies, taken from [18]

.

- The apparent chemical equilibration of strangeness at SIS and AGS energies is surprising – one does not expect to form a plasma, and timescales for the equilibration of strangeness in the hadronic phase are on the order of $\sim$ 80 fm/c [29], much longer than the duration of the hadronic phase – and remains unexplained.
- Most thermal models use vacuum properties of particles which may however be modified (masses and/or widths) at finite temperatures and densities.
- If the system is in thermal equilibrium, the main advantage is that the details of the dynamics can be ignored. However, it would be satisfying to understand microscopically how chemical and thermal equilibrium are reached.

3.3.2 Charmonium production in statistical models

One feature of the statistical models is that the multiplicities of observed particles scale with the volume at hadronization which in turn is proportional to the number of participants in the collision. It was first observed in Ref. [30] that the J/ψ yield per charged hadron at SPS is remarkably constant as a function of the centrality of the collision as shown in Fig. 3.8. Based on this observation, the authors of Ref. [30] argued

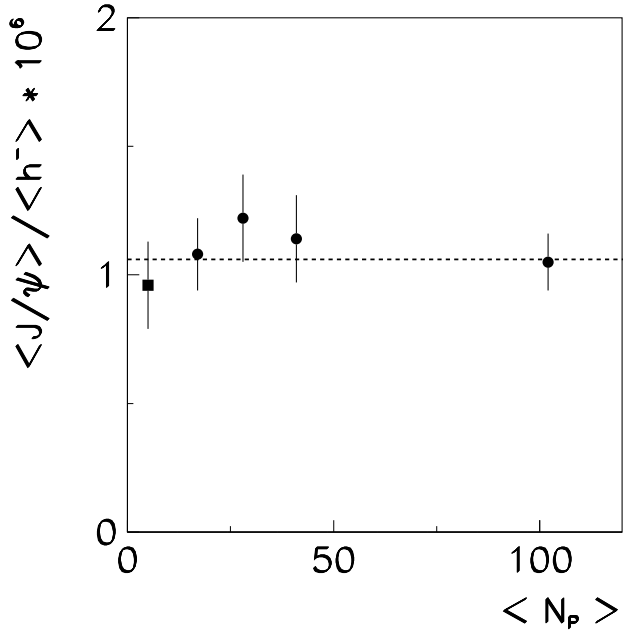

Figure 3.8: J/ψ yield per negatively charged hadron as a function of the number of participants in various collision systems (O-Cu, O-U, S-U and Pb-Pb) at the SPS, from Ref. [30].

that all J/ψ's were created statistically at the hadronization transition. The deduced temperature of $T \simeq 175$ MeV is well in line with the chemical freezeout temperature of light hadron production described in the previous section.

Another consequence of statistical production is that the particle ratios do not depend on the centrality of the collision and are given (in the Boltzmann approximation) by

$$R_{1,2} = \frac{d_1}{d_2} e^{-\frac{m_1 - m_2}{T}} \left(\frac{m_1}{m_2}\right)^{3/2} . \tag{60}$$

The observation made in [31] that for sufficiently central collisions of Pb-Pb nuclei at SPS, the ψ'/ψ ratio approaches its thermal value of $\sim 4\%$, see Fig. 3.9, was also put forward by Braun-Munzinger and Stachel [13] as an argument for statistical charmonium production. Their picture of charmonium production developed in [14, 13, 15] is the following: One calculates the abundances of all known charmed particles as given by statistical models using the parameters (T, μ_B) determined by fit to light hadrons ratios. Hence, charmed particle multiplicities are calculated with Eqs. (57) and (59) upon inclusion of a charm quantum number and its corresponding chemical potential

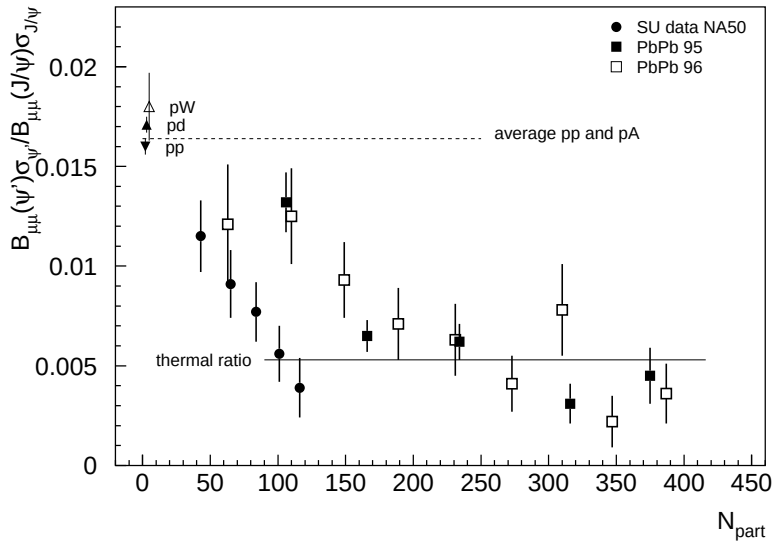

Figure 3.9: ψ'/ψ ratio at SPS, for *S-U* and *Pb-Pb* collisions, taken from [13]. For both systems, the ratio in central collisions approaches its thermal value indicated by the straight line.

μ_c such that

$$\mu_i = b_i\mu_B + s_i\mu_s + c_i\mu_c \ , \tag{61}$$

where μ_c is determined by a zero net charm charge. However, the resulting value of μ_c constrains charm conservation only in the average sense (globally). For the small multiplicities of charmed particles, the grand-canonical ensemble treatment is not valid and one has to conserve charm exactly (*i.e.* locally), within the canonical ensemble [32, 33]. Therefore, the abundances of open-charmed hadrons are suppressed by a so-called "canonical suppression" factor (multiplicities of charmonium states are the same in the canonical and grand-canonical ensemble since they have zero charm charge). Writing

$$N_{op} = \sum N_i \ , \qquad i = D, D^\star, \bar{D}, \bar{D}^\star, \Lambda, \bar{\Lambda}, \cdots \tag{62}$$

$$N_{hid} = \sum N_j \ , \qquad j = \eta_c, \Psi, \cdots \ , \tag{63}$$

the canonical ensemble multiplicities of open-charm states are related to the grand-canonical ones according to

$$N_{op}^{c.e} = N_{op}^{g.c.e}\frac{I_1\left(N_{op}^{g.c.e}\right)}{I_0\left(N_{op}^{g.c.e}\right)} \ , \tag{64}$$

where I_1, I_0 are modified Bessel functions. It is instructive to consider the two extreme

limits of large and small arguments of the Bessel functions. We have

$$\frac{I_1(x)}{I_0(x)} \to \begin{cases} 1\ , & x >> 1 \\ \frac{x}{2}\ , & x << 1 \end{cases} \tag{65}$$

Therefore, for large multiplicities ($N_{op}^{g.c.e} >> 1$), we recover the grand-canonical limit, *i.e.* $N_{op}^{c.e} \sim N_{op}^{g.c.e}$. On the other hand, for small multiplicities ($N_{op}^{g.c.e} << 1$), the canonical abundances are suppressed from the grand-canonical ones by an extra $N_{op}^{g.c.e}/2$ factor, which corresponds to the constrained probability of finding the partner of a produced charmed particle. This is particularly relevant at SPS energies where for central collisions of *Pb-Pb* at $\sqrt{s} = 17.3$ AGeV, one typically expects 0.2 $c\bar{c}$ pair per collision.

Contrary to [30] where no underlying mechanism for the production of $c\bar{c}$ was specified, we use as developed in [15, 14, 13] the dynamically well justified hypothesis that at SPS energies, (and also at RHIC) all $c\bar{c}$ pairs are exclusively created in primordial (hard) parton-parton collisions (secondary creation in a partonic medium has been shown to be negligible even at full RHIC energy [34]). This is motivated by the expectation that heavy flavor production does not equilibrate [35] but is rather determined by the number $N_{c\bar{c}}$ of pairs created in primordial N-N collisions, which is from then on frozen. Thermal equilibration of charm quarks, however, seems possible [36]. Thus the corresponding relaxation times might well satisfy a hierarchy

$$\tau_{c,\bar{c}}^{chem} >> \tau_{FB} >> \tau_{c,\bar{c}}^{th}\ . \tag{66}$$

This necessitates the introduction of a fugacity $\gamma_c = \gamma_{\bar{c}}$ for charm and anti-charm quarks constrained by

$$N_{c\bar{c}} = \frac{1}{2}\gamma_c N_{op}\frac{I_1(\gamma_c N_{op})}{I_0(\gamma_c N_{op})} + \gamma_c^2 N_{hid}\ . \tag{67}$$

Upon solving Eq. (67) for γ_c, we obtain the thermal equilibrium (but chemical off-equilibrium) J/ψ production at the hadronization transition according to

$$N_{J/\psi}^{th} = \gamma_c^2\ V_H \left[n_{J/\psi} + \sum_X \mathcal{BR}(X \to J/\psi)\ n_X \right]\ , \tag{68}$$

where the summation is carried over the charmonium states X with finite decay branching into J/ψ's (feeddown). An important feature of this model is that charmonium production is linked to open-charm production, through the determination of γ_c. In the canonical limit, parametrically, one has $N_{c\bar{c}} \propto \gamma_c^2 V^2$, *i.e.* at fixed $N_{c\bar{c}}$,

$$N_{J/\psi}^{th} \propto \frac{N_{c\bar{c}}}{V}. \tag{69}$$

In the grand-canonical limit, $N_{c\bar{c}} \propto \gamma_c V$ leads to

$$N_{J/\psi}^{th} \propto \frac{N_{c\bar{c}}^2}{V}. \tag{70}$$

Thus we expect that when the open-charm production is large enough to reach the grand-canonical regime, J/ψ production is enhanced growing quadratically with $N_{c\bar{c}}$. We consider in more details the role of this statistical production mechanism for the situation of heavy-ion collision in Sec. 6.1.2.

3.3.3 In-medium effects on charmonium equilibrium numbers

Here we examine how the in-medium effects inferred from lattice calculations and developed in Sec. 3.2 influence the J/ψ equilibrium numbers. Based on recent lattice calculations, low-lying charmonia seem to survive above T_c. This leads to consider the production of J/ψ's in the plasma through the coalescence mechanism and not only at the hadronization transition. The second insight from lattice QCD calculations involves the in-medium modified charm/D-meson masses. Modified masses imply a change in the thermal multiplicities of open-charm which in turn entails a change in charmonium multiplicities through γ_c (even though the mass of the charmonium is remarkably constant across the transition). We therefore compare the J/ψ equilibrium abundances in the plasma and in the hadronic phases for *(i)* the free case using vacuum masses for the open-charm states and *(ii)* in-medium modified charmed particles.

J/ψ equilibrium numbers in the plasma

Since J/ψ's seem to exist in the plasma, as inferred from studies of charmonium spectral functions on the lattice (Fig. 3.3), we consider the statistical production of J/ψ's obtained by coalescence of a c and a $\bar{c}$ quark in the plasma. f^ψ being the thermal J/ψ distribution, the J/ψ equilibrium density is calculated as

$$n_{J/\psi}^{eq} = 3\gamma_c^2 \int \frac{d^3q}{(2\pi)^3} f^\psi(m_\psi, T) \tag{71}$$

where the J/ψ mass is unchanged from its vacuum value and γ_c is determined upon solving Eq. (67) with the number N_{op} of open-charm states given by

$$N_{op} = 2\ V_{FB}(T)\ \gamma_c(T)\ n_c(T)\ , \tag{72}$$

with

$$n_c(T,\gamma_c) = n_{\bar{c}}(T,\gamma_c) \equiv \gamma_c n_c(T) = 6\ \gamma_c \int \frac{d^3q}{(2\pi)^3} f^c(m_c,T)\ . \tag{73}$$

We studied the dependence of Eq. (71) on the charm quark mass. Fig. 3.10 shows the J/ψ equilibrium abundances for situations comparable to SPS and RHIC central collisions. One observes a large sensitivity to the in-medium charm quark mass, with

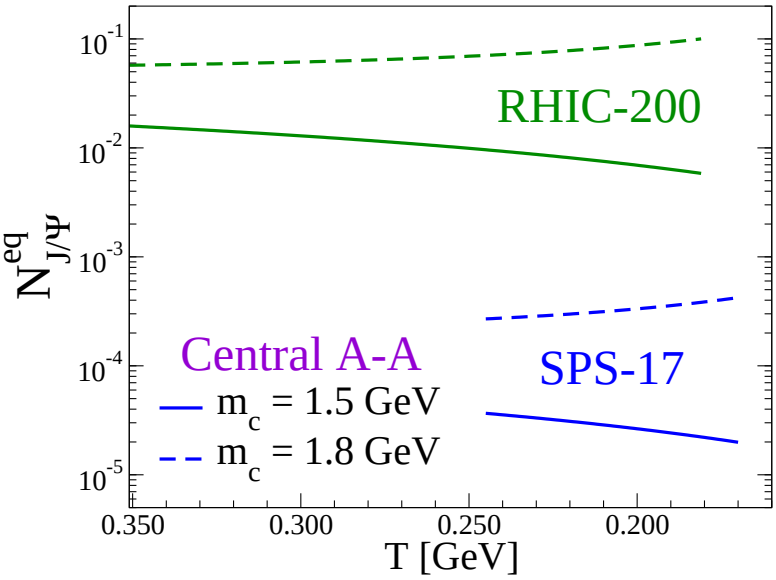

Figure 3.10: Equilibrium J/ψ abundances (assuming $m_\psi(T) \equiv m_\psi^{vac}$) in an isotropic, adiabatically expanding Quark-Gluon Plasma at fixed (anti-) charm quark number $N_{c\bar{c}}$, resembling conditions at RHIC and SPS for two values of the charm quark mass.

larger values of m_c^* requiring a larger fugacity γ_c (at fixed $N_{c\bar{c}}$), and thus entailing a larger equilibrium abundance of charmonium states.

The temperature dependence of J/ψ equilibrium abundances exhibits different behaviors according to the in-medium charm quark mass, see Fig. 3.10. This can be understood if one considers the grand-canonical limit and use approximate thermal densities to rewrite Eqs. (67) and (68) as

$$N_{c\bar{c}} \simeq 6\gamma_c\, V \left(\frac{m_c^* T}{2\pi}\right)^{3/2} e^{-m_c^*/T}\ , \tag{74}$$

$$N_{J/\psi}^{th} \simeq 3\gamma_c^2\, V \left(\frac{m_\psi T}{2\pi}\right)^{3/2} e^{-m_\psi/T}\ . \tag{75}$$

Solving Eq. (74) for γ_c and substituting into Eq. (75) we get

$$N_{J/\psi}^{th} \propto \left(\frac{m_\psi}{m_c^{*2} T}\right)^{3/2} e^{\frac{2m_c^* - m_\psi}{T}}\ . \tag{76}$$

From Eq. (76), we readily see that when $2m_c^* > m_\psi$ (see dashed curves in Fig. 3.10) the J/ψ equilibrium abundances increase as T decreases. Conversely, when $2m_c^* < m_\psi$ the J/ψ equilibrium abundances decrease as T decreases since it becomes energetically favorable to distribute the charm in open-charm states rather than in J/ψ's.

J/ψ equilibrium numbers in the hadronic phase

The effect of the in-medium reduction of the charmed hadron masses on the J/ψ equilibrium numbers in the hadronic phase is completely analogous to varying m_c in the QGP. A reduction of the D-meson masses by ~ 140 MeV at $T_c \sim 170$ MeV lowers the J/ψ equilibrium level by a factor $\simeq 3$. This is illustrated in Fig. 3.11 where the full lines correspond to J/ψ equilibrium numbers in the hadronic phase using vacuum values for the charmed meson masses, to be compared with the dashed lines where the in-medium masses of Fig. 3.5 have been used to calculate the open-charm multiplicities.

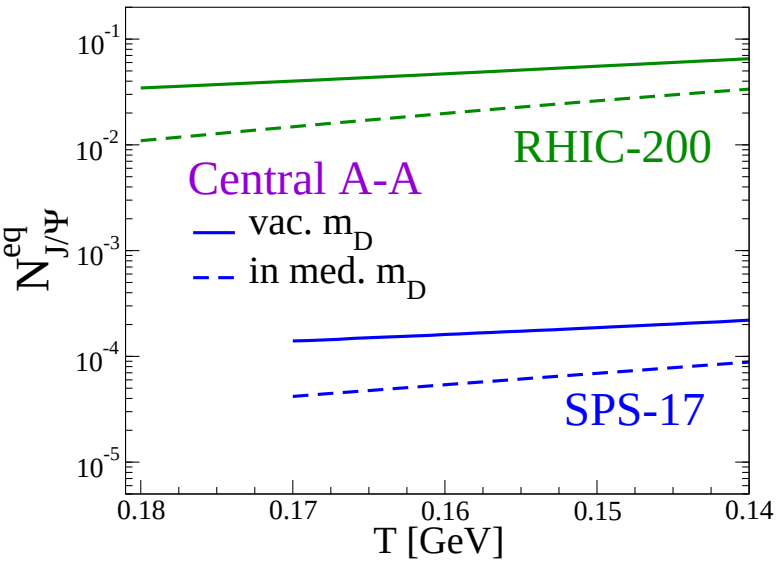

Figure 3.11: J/ψ equilibrium numbers in the hadronic phase (under equivalent conditions as in Fig. 3.10) using free and in-medium hadron masses.

The other noticeable feature of the J/ψ equilibrium abundances in the hadronic phase is that they increase with decreasing temperature, which is a consequence of the increasing γ_c at fixed $N_{c\bar{c}}$ together with $m_\psi < 2m_D$. Therefore, for heavy-ion reactions, this implies that if J/ψ's equilibrate close to T_c, subsequent hadronic reactions would favor additional formation over dissociation. Such a behavior, quite contrary to the commonly assumed hadronic dissociation, has indeed been observed in kinetic and transport model calculations at RHIC [34, 37, 38].

We conclude here our considerations about the equilibrium properties of charm (in matter). We found that statistical J/ψ production was conceivable and we will include it in our two-component model of charmonium production in heavy-ion collisions developed in Chapter 6. In-medium effects on the charmonium yield in heavy-ion collisions will be addressed in Chapter 7.

Bibliography

[1] F. Karsch, Lect. Notes Phys. **583**, 209 (2002), hep-lat/0106019.

[2] F. Karsch, E. Laermann, and A. Peikert, Nucl. Phys. **B605**, 579 (2001), hep-lat/0012023.

[3] D. Blaschke, G. Burau, T. Barnes, Y. Kalinovsky, and E. Swanson, (2002), hep-ph/0210265.

[4] S. Digal, P. Petreczky, and H. Satz, Phys. Lett. **B514**, 57 (2001), hep-ph/0105234.

[5] S. Digal, P. Petreczky, and H. Satz, Phys. Rev. **D64**, 094015 (2001), hep-ph/0106017.

[6] S. Datta, F. Karsch, P. Petreczky, and I. Wetzorke, (2002), hep-lat/0208012.

[7] T. Umeda, K. Nomura, and H. Matsufuru, (2002), hep-lat/0211003.

[8] E. V. Shuryak, (2003), Private communication.

[9] Y. Nambu and G. Jona-Lasinio, Phys. Rev. **122**, 345 (1961).

[10] Y. Nambu and G. Jona-Lasinio, Phys. Rev. **124**, 246 (1961).

[11] S. P. Klevansky, Rev. Mod. Phys. **64**, 649 (1992).

[12] V. Bernard, U. G. Meissner, and I. Zahed, Phys. Rev. **D36**, 819 (1987).

[13] P. Braun-Munzinger and J. Stachel, Phys. Lett. **B490**, 196 (2000), nucl-th/0007059.

[14] P. Braun-Munzinger and J. Stachel, Nucl. Phys. **A690**, 119 (2001), nucl-th/0012064.

[15] M. I. Gorenstein, A. P. Kostyuk, H. Stöcker, and W. Greiner, Phys. Lett. **B509**, 277 (2001), hep-ph/0010148.

[16] R. L. Thews, M. Schroedter, and J. Rafelski, Phys. Rev. **C63**, 054905 (2001), hep-ph/0007323.

[17] P. Braun-Munzinger, I. Heppe, and J. Stachel, Phys. Lett. **B465**, 15 (1999), nucl-th/9903010.

[18] P. Braun-Munzinger, K. Redlich, and J. Stachel, (2003), nucl-th/0304013.

[19] F. Becattini and U. W. Heinz, Z. Phys. **C76**, 269 (1997), hep-ph/9702274.

[20] F. Becattini, (1998), Prepared for Workshop on Nuclear Matter in Different Phases and Transitions, Les Houches, France, 31 Mar - 10 Apr 1998.

[21] P. Braun-Munzinger, D. Magestro, K. Redlich, and J. Stachel, Phys. Lett. **B518**, 41 (2001), hep-ph/0105229.

[22] J. Cleymans, H. Oeschler, and K. Redlich, Phys. Rev. **C59**, 1663 (1999), nucl-th/9809027.

[23] J. Cleymans, H. Oeschler, and K. Redlich, Phys. Lett. **B485**, 27 (2000), nucl-th/0004025.

[24] J. Cleymans, H. Oeschler, and K. Redlich, J. Phys. **G25**, 281 (1999), nucl-th/9809031.

[25] P. Braun-Munzinger, J. Stachel, J. P. Wessels, and N. Xu, Phys. Lett. **B365**, 1 (1996), nucl-th/9508020.

[26] F. Becattini, J. Cleymans, A. Keranen, E. Suhonen, and K. Redlich, Phys. Rev. **C64**, 024901 (2001), hep-ph/0002267.

[27] J. Cleymans and K. Redlich, Phys. Rev. **C60**, 054908 (1999), nucl-th/9903063.

[28] P. Braun-Munzinger and J. Stachel, J. Phys. **G28**, 1971 (2002), nucl-th/0112051.

[29] P. Koch, B. Müller, and J. Rafelski, Phys. Rept. **142**, 167 (1986).

[30] M. Gazdzicki and M. I. Gorenstein, Phys. Rev. Lett. **83**, 4009 (1999), hep-ph/9905515.

[31] H. Sorge, E. V. Shuryak, and I. Zahed, Phys. Rev. Lett. **79**, 2775 (1997), hep-ph/9705329.

[32] E. V. Shuryak, Sov. J. Nucl. Phys. **20**, 295 (1975).

[33] K. Redlich and L. Turko, Zeit. Phys. **C5**, 201 (1980).

[34] P. Braun-Munzinger and K. Redlich, Eur. Phys. J. **C16**, 519 (2000), hep-ph/0001008.

[35] P. Levai, B. Müller, and X.-N. Wang, Phys. Rev. **C51**, 3326 (1995), hep-ph/9412352.

[36] B. Svetitsky, Phys. Rev. **D37**, 2484 (1988).

[37] B. Zhang, C. M. Ko, B.-A. Li, Z.-W. Lin, and S. Pal, Phys. Rev. **C65**, 054909 (2002), nucl-th/0201038.

[38] E. L. Bratkovskaya, W. Cassing, and H. Stöcker, Phys. Rev. **C67**, 054905 (2003), nucl-th/0301083.

Chapter 4

Charmonium Inelastic Reaction Rates

The deviation of the J/ψ yield from nuclear absorption systematics in Pb(158 AGeV)-Pb has triggered extensive theoretical analysis. The responsible underlying mechanisms are still a matter of debate, ranging from destruction in a QGP and/or hadron gas to thermal production at T_c. As stressed previously, this work attempts a comprehensive treatment of all three of these aspects within a minimal set of assumptions, which, in particular, is based on a thermal description of the collision dynamics including Quark-Gluon Plasma formation if the initial conditions are energetic enough. In this chapter, we compute J/ψ dissociation rates for both the plasma and hadronic phases of heavy-ion reactions.

4.1 Charmonium dissociation in the Quark-Gluon Plasma

J/ψ dissociation in a thermalized QGP has been studied in both static and dynamical frameworks. Within the former, one typically evaluates the screening of the heavy quark potential by color charges, whereas the latter involves inelastic parton collisions using, *e.g.* , the QCD analogue of photo-dissociation,

$$g + J/\Psi \rightarrow c + \bar{c} \; . \tag{77}$$

Here we adopt a dynamical approach, accounting however for reduced charmonium binding energies in the plasma.

4.1.1 Reduced charmonium binding energies in the QGP

In vacuum, the open-charm threshold corresponds to a $D\bar{D}$ pair and the binding energy ε_0^Ψ of a charmonium state Ψ is given by

$$\varepsilon_0^\Psi = 2m_D - m_\Psi \ . \tag{78}$$

This gives for the charmonia we consider in this work: $\varepsilon_0^\psi = 640$ MeV, $\varepsilon_0^{\psi'} = 60$ MeV and $\varepsilon_0^\chi \simeq 240$ MeV. However, if a Quark-Gluon Plasma is formed, one expects the open-charm threshold to be reduced due to the screening of the heavy-quark potential and/or a change in asymptotic states (free c and $\bar{c}$ quarks, with $m_c \sim 1.5 - 1.6$ GeV). To evaluate the resulting reduction of the charmonium binding energies in a QGP at temperature T, we follow the work of Karsch, Mehr and Satz [1].

Within the framework of a non-relativistic potential model for a $c\bar{c}$ system, the Hamiltonian is given by

$$H(r,T) = 2m_c - \frac{1}{m_c}\nabla^2 + V(r,T) \ , \tag{79}$$

where m_c is the charm quark mass. At $T = 0$, $V(r, T = 0)$ corresponds to the Cornell potential [2, 3]

$$V(r, T = 0) = \sigma r - \frac{\alpha}{r} \tag{80}$$

with $\sigma = 0.192$ GeV^2 and $\alpha = 0.471$, obtained in [4] to fit the charmonium spectrum. σr corresponds to the linear confining part of the potential at large distances while $-\frac{\alpha}{r}$ represents the Coulombic attraction at short distances. In [1], to account for the color screening between the c and $\bar{c}$ charges, the authors proposed to parameterize the interaction potential $V(r,T)$ as

$$V(r,T) = \frac{\sigma}{\mu_D(T)}\left(1 - e^{-\mu_D(T)r}\right) - \frac{\alpha}{r}e^{-\mu_D(T)r} \ , \tag{81}$$

where $\mu_D(T)$ is the temperature dependent Debye screening mass. For $\mu_D = 0$, one recovers Eq. (80) while for $\mu_D \neq 0$, the potential behaves as $1/r$ at short distances and is exponentially decreasing at large distances with the screening mass $\mu_D(T)$. Note that this potential depends on the temperature exclusively through $\mu_D(T)$. Once the temperature dependence of the potential has been specified, one obtains the dissociation energy for a charmonium state by solving the Schrödinger equation

$$H(r,\mu_D)\phi_{n,l}(r,\mu_D) = E_{n,l}(\mu_D)\phi_{n,l}(r,\mu_D) \ , \tag{82}$$

where n is the principal quantum number and l the orbital quantum number of a charmonium state Ψ ($J/\psi : n = 1,\ l = 0;\ \chi : n = 2,\ l = 1;\ \psi' : n = 2,\ l = 0$). The corresponding dissociation energy is then obtained using

$$E_{diss}^{n,l}(\mu_D) = 2m_c + \frac{\sigma}{\mu_D} - E_{n,l}(\mu_D) \tag{83}$$

which is positive for a bound state and becomes negative for the continuum. The last step consists of specifying the temperature dependence of the Debye screening mass $\mu_D(T)$. To such end, we use the estimate obtained in leading order perturbation theory [5]

$$\mu_D \sim gT\ . \tag{84}$$

Since, strictly speaking, perturbation theory is not really applicable under the moderate plasma temperatures expected even at RHIC energies, we regard the strong coupling constant α_S as an effective parameter to be adjusted to the J/ψ data at SPS. With a typical $g \simeq 1.7$ (inferred from a fit to SPS data on J/ψ centrality dependence), the resulting J/ψ binding energy as a function of temperature is shown in Fig. 4.1. Around

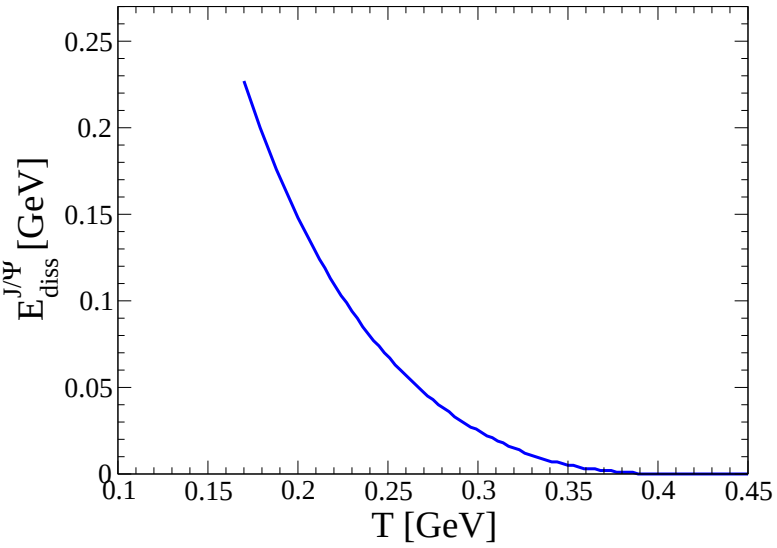

Figure 4.1: Temperature dependence of the J/ψ binding energy in the plasma obtained upon solving the Schrödinger equation with the screened heavy-quark potential according to (81).

$T_c = 170$ MeV, the J/ψ binding energy is $E_{diss} = 250$ MeV, strongly reduced from its vacuum value $\varepsilon_0^{\psi} = 640$ MeV. It keeps decreasing as T increases, reaching $E_{diss} = 100$ MeV at $T = 230$ MeV and vanishing around $T \simeq 360$ MeV. Higher charmonia states such as χ's and ψ' have essentially zero binding energy in the plasma phase.

4.1.2 Parton induced J/ψ breakup

To make contact with heavy-ion collisions, we follow a dynamical approach of J/ψ dissociation in the Quark-Gluon Plasma rather than the static picture of J/ψ dissolution by Debye screening originally suggested by Matsui and Satz in 1986 [6]. We first review the QCD analogue of the photo-dissociation process before turning to the mechanism of inelastic parton scattering which is more efficient to destroy a loosely bound charmonium state.

J/ψ gluo-dissociation

To our knowledge, dynamical dissociation of a J/ψ in the Quark-Gluon Plasma has been mostly discussed using the analogue in QCD of the photo-dissociation process $g + J/\psi \rightarrow c + \bar{c}$ illustrated in Fig. 4.2. Based on the assumption that the binding

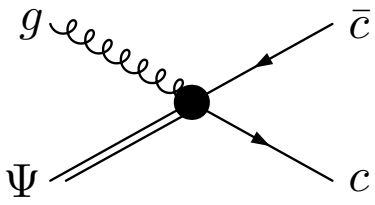

Figure 4.2: J/ψ breakup by the QCD analogue of the photo-dissociation process.

energy ε_0^ψ of the J/ψ is large compared to Λ_{QCD}, Bhanot and Peskin [7, 8] derived the following expression for the gluon-quarkonium cross-section

$$\sigma_{g\Psi}(k) = \frac{2\pi}{3}\left(\frac{32}{3}\right)^2\left(\frac{m_Q}{\varepsilon_0}\right)^{1/2}\frac{1}{m_Q^2}\frac{(k/\varepsilon_0 - 1)^{3/2}}{(k/\varepsilon_0)^5}\ , \tag{85}$$

where k is the momentum of the incoming gluon and m_Q the mass of the heavy-quark. The corresponding thermal averaged cross-section [9]

$$\sigma_{g\Psi}(T) = 65 \text{ mb } \times \frac{\int_{\varepsilon_0}^{\infty} dk k^2 e^{-k/T}(k/\varepsilon_0 - 1)^{3/2}(k/\varepsilon_0)^{-5}}{\int_{\varepsilon_0}^{\infty} dk k^2 e^{-k/T}} \tag{86}$$

is shown in Fig. 4.3 (dashed line). For temperatures relevant at SPS energies ($T \sim 200$ MeV), the cross-section remains sub-millibarn and is not very effective at destroying the J/ψ. Let us stress that the cross-section obtained in Fig. 4.3 is, strictly speaking, only valid when the bound state binding energy ε_0 is large compared to Λ_{QCD}. This limits the

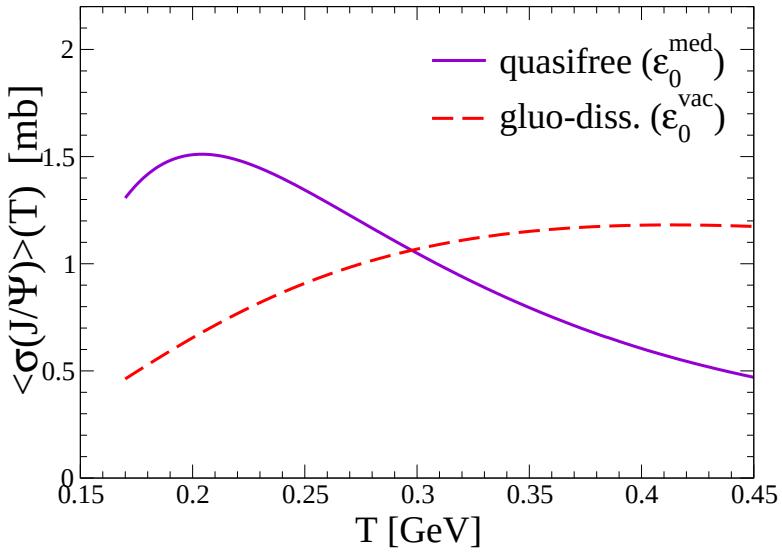

Figure 4.3: Thermal averaged $\sigma_{gJ/\psi}(T)$ cross-sections in a QGP. The dashed line indicates the QCD analogue of the photo-dissociation process and the full line corresponds to our quasifree calculation, see text for details.

applicability of this approach when considering a J/ψ whose binding energy is reduced in the medium and makes it questionable (at best) to treat the ψ' and the χ which have even smaller binding energies. In addition, for such small binding energies, the photo-dissociation process becomes inefficient due to unfavorable breakup kinematics.

Inelastic parton scattering in the quasifree approximation

Having in mind the picture of a loosely bound $c\bar{c}$ pair being destroyed as one of the charm quark interacts with a surrounding parton in the thermal medium, we found [10] that inelastic parton scattering

$$g\ (q,\bar{q}) + J/\psi \to g\ (q,\bar{q}) + c + \bar{c}\ , \tag{87}$$

illustrated in Fig. 4.4 is a more important mechanism (see full line in Fig. 4.3).

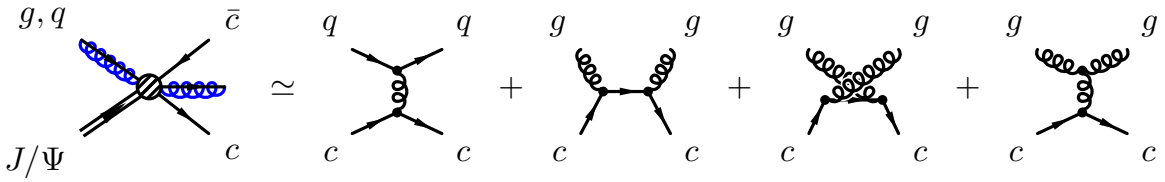

Figure 4.4: Graphs of the quasifree process: Since the charmonium state is loosely bound in the plasma, the interaction of any of the charm quarks with a surrounding parton destroys the $c\bar{c}$ correlation and eventually the J/ψ.

The respective cross-sections are evaluated in quasifree approximation using leading-order pQCD [11] for

$$g + c \to g + c \ , \qquad q + c \to q + c \ . \tag{88}$$

Again, due to the questionability of the use of pQCD, the strong coupling constant α_S which is the main parameter of the calculation is considered as an effective parameter adjusted to the magnitude of J/ψ suppression observed at SPS. The resulting typical values of α_S (~ 0.3) seem quite reasonable.

Another advantage of this formalism to calculate J/ψ interactions in the plasma is that it applies straightforwardly to essentially unbound ψ' and χ states as well, and allows to treat these charmonium states on an equal footing with the J/ψ.

4.1.3 Charmonium dissociation rates

To calculate the magnitude of the J/ψ suppression in a thermal QGP, one needs to convert the previous dissociation cross-sections into dissociation rates. Assuming that the surrounding partons in the medium are in thermal equilibrium at a temperature T, the corresponding thermal dissociation rates are obtained by convolution of the inelastic cross-sections with the thermal distribution functions of the surrounding partons

$$\Gamma^{\Psi}_{diss} = \sum_{i=q,g} \int_{k_{min}}^{\infty} \frac{d^3k}{(2\pi)^3} f^i(k,T) v_{rel} \sigma^{\Psi}_{diss}(s) \ , \tag{89}$$

where k_{min} denotes the minimal on-shell momentum of a quark or gluon from the heat bath necessary to dissolve an in-medium charmonium bound state Ψ into a free $c\bar{c}$ pair. Here, $s = (p_{q,g} + p_\psi)^2$ and we work in the static approximation ($\vec{p}_\psi = 0$). The thermal distribution functions read

$$f^i(k,T) = \frac{1}{\exp\left(\frac{\sqrt{k^2+m^2}}{T}\right) - 1} \ , \qquad i = g \tag{90}$$

$$f^i(k,T) = \frac{1}{\exp\left(\frac{\sqrt{k^2+m^2}}{T}\right) + 1} \ , \qquad i = u,d,s \tag{91}$$

where we have included thermal quasiparticle masses for light quarks and gluons [12]

$$m^2_{u,d} = \frac{g^2T^2}{6} \ , \tag{92}$$

$$m^2_s = m^2_0 + \frac{g^2T^2}{6} \ , \tag{93}$$

$$m^2_g = \frac{g^2T^2}{2} \ , \tag{94}$$

where g is the same strong coupling constant used in the quasifree calculation. The resulting J/ψ dissociation rates as a function of temperature are given in Fig. 4.5 for the different dissociation cross-sections considered in this work. The full line corresponds to

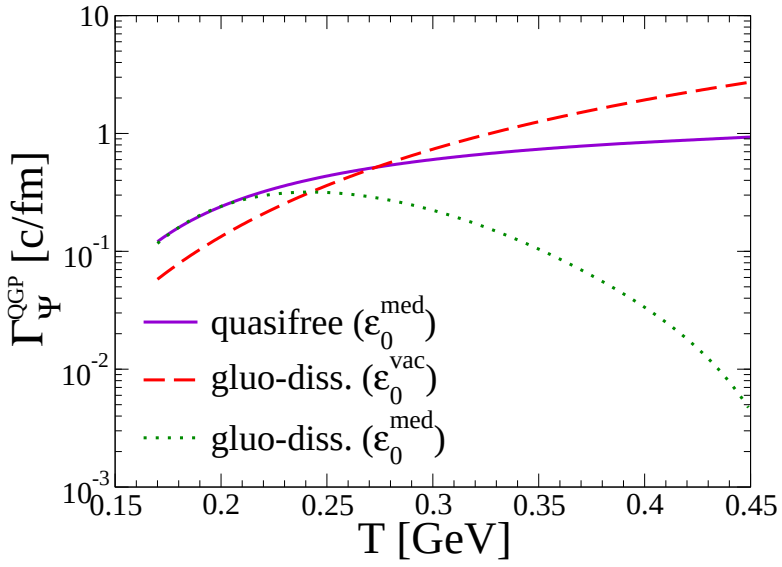

Figure 4.5: Dissociation rates for a J/Ψ in a QGP as a function of temperature. The full curve corresponds to the leading-order QCD process for quasifree $g, q + c \to g, q + c$ scattering with *in-medium* J/Ψ bound state energies. The dashed (dotted) curve results from the gluo-dissociation mechanism $gJ/\Psi \to c\bar{c}$, assuming the *vacuum* (in-medium) dissociation energy.

the quasifree process and for temperatures relevant at SPS, it is more efficient in dissolving J/ψ's than gluo-dissociation (dashed line). At higher temperatures this tendency is reversed, mostly due to an increasing Debye mass which suppresses the t-channel gluon-exchange graphs for $g(q, \bar{q}) + J/\psi \to g(q, \bar{q}) + c + \bar{c}$. The dotted line indicates the results of the gluo-dissociation process accounting, however, for an in-medium reduced binding energy ($\varepsilon_0 \to \varepsilon(T)$ in Eq. (85)). Under such conditions, the gluo-dissociation process becomes increasingly inefficient as the temperature increases due to the fact that the absorption of the incoming gluon (whose average energy is $3T$) is more difficult as the open-charm threshold moves toward the J/ψ mass. At temperatures around T_c, where kinematics constraints are less pronounced, the quasifree calculation and the gluo-dissociation process including in-medium binding energies give very similar results.

Finally, to make contact with the time scales encountered in heavy-ion collisions, we plot in Fig. 4.6 the lifetimes τ_Ψ^{QGP} of J/ψ, ψ' and χ in the plasma as a function of

temperature. The latter are related to the dissociation rates Γ^{Ψ}_{diss} through

$$\tau^{QGP}_{\Psi} = \left(\Gamma^{\Psi}_{diss}\right)^{-1} \ . \tag{95}$$

The full (dashed) line indicates the J/ψ (ψ', χ) lifetime. Close to T_c, the vanishing binding energies for ψ' and χ entail lifetimes which are about a factor of three below the one for J/ψ-mesons.

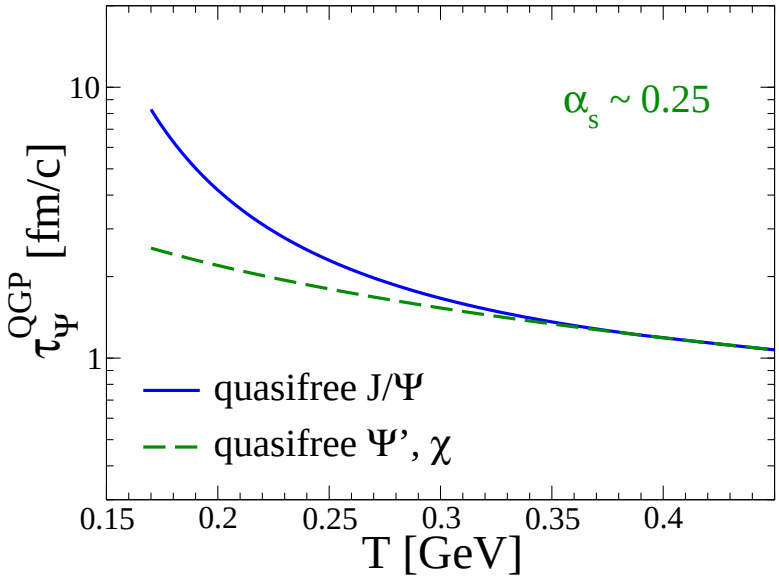

Figure 4.6: Lifetimes of a J/ψ (ψ', χ) in a thermalized QGP as a function of temperature T using the quasifree dissociation process. The full curve corresponds to the J/ψ ($\varepsilon^{\psi} \neq 0$) while the dashed curve illustrates $\varepsilon = 0$ (ψ', χ).

4.2 Hadronic interactions of charmonium

Subsequent to quark-gluon plasma dissociation, when the system converts to the hadronic phase, charmonia undergo further interactions with surrounding hadrons. There are a number of theoretical models for $J/\psi + hadron$ processes [9, 13, 14, 15, 15, 16, 17, 18, 19] whose results span an appreciable magnitude. Calculations involving excited charmonia [20], such as ψ' and χ (which contribute to the J/ψ yield via electromagnetic feeddown), are scarce. Consequently, the impact of inelastic hadronic scattering is not very well under control. An illustration of the current status of the theory is shown in Fig. 4.7, taken from Ref. [18]. The band, which is the main result of [18], reflects the pion-induced dissociation cross-section as assessed within a QCD sum rule

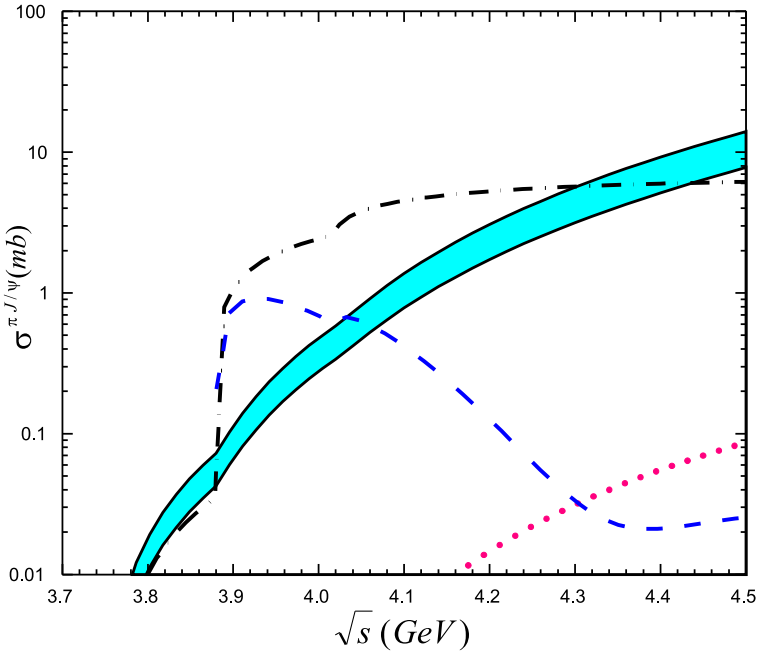

Figure 4.7: $\pi\ J/\psi \to D\bar{D}, D^*\bar{D}, D\bar{D}^*$ dissociation cross sections in various approaches; band: QCD sum rules [18], dotted line: short-distance QCD [9], dashed-dotted line: meson-exchange [21], dashed line: non-relativistic constituent quark model [16].

analysis. It is in reasonable agreement with evaluations from both constituent quark-model estimates [16, 22] as well as meson-exchange calculations [13, 15, 21, 17] (once soft form factors with cutoffs $\Lambda \sim 1$ GeV are included), but significantly above earlier short-distance QCD calculations [9] based on gluo-dissociation [8] folded with the (very soft) gluon distribution functions within light hadrons. ρ- [14, 17, 15] and nucleon-induced [14, 23] break-up cross sections tend to be somewhat larger. But even under rather extreme assumptions, *e.g.* an average cross-section of 1 mb and a total hadron density n_{had}=3$n_0$$\simeq$0.5 fm^{-3}, the chemical relaxation time, τ_ψ=$[\langle\sigma v\rangle n_{had}]^{-1}$$\simeq$30-40 fm/c, is well above typical hadronic fireball lifetimes.

4.2.1 $SU(4)$ effective theory of J/ψ interactions with light hadrons

As a baseline calculation, we reproduce results obtained first by Haglin [14], Lin and Ko [17], Haglin and Gale [15] within a $SU(4)$ effective theory.

$SU(4)$ Lagrangian

The starting point is a $SU(4)$-flavor symmetric effective Lagrangian formulated with 4-by-4 pseudoscalar and vector meson matrices. In the limit of $SU(4)$ invariance, the

free Lagrangian for pseudoscalar and vector mesons reads

$$\mathcal{L}_0 = Tr\left(\partial_\mu P^\dagger \partial^\mu P\right) - \frac{1}{2} Tr\left(F^\dagger_{\mu\nu} F^{\mu\nu}\right) \ , \tag{96}$$

where $F_{\mu\nu} = \partial_\mu V_\nu - \partial_\nu V_\mu$ and P and V corresponds to the pseudo-scalar and vector meson matrices in $SU(4)$ written as

$$P = \frac{1}{\sqrt{2}} \begin{pmatrix} \frac{\pi^0}{\sqrt{2}} + \frac{\eta}{\sqrt{6}} + \frac{\eta_c}{\sqrt{12}} & \pi^+ & K^+ & \bar{D^0} \\ \pi^- & -\frac{\pi^0}{\sqrt{2}} + \frac{\eta}{\sqrt{6}} + \frac{\eta_c}{\sqrt{12}} & K^0 & D^- \\ K^- & \bar{K^0} & -\sqrt{\frac{2}{3}}\eta + \frac{\eta_c}{\sqrt{12}} & D_S^- \\ D^0 & D^+ & D_S^+ & -\frac{\eta_c}{\sqrt{12}} \end{pmatrix} \tag{97}$$

and,

$$V = \frac{1}{\sqrt{2}} \begin{pmatrix} \frac{\rho^0}{\sqrt{2}} + \frac{\omega}{\sqrt{6}} + \frac{J/\psi}{\sqrt{12}} & \rho^+ & K^{\star +} & \bar{D^{\star 0}} \\ \rho^- & -\frac{\rho^0}{\sqrt{2}} + \frac{\omega}{\sqrt{6}} + \frac{J/\psi}{\sqrt{12}} & K^{\star 0} & D^{\star -} \\ K^{\star -} & \bar{K^{\star 0}} & -\sqrt{\frac{2}{3}}\omega + \frac{J/\psi}{\sqrt{12}} & D_S^{\star -} \\ D^{\star 0} & D^{\star +} & D_S^{\star +} & -3\frac{J/\psi}{\sqrt{12}} \end{pmatrix} \tag{98}$$

Interactions are generated from the free Lagrangian by replacing the spacetime derivative with a gauge covariant one

$$\partial_\mu \rightarrow D_\mu = \partial_\mu + \left[-\frac{ig}{2} V_\mu \ , \quad \right] \ . \tag{99}$$

Using the hermiticity of P and V leads to the following effective Lagrangian

$$\begin{aligned} \mathcal{L} = \mathcal{L}_0 \ &+ \ igTr\left(\partial^\mu P [P, V_\mu]\right) - \frac{g^2}{4} Tr\left([P, V_\mu]^2\right) \\ &+ \ igTr\left(\partial^\mu V^\nu [V_\mu, V_\nu]\right) + \frac{g^2}{8} Tr\left([V_\mu, V_\nu]^2\right) \ . \end{aligned} \tag{100}$$

The terms of order g correspond to 3-point vertices while the terms of order g^2 generate 4-point interactions. From Eq. (100), one can extract the Lagrangians relevant for charmonium hadronic interactions whose expressions are given in Appendix B. Although the $SU(4)$ symmetry is strongly broken by the c-quark mass, the hope is that symmetry-breaking effects are largely accounted for by the use of the hadronic *physical* masses in the calculations of the different processes.

Before we turn to the detailed calculation of the J/ψ hadronic interactions, let us mention a few words about the determination of the coupling constants entering Eq. (100). We employ coupling constants as calibrated by Haglin and Gale in Ref. [15] based

on the $\rho \to \pi\pi$ decay to fix the gauge coupling, which results in $K^\star$ widths consistent within 10% of experiments and $D^\star$ widths in agreement with other phenomenological determinations of the coupling constants [14, 17]. Other choices are possible [18, 24] and the lack of experimental constraints renders it difficult to discriminate between different sets of coupling. Our choice of couplings has also been guided by results obtained within constituent quark model approaches to describe hadronic J/ψ interactions [20].

J/ψ cross-sections with pions and rhos

Within the previous model, we study the interactions of J/ψ with pions and rhos which are the most abundant mesons in the heat bath. The Lagrangian (100) leads to the following J/ψ interactions with pions and rhos (for simplicity, we have neglected interactions with kaons which are also included in the Lagrangian (100))

$$\pi + J/\psi \to D + \bar{D}^\star, \bar{D} + D^\star \tag{101}$$

$$\rho + J/\psi \to D + \bar{D} \tag{102}$$

$$\rho + J/\psi \to D^\star + \bar{D}^\star \ . \tag{103}$$

Other processes, *e.g.* $J/\psi + \pi \to \eta_c + \rho$, involve vector-vector-pseudo-scalar vertices which are part of the Lagrangian (100) and have not been included. Fig. 4.8 displays the Feynman graphs for the three processes above and the corresponding amplitudes can be found in Appendix B as well as the calculations of the cross-sections for Eqs. (101), (102) and (103). The latter are shown in Fig. 4.9 (full lines) as a function of the cms energies of the incoming particles.

- The resulting $J/\psi+\pi$ cross-section rises quickly above threshold to level-off around 6 mb. This may seem a somewhat large value but the effective hadronic theory has to be supplemented with vertex form factors, to be discussed in the next section, which reduce the magnitude of the scattering processes.

- The $J/\psi + \rho \to D\bar{D}$ is exothermic and decreases very rapidly with increasing cms energy. Overall, this process gives a small contribution to the inelastic J/ψ break-up in the hadronic phase.

- The $J/\psi + \rho \to D^\star\bar{D}^\star$ cross-section depends weakly on the cms energy and gives a somewhat comparable contribution as the $J/\psi + \pi$ process.

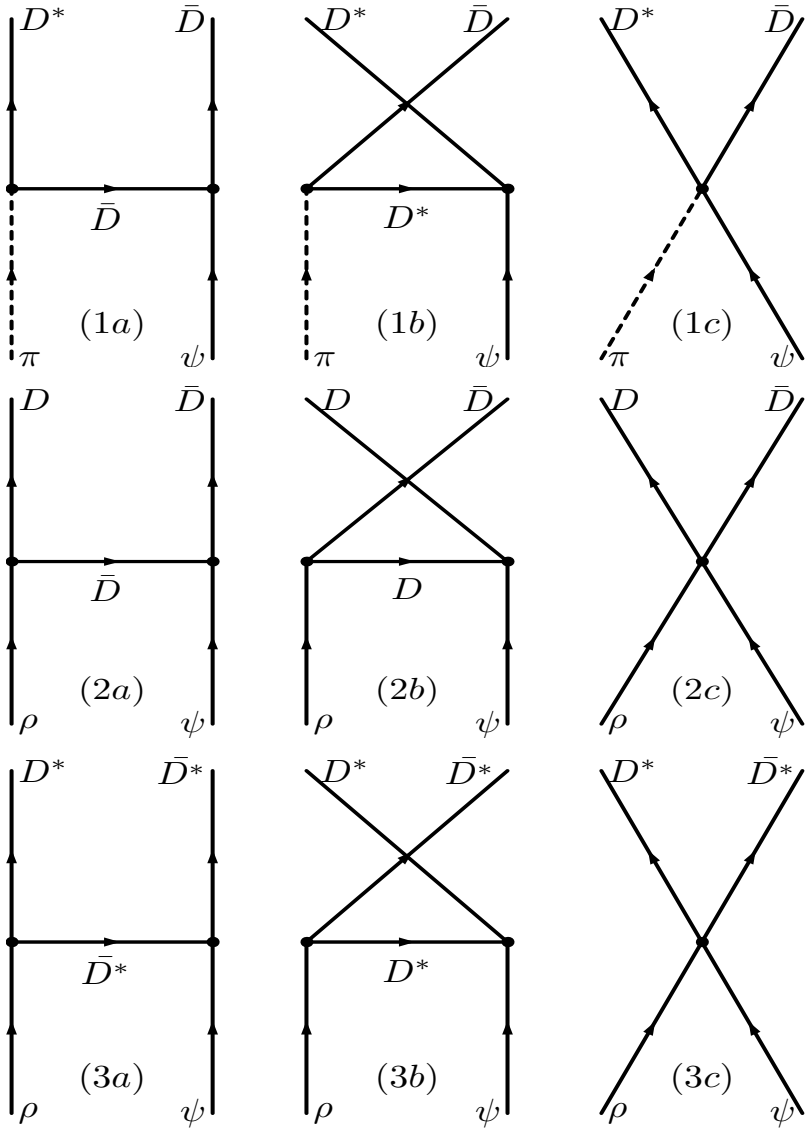

Figure 4.8: Feynman diagrams for J/ψ break-up in the hadronic phase. First row: $J/\psi + \pi \to D^\star \bar{D}$, second row: $J/\psi + \rho \to D\bar{D}$ and last row: $J/\psi + \rho \to D^\star \bar{D}^\star$.

Effects of form factors

The effective hadronic theory is not applicable at very short distances and is therefore supplemented by vertex form factors to simulate finite size effects and take into account the composite nature of hadrons. Since there is little experimental information on form factors for charmonia and charmed mesons, we rely on simple assumptions to introduce the form factors in the theory, especially regarding the 4-point vertices.

Non-covariant form factors

As done previously by Lin and Ko in [17], for simplicity we use the following monopole form factors at the 3-point vertices,

$$f_t = \frac{\Lambda^2}{\Lambda^2 + \vec{q_t}^2} \ , \tag{104}$$

and

$$f_u = \frac{\Lambda^2}{\Lambda^2 + \vec{q_u}^2} \ , \tag{105}$$

respectively in the t-channel and u-channel of the graphs from Fig. 4.8. Λ is a cutoff parameter which sets the upper energy scale up to which the hadronic effective theory is believed to apply. $\vec{q_t}^2$ (respectively $\vec{q_u}^2$) is the squared three-momentum transfer in the center of mass frame given by $\vec{q_t}^2 = (\vec{p_1} - \vec{p_3})^2_{cm}$ (respectively $\vec{q_u}^2 = (\vec{p_1} - \vec{p_4})^2_{cm}$) for the t- (respectively u-) channels. For the contact terms, it is assumed that the form factors can be written as

$$f_c = \left(\frac{\Lambda^2}{\Lambda^2 + \vec{q}^2} \right)^2 \tag{106}$$

where $\vec{q}^2$ is the averaged squared three-momentum transfer in the t and u channels ,

$$\vec{q}^2 = \frac{1}{2} \left[(\vec{p_1} - \vec{p_3})^2 + (\vec{p_1} - \vec{p_4})^2 \right]_{cm} = p_i^{\star 2} + p_f^{\star 2} \tag{107}$$

In principle, one can introduce different cutoff values for the different vertices, according, *e.g.* to the mass of the incoming mesons and/or the mass of the exchanged meson. However, for simplicity, we use a common value of Λ for all the interaction vertices. In Fig. 4.9, we study the effects of form factors for a common value of $\Lambda = 1$ GeV or $\Lambda = 2$ GeV. The form factors strongly reduce the magnitude of the J/ψ hadronic interactions, to a mb or sub-mb level. Even if the calculations are shown to be rather sensitive to the precise value of Λ, overall, when form factors are included, the J/ψ seems to interact only mildly with the surrounding hadrons. We checked that up to the choice of coupling

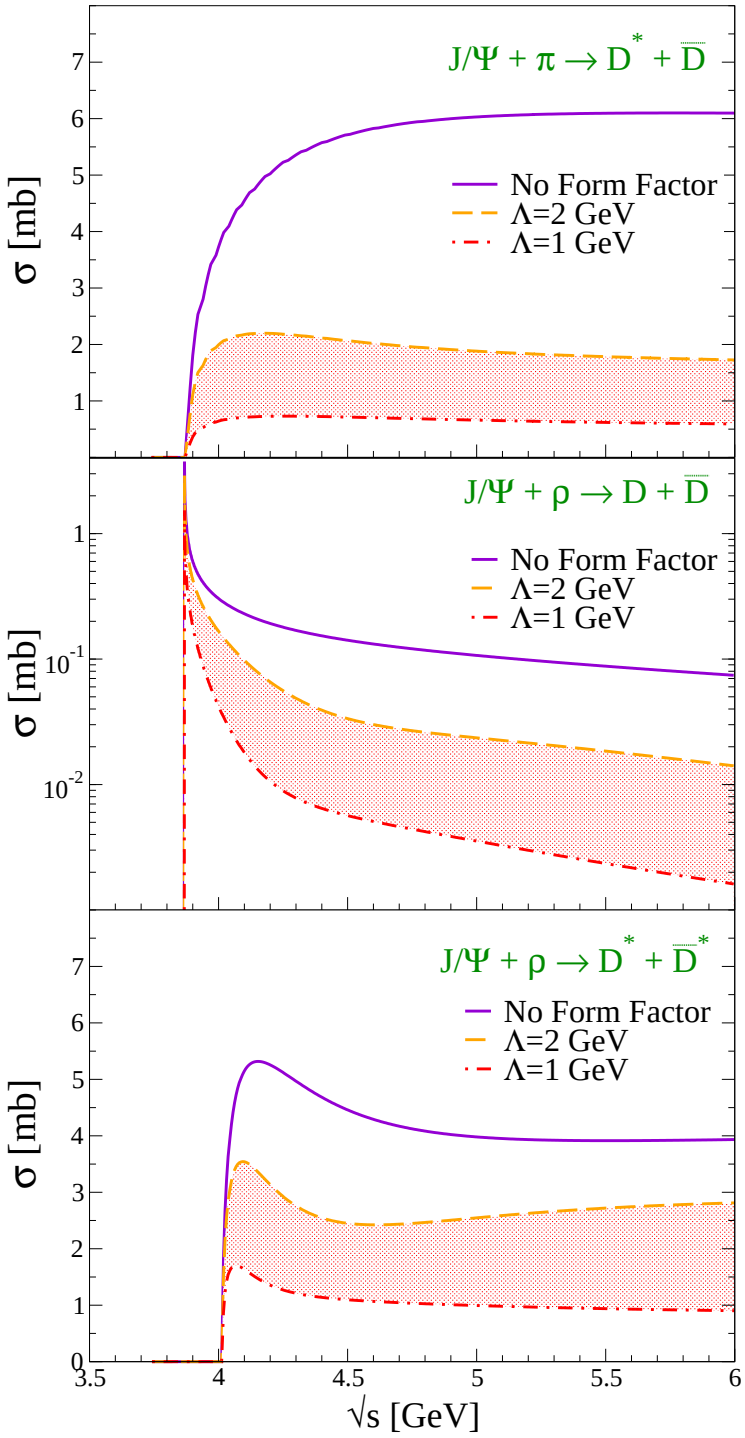

Figure 4.9: Hadronic cross-sections including form factors for $J/\psi+\pi \to D+\bar{D}^{\star}$ (upper plot), $J/\psi+\rho \to D+\bar{D}$ (middle plot) and $J/\psi+\rho \to D^{\star}+\bar{D}^{\star}$ (lower plot). The full curves correspond to calculations without form factors while the band enclosed between the dashed curve ($\Lambda = 2$ GeV) and the dot-dashed curve ($\Lambda = 1$ GeV) reflects the sensitivity of the calculation to the choice of cutoff parameter Λ.

constants and the implementation of form factors, our calculations are consistent with the original results of [14, 17, 15].

Gauge-invariant form factors

As first noted in [15], the form chosen in Eq. (106) for the contact term breaks gauge invariance (in this model, vector mesons are treated as gauge particles which have the quantum numbers of the photon. Therefore, the corresponding amplitudes must satisfy gauge invariance in the electromagnetic sector) which is possible to restore by introducing appropriate counter-terms. Following Haglin and Gale [15], we discuss how to achieve a gauge invariant theory using the $J/\psi + \pi$ cross-section as an example, and we study the sensitivity of our results to the choice of form factors. The introduction of form factors at the three-point vertices amounts to multiplying the matrix elements of the (u-) t-channels by the product of two monopole form factors, *i.e.* $\mathcal{M}_{1a} \to \mathcal{M}_{1a} \times f_t^2$ and $\mathcal{M}_{1b} \to \mathcal{M}_{1b} \times f_u^2$, where $\mathcal{M}_{1a}$ and $\mathcal{M}_{1b}$ are the matrix elements of the graphs $(1a)$ and $(1b)$ from Fig. 4.8. It remains to introduce form factors for the contact term $(1c)$ which preserve gauge invariance. To do so [25, 15], one writes the most general (respecting the symmetry properties of the interaction) 4-point interaction, *i.e.* one makes the substitution (ignoring the overall coupling constant)

$$\begin{aligned} \mathcal{M}_{1c} = -g^{\mu\nu} \to A g^{\mu\nu} &+ B\,(p_D^\mu p_\pi^\nu + p_\pi^\mu p_D^\nu) + C\,(p_{D^\star}^\mu p_\pi^\nu + p_\pi^\mu p_{D^\star}^\nu) \\ &+ D\,(p_\pi^\mu p_\pi^\nu + p_D^\mu p_D^\nu) + E\,(p_\pi^\mu p_\pi^\nu + p_{D^\star}^\mu p_{D^\star}^\nu)\ , \end{aligned} \tag{108}$$

where the coefficients A, B, C, D and E are determined using gauge invariance which requires the current conservation laws

$$p_{j\mu} \mathcal{M}^{\mu\nu} = 0. \tag{109}$$

to be satisfied. Here, $p_{j\mu}$ corresponds to the 4-momentum of the external vector meson j. One possible solution (gauge invariance alone does not allow to uniquely determine the coefficients A, B, C, D and E) is given by

$$A = -f_t^2 \tag{110}$$

$$B = D = \frac{f_t^2 - f_u^2}{p_{J/\psi}.p_\pi + p_{J/\psi}.p_D} \tag{111}$$

$$C = E = 0 \tag{112}$$

We show in Fig. 4.10 the resulting $J/\psi + \pi \to D + \bar{D}^{\star}$ cross-section using Lorentz invariant form factors as in Ref. [15],

$$f_t = \frac{\Lambda^2}{\Lambda^2 + |t - m_D^2|} \quad \text{and} \quad f_u = \frac{\Lambda^2}{\Lambda^2 + |u - m_D^2|} \,, \tag{113}$$

along with the 4-point interaction vertex determined by Eqs. (108) and (110)-(112) which renders the full amplitude $\mathcal{M}_1$ Lorentz and gauge invariant. They are compared

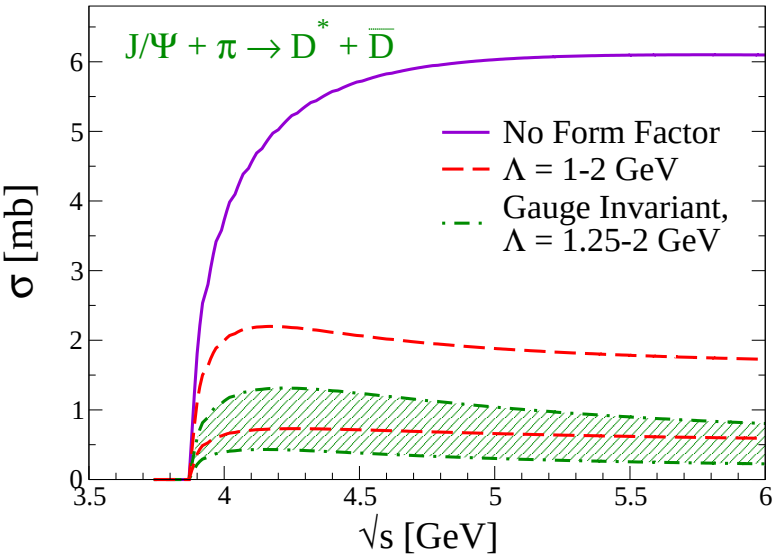

Figure 4.10: Comparison of different choices of form factors functional for the $J/\psi + \pi$ cross-section. Full line: without form factors. Dot-dashed line: Lorentz and gauge invariant form factors with cutoff $\Lambda = 1.25 - 2$ GeV (similar to original work from Haglin and Gale in [15]). Dashed line: Form factors from Eqs. (104)-(106) with $\Lambda = 1 - 2$ GeV.

with our previous simple choice of non-covariant monopole form factors using a cutoff value of $\Lambda = 1$ GeV. The two different implementations of form factors into the hadronic theory agree rather well with eachother, certainly within the overall accuracy of the model. Therefore, for simplicity, in the remaining part of this work, we will use the form factors given by Eqs. (104)-(106) using a common value of $\Lambda = 1$ GeV.

Anomalous processes

We furthermore investigated the role of so-called anomalous processes such as $\pi + J/\Psi \to \eta_c + \rho$, $\pi + J/\Psi \to \eta_c + b_1$, and $\rho + J/\Psi \to \eta_c + \pi$, suggested in Ref. [15]. In there, the relevant hadronic coupling constants, *e.g.* $g_{J/\Psi\omega\eta_c}$, have been estimated applying the vector dominance model (VDM) to the radiative decay $J/\Psi \to \gamma\eta_c$. We believe, however,

that this procedure leads to a significant overprediction of the hadronic coupling, for the following reason. For vertices carrying identical quantum number structure, namely $J/\Psi\omega\eta$ and $J/\Psi\omega\eta'$, both hadronic and corresponding radiative decay information is available from experiment. One finds [26],

$$\Gamma(J/\Psi \to \omega\eta)/\Gamma_{tot} = 1.6 \times 10^{-3}, \qquad \Gamma(J/\Psi \to \omega\eta')/\Gamma_{tot} = 1.7 \times 10^{-4} \ ,$$
$$\Gamma(J/\Psi \to \gamma\eta)/\Gamma_{tot} = 8.6 \times 10^{-4}, \qquad \Gamma(J/\Psi \to \gamma\eta')/\Gamma_{tot} = 4.3 \times 10^{-3} \ ,$$

i.e. , the hadronic branching ratios are comparable or even below the radiative ones. This is in marked contradiction to VDM within which the latter are suppressed by a factor $(e/g_\omega)^2$ which is much smaller than the moderate increase in phase space due to the final state decay momenta (also note that VDM is more strongly violated with increasing mass of the pseudoscalar meson). Thus it appears that VDM cannot be applied, and that an accordingly reduced $g_{J/\Psi\omega\eta_c}$ coupling renders the pertinent t-channel ω exchange processes in $\pi + J/\Psi \to \eta_c + \rho$ and $\pi + J/\Psi \to \eta_c + b_1$ negligible. We therefore decided not to include anomalous processes in our analysis.

4.2.2 Constituent quark model based approaches

The fact that the $SU(4)$ symmetry of the Lagrangian (100) is severely broken due to the large quark mass, in addition to the uncertainty related to the coupling constants, has raised criticism. To establish the J/ψ hadronic interactions on a firmer ground, we compare the cross-sections obtained in Fig. 4.10 to the ones obtained by Wong, Barnes and Swansson [16] using a constituent quark model approach.

The authors of [16] (see also [22] for a similar approach) start from a non-relativistic quark potential model writing an interquark Hamiltonian which includes a Coulomb term, a linear confining term and a spin-spin hyperfine interaction. The parameters entering the Hamiltonian are fitted to the meson spectrum and, then, fully determine the wavefunctions of the external mesons. One can then evaluate the meson-meson scattering amplitudes at the Born order assuming a constituent interchange scattering mechanism. Their results [16] for the $J/\psi + \pi$ inelastic break-up cross-section are shown in Fig. 4.7 (dashed line) and compared to meson exchange calculations (dot-dashed line). The two different approaches yield rather similar results. Both cross-sections rise sharply just above threshold to reach peak values of ~ 1 mb. In the effective Lagrangian approach, they do not fall off as quickly as in the constituent quark based calculations,

however, the difference between the two approaches at large $\sqrt{s}$ has little impact on the hadronic dissociation rates.

4.3 Charmonium dissociation rates in the hadronic phase

4.3.1 J/ψ dissociation

We proceed to calculate the J/ψ dissociation rate in the hadronic phase using the J/ψ hadronic cross-sections of Fig. 4.9. As in Sec. 4.1.3, the dissociation rates are given by the convolution of the thermal distribution functions with the inelastic cross-sections. Under the assumption that the particles follow a Boltzmann distribution, this can be conveniently expressed as

$$\Gamma_{diss}^{HAD} = \frac{g_a T^3}{8\pi^2} \frac{\int_{z_{min}}^{\infty} dz \lambda \left(z^2T^2, m_a^2, m_{J/\psi}^2\right) \sigma_{aJ/\psi}\left(s = z^2T^2\right) K_1(z)}{\frac{m_{J/\psi}^2}{T^2} K_2\left(\frac{m_{J/\psi}}{T}\right)} \ , \tag{114}$$

where $a = \pi, \rho$, $s = (p_\psi + p_a)^2$ and λ is the usual kinematical function

$$\lambda\left(x^2, y^2, z^2\right) = \left[x^2 - (y+z)^2\right]\left[x^2 - (y-z)^2\right] \ . \tag{115}$$

Writing $z = \sqrt{s}/T$, the threshold of the process is given by

$$z_{min} = max\left(\frac{m_1 + m_2}{T}, \frac{m_3 + m_4}{T}\right) \ . \tag{116}$$

The resulting dissociation rates are displayed in Fig. 4.11 as a function of the temperature of the hadron gas. The main contribution to the J/ψ dissociation is given by the $J/\psi + \rho \to D^\star + \bar{D}^\star$ process (dot-dashed line) which is slightly more effective than the pion process (dashed line). The $J/\psi + \rho \to D + \bar{D}$ (dotted line) is rather small. The sum of the three processes we have considered corresponds to the full line in Fig. 4.11. With a value of $\Gamma_{diss}^{HAD} \simeq 1$ MeV at $T = 170$ MeV, the hadronic phase, in the absence of in-medium effects, is very ineffective at destroying J/ψ's.

4.3.2 ψ' and χ dissociation

As mentioned previously, ψ' and χ hadronic interactions are even more difficult to assess than the J/ψ ones within meson exchange models. To obtain an estimate that

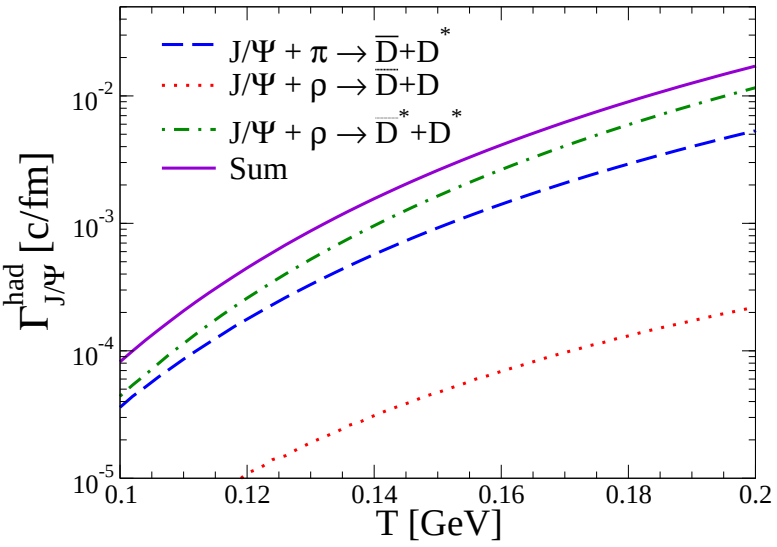

Figure 4.11: J/ψ dissociation rates by pions and rhos as a function of the temperature T of the hadron gas. The full line is the sum of the three contributions, $J/\psi+\pi$ (dashed line), $J/\psi+\rho \to D^\star + \bar{D}^\star$ (dot-dashed line) and $J/\psi+\rho \to D+\bar{D}$ (dotted line).

can be used in our calculations of the J/ψ yield in heavy-ion collisions, we assume a geometric scaling of the calculated J/ψ cross-sections with the squared ratio of the respective charmonium radii. Hence, we use

$$\Gamma^{HAD}_{\psi'} = \left(\frac{r_{\psi'}}{r_{J/\psi}}\right)^2 \Gamma^{HAD}_{J/\psi} \simeq 3.73\ \Gamma^{HAD}_{J/\psi}\ , \tag{117}$$

and

$$\Gamma^{HAD}_{\chi} = \left(\frac{r_{\chi}}{r_{J/\psi}}\right)^2 \Gamma^{HAD}_{J/\psi} \simeq 2.36\ \Gamma^{HAD}_{J/\psi} \tag{118}$$

where the values of the different charmonium radii obtained in non-relativistic potential models are taken from Ref. [27]

$$r_{J/\psi} = 0.45 \text{ fm} \tag{119}$$

$$r_{\psi'} = 0.88 \text{ fm} \tag{120}$$

$$r_{\chi} = 0.70 \text{ fm}\ . \tag{121}$$

The corresponding lifetimes we obtain are shown in Fig. 4.12. The assumption of geometric scaling for the ψ' and χ cross-section lacks theoretical justification, however, it is further supported by comparison with constituent quark model approaches [16] in which ψ' and χ are directly accessible to calculations. In Fig. 4.13, we compare the rates obtained for the $\Psi+\pi$ interactions using *(i)* the results of the quark interchange model of [16] which give cross-sections for all three charmonia J/ψ, ψ' and χ and *(ii)* our

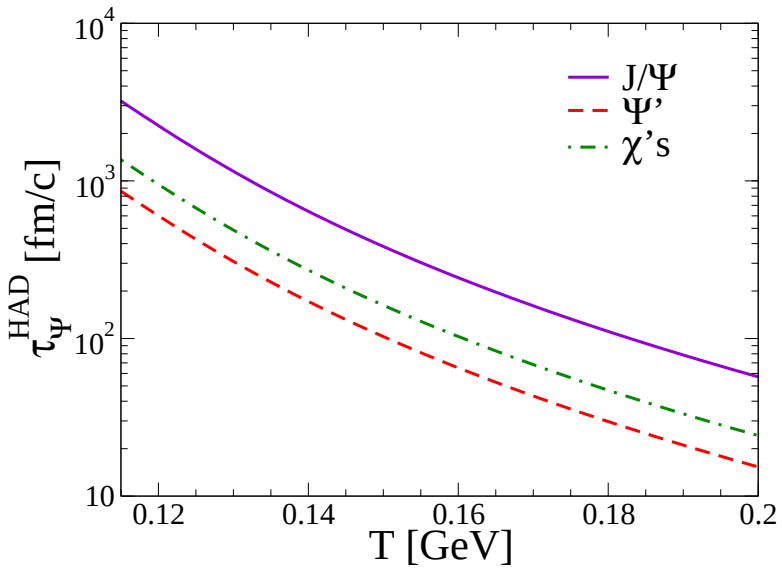

Figure 4.12: Lifetimes of charmonia in the hadronic phase as a function of temperature. The ψ' (dashed line) and the χ (dot-dashed line) lifetimes are deduced from the J/ψ lifetime (solid line) using geometric scaling.

results within an $SU(4)$ effective theory for the J/ψ supplemented by geometric scaling for ψ' and χ. The agreement is rather reasonable, especially in the region of interest

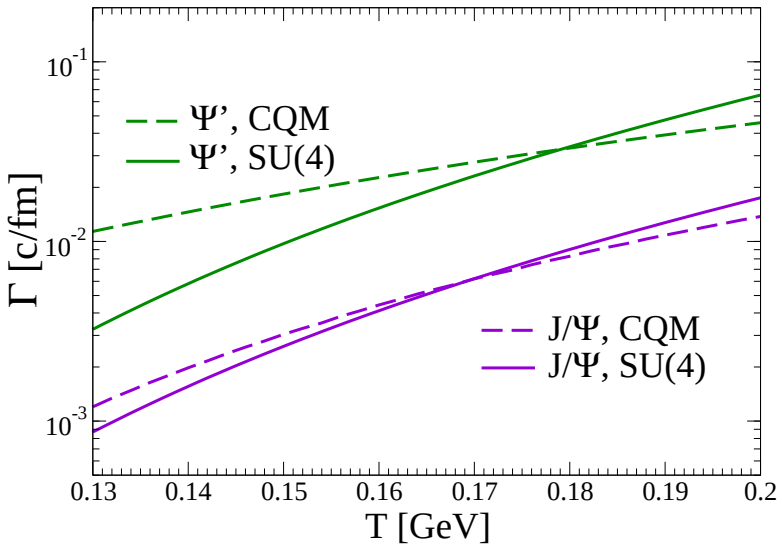

Figure 4.13: Comparison of the dissociation rates for $\Psi + \pi$ between a constituent quark model approach (set of dashed curves) and a $SU(4)$ effective theory including geometric scaling (set of full curves). See text for details.

(*i.e.* slightly below T_c), given the assumption of geometric scaling of the cross-sections. Overall, the lifetimes of charmonia in the hadronic phase are significantly longer than the typical duration of the hadronic phase in heavy-ion collisions, entailing a mild hadronic

suppression.

4.4 In-medium effects in the hadronic phase

At this point, although the impact of inelastic hadronic scattering is not very well under control, most calculations, including recent ones based on quark exchange models or on $SU(4)$ symmetric effective Lagrangians, seem to indicate a rather moderate influence of the hadronic medium on the J/ψ. The situation may change if additional medium effects are present, most notably reduced D-meson masses, as discussed in Chapter 3. From a practical point of view, the lowering of the $D\bar{D}$ threshold has several consequences among which *(i)* the increased phase space accelerates the inelastic reactions and *(ii)* excited charmonia may move above threshold.

4.4.1 Medium effects on J/ψ hadronic interactions

If the D-meson mass gets reduced, possibly due to chiral symmetry restoration as discussed in Sec. 3.2.2, one expects stronger hadronic interactions. We repeated the calculations of the $J/\psi + \pi, \rho$ cross-sections including reduced temperature dependent D-meson masses, according to Fig. 3.5. Our results are displayed in Fig. 4.14 for the $J/\psi + \pi$ process for different temperatures achieved in the hadronic phase. The

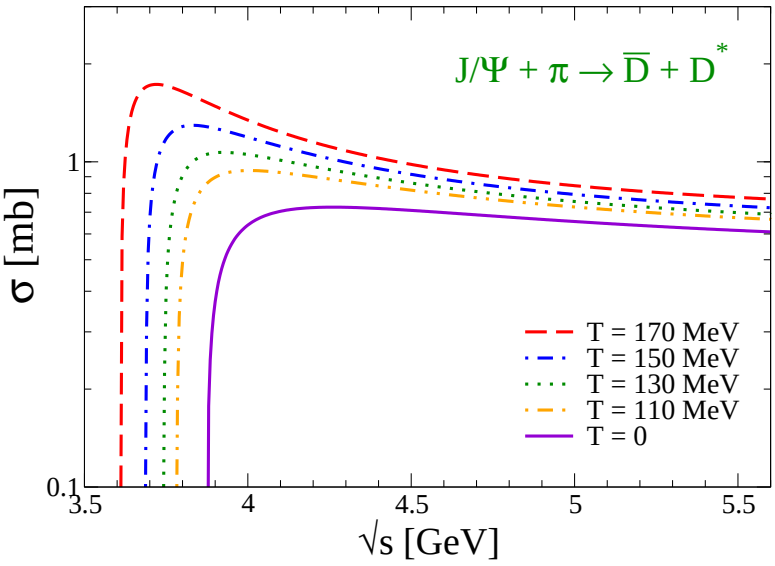

Figure 4.14: $J/\psi + \pi \to D + \bar{D}^{\star}$ cross-sections as a function of the cm energy of the collisions for different temperatures (see curve labels) including reduced in-medium D-meson masses.

reduced D-meson masses substantially increase the $J/\psi+\pi$ cross-section (similar results are obtained for results involving the ρ-meson) and lower the threshold of the process. However, despite the increase due to medium effects in the hadronic phase, the hadronic dissociation rates remain smaller than their QGP counterparts, see Sec. 4.1.3.

4.4.2 ψ' in-medium decay

The other consequence of reduced D-meson masses is related to higher-lying charmonia states which are near the open-charm threshold. For example, in vacuum, the ψ' ($m_{\psi'} = 3.686$ GeV) is only 60 MeV below the open-charm threshold ($2m_D = 3.74$ GeV). As the D-meson mass is reduced, the ψ' may move above threshold and be allowed to directly decay into a $D\bar{D}$ pair. When considering in-medium effects on J/ψ yields in heavy-ion collisions (Chapter 7), we allow for such decays. However, as was first noted by Friman *et al.* [28], the naive extrapolation of the decay rate according to the increase of the available phase space needs to be reevaluated taking into account effects of nodes in the wavefunction. Fig. 4.15, taken from Ref. [28], shows the width of excited charmonia, calculated parametrically as a function of the D-meson mass, taking into account precise charmonium wavefunctions. Upon folding the ψ' width with our temperature

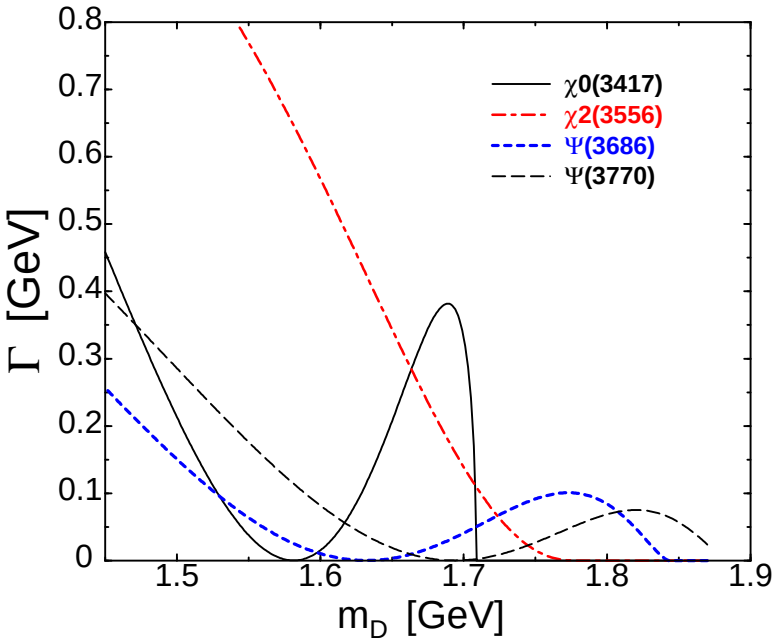

Figure 4.15: Calculations of the width of excited charmonia as a function of the D-meson mass, taken from Ref. [28].

dependence of the D-meson mass, we obtain the decay rate of the ψ' into a $D\bar{D}$ pair in

the medium, as a function of temperature. We used the results of Ref. [28] to include this process in our study of in-medium effects on J/ψ production which has important consequences, most notably on ψ'/ψ ratio.

Bibliography

[1] F. Karsch, M. T. Mehr, and H. Satz, Z. Phys. **C37**, 617 (1988).

[2] E. Eichten, K. Gottfried, T. Kinoshita, K. D. Lane, and T.-M. Yan, Phys. Rev. **D17**, 3090 (1978).

[3] E. Eichten, K. Gottfried, T. Kinoshita, K. D. Lane, and T.-M. Yan, Phys. Rev. **D21**, 203 (1980).

[4] S. Jacobs, M. G. Olsson, and C. Suchyta III, Phys. Rev. **D33**, 3338 (1986).

[5] E. V. Shuryak, Phys. Lett. **B78**, 150 (1978).

[6] T. Matsui and H. Satz, Phys. Lett. **B178**, 416 (1986).

[7] M. E. Peskin, Nucl. Phys. **B156**, 365 (1979).

[8] G. Bhanot and M. E. Peskin, Nucl. Phys. **B156**, 391 (1979).

[9] D. Kharzeev and H. Satz, Phys. Lett. **B334**, 155 (1994), hep-ph/9405414.

[10] L. Grandchamp and R. Rapp, Phys. Lett. **B523**, 60 (2001), hep-ph/0103124.

[11] B. L. Combridge, Nucl. Phys. **B151**, 429 (1979).

[12] M. LeBellac, *Thermal field theory*, Cambridge University Press, Cambridge, USA (1996).

[13] S. G. Matinian and B. Müller, Phys. Rev. **C58**, 2994 (1998), nucl-th/9806027.

[14] K. L. Haglin, Phys. Rev. **C61**, 031902 (2000), nucl-th/9907034.

[15] K. L. Haglin and C. Gale, Phys. Rev. **C63**, 065201 (2001), nucl-th/0010017.

[16] C.-Y. Wong, E. S. Swanson, and T. Barnes, Phys. Rev. **C65**, 014903 (2002), nucl-th/0106067.

[17] Z.-W. Lin and C. M. Ko, Phys. Rev. **C62**, 034903 (2000), nucl-th/9912046.

[18] F. O. Duraes, H. C. Kim, S. H. Lee, F. S. Navarra, and M. Nielsen, (2002), nucl-th/0211092.

[19] F. S. Navarra, M. Nielsen, and M. R. Robilotta, Phys. Rev. **C64**, 021901 (2001), nucl-th/0103051.

[20] C.-Y. Wong, E. S. Swanson, and T. Barnes, Phys. Rev. **C62**, 045201 (2000), hep-ph/9912431.

[21] Y. Oh, T. Song, and S. H. Lee, Phys. Rev. **C63**, 034901 (2001), nucl-th/0010064.

[22] K. Martins, D. Blaschke, and E. Quack, Phys. Rev. **C51**, 2723 (1995), hep-ph/9411302.

[23] W. Liu, C. M. Ko, and Z.-W. Lin, Phys. Rev. **C65**, 015203 (2002).

[24] A. Deandrea, G. Nardulli, and A. D. Polosa, (2003), hep-ph/0302273.

[25] J. Kapusta, P. Lichard, and D. Seibert, Phys. Rev. **D44**, 2774 (1991).

[26] Particle Data Group, D. E. Groom *et al.*, Eur. Phys. J. **C15**, 1 (2000).

[27] R. Vogt, Phys. Rept. **310**, 197 (1999).

[28] B. Friman, S. H. Lee, and T. Song, Phys. Lett. **B548**, 153 (2002), nucl-th/0207006.

Chapter 5

Thermal Fireball Description of Heavy-Ion Collisions

To calculate the final number of J/ψ's remaining in the system after the plasma and hadronic phases, we need to convolute the dissociation rates of Chapter 4 with the space-time history of the heavy-ion collision. To describe how the system created in the collision of two heavy nuclei expands over time, a few suitable approaches are conceivable, among which are hydrodynamical, transport and thermal fireball models.

In hydrodynamical models of heavy-ion collisions (see [1] for a recent review), the assumption is made that the strong interaction maintains local thermal equilibrium so that the system can be divided into elementary cells in which thermodynamical quantities such as temperature, energy density and pressure are well defined. The system expands according to the conservation of the energy-momentum tensor $\partial_\mu T^{\mu\nu} = 0$ supplemented by continuity equations for conserved currents $\partial_\mu j_B^\mu$, $\partial_\mu j_S^\mu = 0$ where j_B^μ and j_S^μ are the baryon number and strangeness currents. Hydrodynamical models require three inputs: the equation of state (EOS) of the expanding matter, as well as the initial conditions and a freeze-out prescription. Such models have proven rather successful at describing collective phenomena, *e.g.* radial and elliptic flows in heavy-ion collisions.

Another large class of models attempting to describe heavy-ion collisions is constituted by transport models, reviewed in [2]. Their starting point is a set of coupled Boltzmann equations for the phase-space distributions f_i of particle i. The change in f_i due to the motion of particle i in the average potential field produced by other particles equals a collision term which evaluates the two-body scattering rate of particle i

(as well as its production/decay rates) with other particles in the medium. Transport models rely on empirical information to input the in-medium potentials and the 2-to-2 cross-sections involved in the Boltzmann equation. They have been successfully used to reproduce single-particle spectra, to study strangeness exchange reactions and HBT radii.

There is an abundant literature on hydrodynamic and transport models, however in this work we use a simplified picture of the reaction dynamics taking place in the course of a heavy-ion collision. To model the space-time evolution of the system, we employ a schematic thermal fireball expansion [3, 4], which however, incorporates essential features of hydrodynamical calculations.

5.1 Thermal fireball model

We assume that the system is equilibrated after a formation time τ_0, similar to the formation time used in hydrodynamical calculations. From then on, the system expands homogeneously and isentropically, at fixed entropy per baryon $S/N_B = s/n_B$ where the total entropy $S = sV_{FB}$ and the net baryon number $N_B = n_B V_{FB}$ are related to the corresponding densities via the time-dependent 3-volume V_{FB}. The volume prescription sets the time scale of the evolution and we model it in cylindrical symmetry, according to

$$V_{FB}(\tau) = (z_0 + v_z\tau + \frac{1}{2}a_z\tau^2)\pi(r_0 + \frac{1}{2}a_\perp\tau^2)^2 \ , \tag{122}$$

where r_0 denotes the initial transverse overlap of the two colliding nuclei at given impact parameter b. The expansion parameters $\{v_z, a_z, a_\perp\}$ are adjusted in line with hydro-calculations to reproduce observed flow velocities in connection with (thermal) freezeout times of $\tau_{fo} \simeq 10 - 14$ fm/c. The parameter z_0 is equivalent to the formation time τ_0 (in the Bjorken limit $z_0 \simeq \tau_0\Delta y$), specifying the initial conditions of the evolution. We alternatively used two fireballs, to conveniently cover the whole rapidity window of particle production in Pb(160 AGeV)-Pb collisions at SPS and one fireball, which may be more realistic when applied to the coalescence of charm quarks (due to the strong longituninal flow, it is hardly conceivable that charm could coalesce over more than two units of rapidity). Note, however, that the sensitivity of our results to the number of fireballs employed is rather small (*e.g.*, to describe the J/ψ centrality dependence at SPS, switching from one fireball to two fireballs entails a change in our effective

parameter α_s smaller than 10%).

5.1.1 Phases of the fireball

At any given time τ, the fireball volume $V_{FB}(\tau)$ specifies the temperature of the system through the corresponding entropy density $s(\tau) = S/V_{FB}(\tau)$ in either the hadronic or the QGP phase. The latter is modelled by a ideal gas of massive quarks and gluons. Hence, the entropy density in the QGP at a temperature T is given by

$$s(\tau) = \frac{g}{2\pi^2} m^3 \sum_{k=1}^{\infty} (\pm)^{k+1} \frac{K_3\left(k\frac{m}{T}\right)}{k} \quad , \begin{cases} + : \text{ gluons} \\ - : \text{ quarks} \end{cases} \tag{123}$$

where g are degeneracies and the masses m correspond to thermal quasiparticle masses as in Eqs. (92)-(94). In the hadronic phase, we use a resonance gas equation of state including the 37(37) lowest lying mesons (baryons). A similar hadron gas equation of state was recently compared to lattice data in [5] and is seen to provide a good description of the hadronic phase EOS from the lattice (see Fig. 5.1). At T_c, the critical

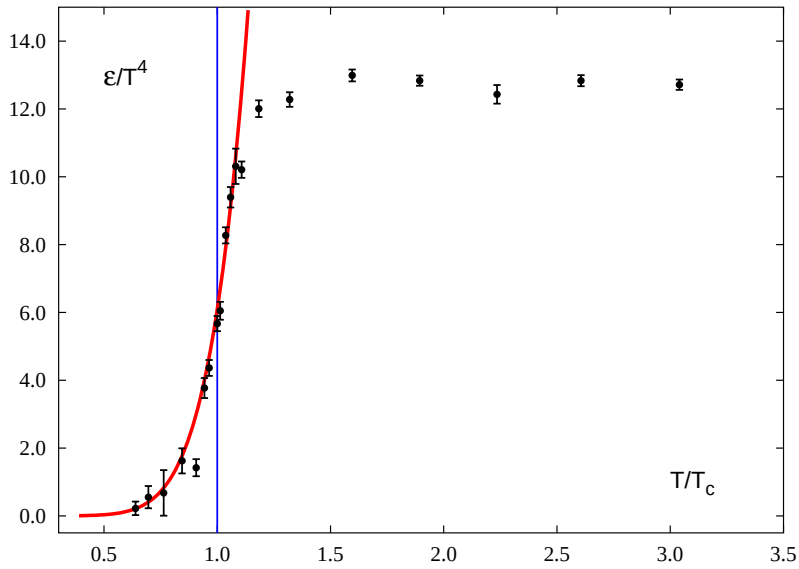

Figure 5.1: Comparison of a resonance gas equation of state with lattice data, taken from Ref. [5]

entropy density calculated in the plasma phase s^c_{QGP} is roughly twice as large as the critical entropy density calculated in the hadronic phase s^c_{HAD}, also quite reminiscent of the rapid entropy increase around T_c observed in lattice QCD calculations. If $s(\tau)$ lies in between the entropy densities s^c_{QGP} and s^c_{HAD}, a standard mixed phase construction

[6] is employed at the critical temperature T_c,

$$\frac{S}{V_{FB}(\tau)} = f\ s^c_{HAD} + (1-f)\ s^c_{QGP} \tag{124}$$

which determines the volume partitions f and $(1-f)$ for hadronic and quark-gluon matter respectively. Thus, we obtain the typical temperature profiles displayed in Fig. 5.2 for central collisions at SPS and RHIC. At SPS, for central collisions ($N_p = 360$),

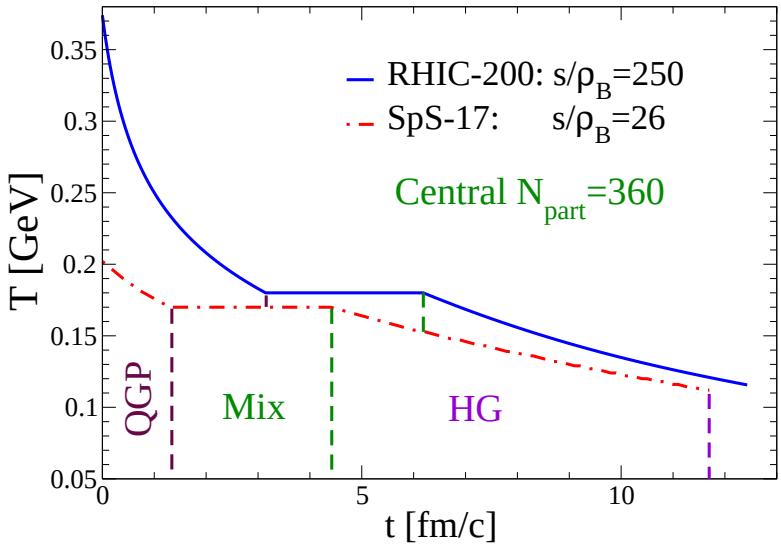

Figure 5.2: Typical temperature profiles at SPS ($\sqrt{s_{NN}} = 17.3$ GeV, dot-dashed line) and RHIC ($\sqrt{s_{NN}} = 200$ GeV, full line) for central collisions ($N_{part} = 360$) of heavy nuclei.

the QGP phase lasts for $1-2$ fm/c and the mixed phase continues up to $4-5$ fm/c. At RHIC, due to the more energetic conditions, the plasma phase lasts up to $3-4$ fm/c with the mixed phase continuing up to $6-7$ fm/c.

5.1.2 Initial conditions, centrality and energy dependence of the fireball

The initial conditions of the collision are specified via the quantities z_0, r_0 and the entropy over baryon number ratio s/n_B (sometimes referred to as specific entropy) which are impact parameter and/or energy dependent.

z_0 is taken in connection with formation times $\tau_0 \simeq 1$ fm/c at SPS and $\tau_0 \simeq 1/3$ fm/c at RHIC. It is conceivable that z_0 also depends on the impact parameter b of the collision, since it is expected that for peripheral collisions, the less energetic conditions lead to longer equilibration times or even partial equilibration. However, due to the lack

of theoretical handle on the impact parameter dependence of τ_0, we kept z_0 constant unless otherwise stated.

r_0 is a geometrical quantity which characterizes the overlap of the two colliding nuclei in the transverse plane. Therefore, it is expected to depend only on the impact parameter of the collision and we calculate it as follows: we evaluate within a Glauber model the density of participant nucleons in the transverse plane. Due to the Wood-Saxon parameterization of the nuclear profile of the colliding nuclei, the distribution of participant nucleons does not have sharp edges and we apply a cutoff at the distance $r \equiv r_0$ when the density has dropped by a factor $1/e$ with respect to its maximal value. This defines our initial volume inside which the number of participant nucleons given by a Glauber calculation is distributed homogeneously.

The entropy over baryon number is determined to reproduce the correct multiplicities of observed particles and its value grows from $s/n_B = 26$ at SPS to $s/n_B = 250$ at RHIC. It is fully consistent with the (T, μ_B) chemical freeze-out parameters inferred from hadro-chemistry analysis [7, 8]. The total entropy of the system at a given impact parameter is then obtained by multiplying the s/n_B ratio by the number of net baryons included in the rapididty range covered by the fireball. The centrality dependance of the net baryon number is assumed to be proportional to the number of participants whose distributions as a function of the impact parameter b are shown in Fig. 5.3 for the three different systems we have considered: *S-U*, *Pb-Pb* at SPS and *Au-Au* at RHIC.

Note that the parameters $\{v_z, a_z, a_\perp\}$ are also centrality dependent since we expect less stopping (*i.e.* $v_z^{peri.} > v_z^{cent.}$) and smaller pressure gradient (*i.e.* $a_\perp^{peri.} < a_\perp^{cent.}$) in peripheral collisions compared to central ones. However, the sensitivity of our results with respect to these variations is small.

We take into account the cms energy dependence of T_c (less stopping entails a smaller μ_B and hence a larger T_c) which increases smoothly from $T_c = 170$ MeV at SPS to $T_c = 180$ MeV at RHIC. The baryon and strangeness chemical potential at T_c are inferred from $\bar{p}/p$ and $\bar{\Lambda}/\Lambda$ ratio and their energy dependence is shown in Fig. 5.4. It was recently realized [9] that at RHIC, the experimental fact of anti-baryon conservation affects appreciably the evolution of the hadronic phase. This is implemented using an effective baryon chemical potential μ_B^{eff} which results in a much faster cooling of the system as well as larger baryon chemical potential at thermal freezeout (compared to previous hydro calculations [10]). Thus, we observe that the baryon chemical potentials μ_B have (approximately) a linear temperature dependence, from their value at chemical

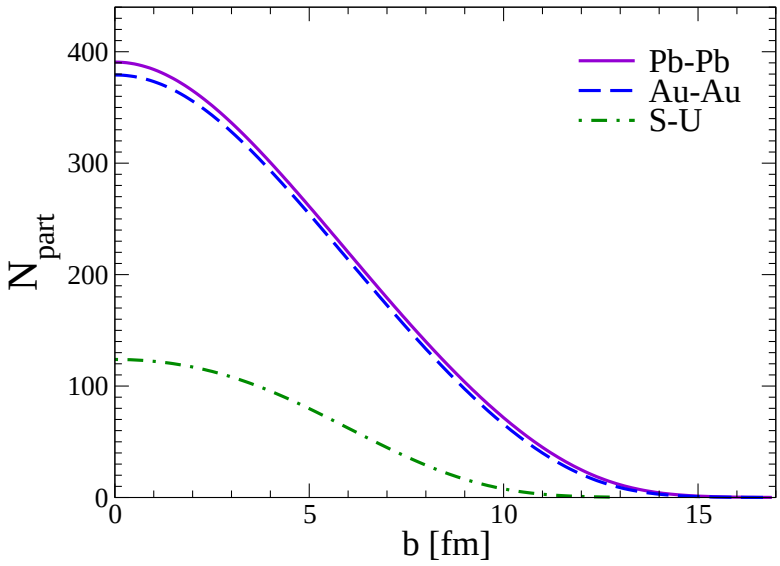

Figure 5.3: Number of participant nucleons versus the impact parameter b of the collision within a Glauber picture for three different systems: *S-U*, *Pb-Pb* at SPS and *Au-Au* at RHIC.

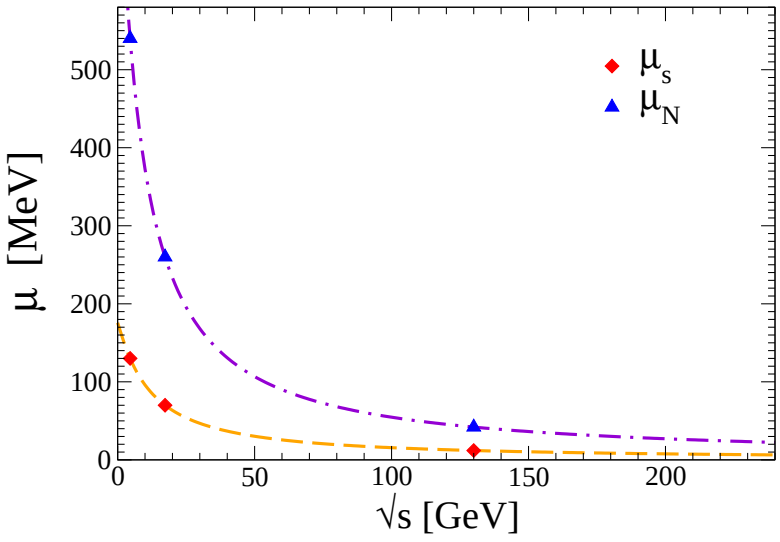

Figure 5.4: Excitation function of the baryon chemical potential $\mu_B(T_c)$ (dot-dashed line) and the strangeness chemical potential $\mu_s(T_c)$ (dashed line). The points correspond to extracted values from particle ratios, while the curve correspond to empirical fits.

freezeout to essentially $\mu_B \simeq m_N$ at $T = 0$.

The thermal fireball model includes light-hadron chemical potentials (required to maintain the numbers of particles which do not decay strongly: pions, kaons, ...) which build up in the hadronic phase when the system cools down from the chemical freeze-out to the thermal freeze-out. To reproduce, the observed pion multiplicities, the pion chemical potential typically reaches $\mu_\pi \simeq 80$ MeV at thermal freeze-out.

Finally, we also accounted for $10 - 20\%$ variations in s/n_B with centrality following particle production systematics reported by NA49 [11] and PHOBOS [12].

5.1.3 Successes and limitations of the fireball model

It is important to emphasize the general approach we have adopted in this work: As mentioned in the Introduction, we tried to develop a consistent picture of heavy-ion collisions including, but not limited to, charmonium production. Despite the few quantities entering the thermal fireball model, we do not consider them as actual parameters of the calculation of the charmonium yield in heavy-ion collisions. Our fireball evolution had been developed earlier to calculate dilepton production in heavy-ion collisions [13]. The same framework was also used to resolve the anti-proton puzzle at SPS and RHIC [14] and to evaluate direct photon production [15]. The idea is to attempt, within this common fireball evolution, a coherent picture of the hadro-chemistry, the space-time evolution, as well as dilepton and charmonium production in heavy-ion collisions.

We, however, keep in mind that fireball models give a rather simplified picture of the reaction dynamics of a heavy-ion collision. The uniform temperature and density profiles of the fireball should be understood as an average of hydrodynamical calculations. In addition, the formation time τ_0 bears appreciable uncertainty (as in hydrodynamics), especially for peripheral collisions where the validity of fireball models is not really established. We nevertheless expect to capture the main features of the space-time evolution of the system, at least for central to mid-central collisions.

Bibliography

[1] P. F. Kolb and U. Heinz, (2003), nucl-th/0305084.

[2] W. Cassing and E. L. Bratkovskaya, Phys. Rept. **308**, 65 (1999).

[3] R. Rapp and J. Wambach, Eur. Phys. J. **A6**, 415 (1999), hep-ph/9907502.

[4] R. Rapp and E. V. Shuryak, Phys. Lett. **B473**, 13 (2000), hep-ph/9909348.

[5] P. Braun-Munzinger, K. Redlich, and J. Stachel, (2003), nucl-th/0304013.

[6] K. Kajantie, J. Kapusta, L. D. McLerran, and A. Mekjian, Phys. Rev. **D34**, 2746 (1986).

[7] P. Braun-Munzinger, I. Heppe, and J. Stachel, Phys. Lett. **B465**, 15 (1999), nucl-th/9903010.

[8] P. Braun-Munzinger, D. Magestro, K. Redlich, and J. Stachel, Phys. Lett. **B518**, 41 (2001), hep-ph/0105229.

[9] R. Rapp, Phys. Rev. **C66**, 017901 (2002), hep-ph/0204131.

[10] P. Huovinen, P. F. Kolb, U. W. Heinz, P. V. Ruuskanen, and S. A. Voloshin, Phys. Lett. **B503**, 58 (2001), hep-ph/0101136.

[11] NA49 Collaboration, J. Bachler *et al.*, Nucl. Phys. **A661**, 45 (1999).

[12] PHOBOS Collaboration, B. B. Back *et al.*, Phys. Rev. **C65**, 061901 (2002), nucl-ex/0201005.

[13] R. Rapp and J. Wambach, Adv. Nucl. Phys. **25**, 1 (2000), hep-ph/9909229.

[14] R. Rapp and E. V. Shuryak, Phys. Rev. Lett. **86**, 2980 (2001), hep-ph/0008326.

[15] S. Turbide, R. Rapp, and C. Gale, (2003), hep-ph/0308085.

Chapter 6

Two-Component Model of Charmonium Production in Heavy-Ion Collisions

On the one hand, according to the "standard" suppression picture of Matsui and Satz [1], in heavy-ion collisions, J/ψ's are produced in early hard N-N collisions and are then subjected to nuclear, plasma (if any) and hadronic suppression. Within this scenario, the number of J/ψ's remaining at the end of the collision, which we refer to as "direct" J/ψ's, can be calculated by integrating the plasma and hadronic dissociation rates detailed in Chapter 4 over the space-time history of the collision given by our fireball model of Chapter 5.

On the other hand, following the recent suggestion that statistical hadronization provides another mechanism for J/ψ production in heavy-ion collisions, some authors [2, 3, 4, 5] have attempted to describe the J/ψ yield in *Pb-Pb* collisions at SPS solely in terms of statistical production as delineated in Sec. 3.3.2. However, a common assumption shared by the latter models is that the primordial production of J/ψ is absent: J/ψ's either do not form or are fully destroyed in the plasma, which at SPS energies, with expected plasma lifetimes of $1 - 2$ fm/c in conjunction with initial temperatures below 250 MeV is hardly conceivable. In addition, to reproduce the observed J/ψ yield in central *Pb-Pb* collisions at SPS, statistical models require a significant (up to a factor $\times 3$) increase in the open-charm production which is not easily justified theoretically.

This led us to propose in [6] a two-component model for charmonium production in heavy-ion collisions. It incorporates both *(i)* a primordial yield (subject to subsequent

dissociation) as well as *(ii)* a thermal contribution from statistical recombination of c and $\bar{c}$ quarks at the hadronization transition. Both components are evaluated within the common thermal fireball framework described in the previous chapter. Another important feature is that we refrain from invoking any "anomalous" open-charm enhancement.

6.1 Two-component model

We first describe the two separate components which make up the observed J/ψ yield in heavy-ion collisions. Let us mention that in the remainder of this chapter, we will not consider any medium effects (besides the reduction of charmonia binding energies in the plasma, entering the quasifree dissociation calculation). Medium effects on the J/ψ yield will be assessed separately in Chapter 7.

6.1.1 "Direct" component

The direct component corresponds to the J/ψ's that are initially produced in hard N-N collisions and subjected to various suppression mechanisms. Therefore the corresponding yield is given by the product of the initial hard production times the survival probabilities for a charmonium state Ψ at the end of the collision. The latter are calculated as follows: we start from the evolution equation for the number of each charmonium species i ($i = J/\psi, \psi', \chi$) in the system at time τ,

$$\frac{dN_i(\tau)}{d\tau} = -\Gamma^i_{diss} N_i(\tau) \ . \tag{125}$$

The destruction rate Γ^i_{diss} is specified according to the phase and temperature $T(\tau)$ of the system,

$$\Gamma^i_{diss} = \begin{cases} \Gamma^i_{QGP} \ , & T > T_c \\ f\Gamma^i_{HG} + (1-f)\Gamma^i_{QGP} \ , & T = T_c \\ \Gamma^i_{HG} \ , & T < T_c \end{cases} \tag{126}$$

with f given by Eq. (124), Γ^i_{QGP} and Γ^i_{HG} from Secs. 4.1.3 and 4.3. Eq. (125) is readily integrated to obtain the survival probability at time τ during the collision,

$$\mathcal{S}^i_{QGP+HG}(\tau) = e^{-\int_0^\tau \Gamma^i_{diss}(\tau')d\tau'} \ . \tag{127}$$

The final survival probability, $\mathcal{S}_{QGP+HG}$, relevant for experimental observables is given by the value of $\mathcal{S}^i_{QGP+HG}(\tau)$ at the moment of thermal freeze-out, τ_{fo}, where all hadrons

cease to interact. Note that $\mathcal{S}^i_{QGP+HG}$ depends on the impact parameter b of the collision through the space-time evolution of the system.

Fig. 6.1 shows J/ψ and ψ' survival probabilities at full SPS and RHIC energies for central collisions ($N_{part} = 360$) as a function of time with a value of $g = 1.7$ for the strong coupling constant (which provides reasonable agreement with SPS data to be discussed below). Most of the suppression originates from the plasma and mixed phases, with

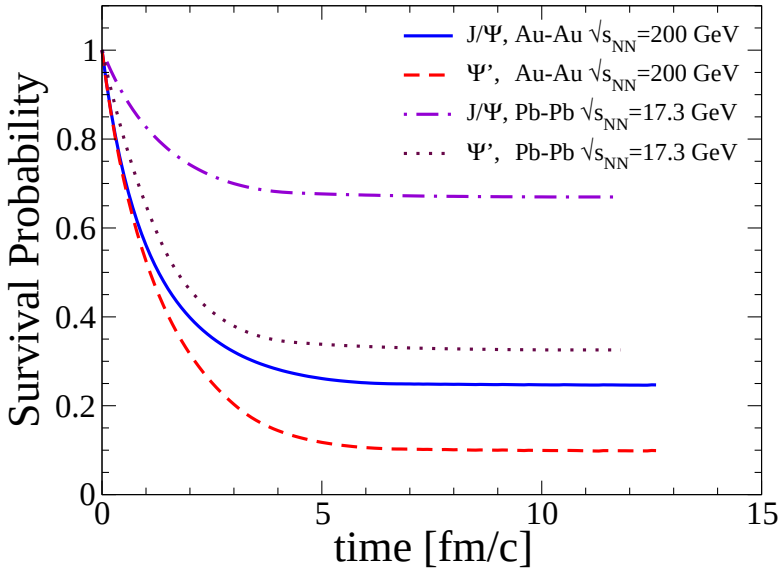

Figure 6.1: Survival probability of J/ψ (dot-dashed line: SPS, solid line: RHIC) and ψ' (dotted line: SPS, dashed line: RHIC) for central collisions ($N_{part} = 360$) as a function of time. The curves are obtained upon integration of the dissociation rates calculated in Secs. 4.1.3 and 4.3.

hadronic effects playing little role. Under SPS conditions, the destruction of ψ' states (dotted line) turns out to be far from complete (with a fraction of about 1/3 remaining at the end of the collision); this may in fact point at a lack of our understanding of the hadronic ψ' interactions, since *(i)* it will cause problems in describing the measured ψ'/ψ ratio (see Sec. 6.2.3), and *(ii)* it appears to be incompatible with recent interpretations of lattice calculations [7, 8] which claim a dissolution of the ψ' in the hadronic phase (although no statement about time-scales could be made). As expected, the overall dissociation is much stronger at RHIC (full line: J/ψ; dashed line: ψ'), although 25% of primordial J/ψ's endure the evolution.

For a combination of the (suppressed) primordial production with the statistical one it is necessary to convert the survival probabilities into absolute yields. At a given impact parameter b, the number of J/ψ mesons initially produced in hard N-N collisions

is

$$N^0_{J/\psi}(b) = \sigma^{J/\psi}_{pp} ABT_{AB}(b) \ . \tag{128}$$

Data on charmonium production in p-p collisions in the RHIC energy regime still bear appreciable uncertainties. The PHENIX collaboration reported [9]

$$\sigma^{J/\psi}_{pp} = 3.99 \pm 0.61(\text{stat}) \pm 0.58(\text{sys}) \pm 0.40(\text{abs}) \ \mu\text{b} \ , \sqrt{s_{NN}} = 200 \ \text{GeV} \tag{129}$$

where $\sigma^{J/\psi}_{pp}$ has not been corrected for feeddown from ψ' and χ's. This is somewhat in between a phenomenological fit based on low-energy systematics, the so-called Schuler parameterization [10], giving $\sigma^{J/\psi}_{pp}(\sqrt{s} = 200 \ \text{GeV}) = 1.0\mu\text{b}$ and the simple ansatz $\sigma^{J/\psi}_{pp} = f\sigma^{c\bar{c}}_{pp}$ with $f \simeq 0.025$ [11] (which, together with LO pQCD extrapolations of open-charm production, also reproduces low-energy data and leads to $\sigma^{J/\psi}_{pp}(\sqrt{s} = 200 \ \text{GeV}) = 8.75 \ \mu\text{b}$). This obviously introduces appreciable uncertainties in establishing the J/ψ yield arising from primordial production mechanisms.

In addition, higher charmonium states (in particular ψ' and various χ states) contribute significantly to the measured J/ψ abundance via strong and electromagnetic decays (feeddown). Since these resonances have different hadronic and plasma cross sections, the distinction between prompt and secondary J/ψ's has to be made. Consequently, the total number of J/ψ's stemming from primordial charmonium states after nuclear, plasma and hadronic suppression, becomes

$$N^{dir}_{J/\psi}(b) = \sigma^{J/\psi}_{pp} ABT_{AB}(b) \mathcal{S}_{nuc} \left[0.6\mathcal{S}^{J/\psi}_{QGP+HG} + 0.08\mathcal{S}^{\psi'}_{QGP+HG} + 0.32\mathcal{S}^{\chi}_{QGP+HG} \right] \ . \tag{130}$$

6.1.2 "Statistical" component

Statistical models [12, 13] and their application to charmonium production [3, 4, 5, 14] have already been discussed in detail in Sec. 3.3.2. The thermal equilibrium (but chemical off-equilibrium) J/ψ yield takes the form

$$N^{th}_{J/\psi} = \gamma_c^2 V_H n_{J/\psi} \ . \tag{131}$$

Here, V_H denotes the fireball volume from Sec. 5.1 at the moment when hadronization is complete, $V_H \equiv V_{FB}(\tau = \tau_H)$. We recall that γ_c is obtained upon solving

$$N_{c\bar{c}} = \frac{1}{2}\gamma_c \ n_{op} \ V_H \ \frac{I_1 \left(\gamma_c n_{op} V_H\right)}{I_0 \left(\gamma_c n_{op} V_H\right)} + \gamma_c^2 n_{hid} V_H \ , \tag{132}$$

to account for the chemical off-equilibrium situation (in the charm sector) encountered in heavy-ion collisions at SPS and RHIC energies. The actual value of $N_{c\bar{c}}$ depends on

both collision energy and impact parameter. The former dependence is inferred from PYTHIA computations [15] upscaled by an empirical K-factor ($K \sim 5$) extracted from a best fit to existing pN and πN data [16]. Such an extrapolation to RHIC energies compares well with recent measurements from the PHENIX collaboration which found [15]

$$\sigma_{pp}^{c\bar{c}} = 380 \pm 60(\text{stat}) \pm 200(\text{sys}) \ \mu\text{b} \ , \sqrt{s_{NN}} = 130 \ \text{GeV} \tag{133}$$

using single-electron p_T-spectra to infer indirectly $\sigma_{pp}^{c\bar{c}}$. At full RHIC energy, preliminary results indicate $\sigma_{pp}^{c\bar{c}}(\sqrt{s} = 200GeV) \simeq 650\mu$b (with large error bars). Such cross-sections are larger than the next-to-leading order pQCD estimates [17, 18] which gives $\sigma_{pp}^{c\bar{c}} \simeq 350\mu$b at full RHIC energy.

By construction, statistical charmonium production at T_c is only active for c and $\bar{c}$ that emerge from a deconfined environment prior to recombination. Therefore, in peripheral collisions where the initial volume is only partially filled with the QGP phase, only a fraction of the $c\bar{c}$ pairs is available for coalescence. Accordingly, the hadronization volume which enters Eq. (132) arises from the initial volume in the plasma phase after expansion and $N_{c\bar{c}}$ is distributed between the plasma and hadronic phases following the respective volume partitions.

Eq. (131) is valid if (anti-) charm quarks are kinetically equilibrated, *i.e.* the momentum distribution of c and $\bar{c}$ quarks is thermal which is questionable under SPS and even RHIC conditions. We therefore implement the following correction: we introduce a thermalization time τ_{eq} for c and $\bar{c}$ quarks, approximated as $\tau_{eq} = 1/n\sigma$, where n is the total density of quark- and gluon-quasiparticles in the system, and σ is the elastic scattering cross section for the processes $g(q,\bar{q}) + c(\bar{c}) \to g(q,\bar{q}) + c(\bar{c})$. Within a relaxation time approach, the relative reduction $\mathcal{R}$ in thermal J/ψ formation is then estimated as

$$\mathcal{R} = \left[1 - \exp\left(-\int_0^{\tau_H} \frac{d\tau}{\tau_{eq}}\right)\right] \ , \tag{134}$$

where τ_H is the time at which hadronization is completed. Our expression for the number of J/ψ's produced at the hadronization transition by coalescence of a c and $\bar{c}$ quark is thus modified according to

$$N_{J/\psi}^{th} = \gamma_c^2 \ V_H \ n_{J/\psi} \mathcal{R} \ . \tag{135}$$

We have checked that our results do not change significantly with the definition adopted for τ_H. The latter is not a sharply defined quantity since the mixed phase lasts for a few

fm/c. However, smaller values of τ_H (*e.g.*, if taken in the middle of the mixed phase) lead to smaller volumes and larger γ_c implying an increase in thermal J/ψ production which, in turn, is (partially) compensated by a lesser degree of thermalization through a smaller value of $\mathcal{R}$.

The charmonia statistically produced at the hadronization transition are still subject to reinteractions in the hadronic phase, so that their final contribution to the observed J/ψ yield is accounted for via

$$N_{J/\psi}^{th} = \gamma_c^2 \; V_H \left[n_{J/\psi} \; \mathcal{S}_{HG}^{J/\psi} + \sum_X n_X \; \mathcal{S}_{HG}^X BR(X \to J/\psi) \right] \; \mathcal{R} \; , \tag{136}$$

where the summation is carried over the charmonium states X with finite decay branching into J/ψ's (feeddown).

6.2 Comparison with experiments at SPS

By combining the two sources of charmonium as discussed in the previous sections, we now turn to applications to heavy-ion collisions at SPS energy ($\sqrt{s}_{NN} = 17.3$ GeV). We first address the observable that has drawn the most attention, *i.e.* the centrality dependence of the J/ψ yield, and then investigate the ψ'/ψ ratio.

6.2.1 Centrality dependence of J/ψ production

One important finding of the NA38 and NA50 experiments at CERN is that the J/ψ yield in p-p and p-A collisions with light and heavy targets is well explained by hard production coupled with nuclear absorption, cf. Sec. 2.3. Thus, any attempt to describe the J/ψ yield in heavy-ion collisions should reproduce this feature. In particular, for very peripheral collisions involving only a few participant nucleons, the J/ψ suppression pattern should coincide with nuclear absorption.

In our two-component model, the total number of observed J/ψ's is the sum of direct and statistical production according to Eqs. (130) and (136), respectively,

$$N_{J/\psi} = N_{J/\psi}^{dir} + N_{J/\psi}^{th} \; . \tag{137}$$

Both terms on the right-hand side depend on centrality (via the impact parameter b) and collision-energy. For very peripheral collisions in the SPS regime, the initial conditions are not energetic enough to induce a transition into the QGP. Therefore, the J/ψ source

of statistical recombination at T_c is absent; at the same time the hadronic interactions are not frequent enough to induce sizable effects. Thus, for large impact parameters our approach is consistent with the NA38/NA50 results.

For a detailed comparison with data, we need to evaluate the ratio $B_{\mu\mu}\sigma^{J/\psi}/\sigma^{DY}$ commonly displayed by NA38/NA50 as a function of the transverse energy deposited in their calorimeter. Following the treatment outlined in Sec. 2.3, we convolute our theoretical results (which are obtained as a function of the impact parameter b) with the probability distribution $\mathcal{P}(E_T, b)$. This amounts to replacing the numerator in Eq. (39) by the expression

$$B_{\mu\mu}\sigma_{J/\psi}(E_T) = B_{\mu\mu}\sigma^{pp}_{J/\psi}\int d^2b\, \mathcal{P}_{AB}(E_T,b) \times \left[\mathcal{S}_{nuc}\mathcal{S}_{QG+H} + N^{th}_{J/\psi}/(\sigma^{pp}_{J/\psi}ABT_{AB}(b))\right] T_{AB}(b)\ . \qquad (138)$$

Our results are compared to NA38/NA50 data in Fig. 6.2 for both the S(200 AGeV)-U (left panel) and Pb(158 AGeV)-Pb (right panel) systems. At all centralities, direct pro-

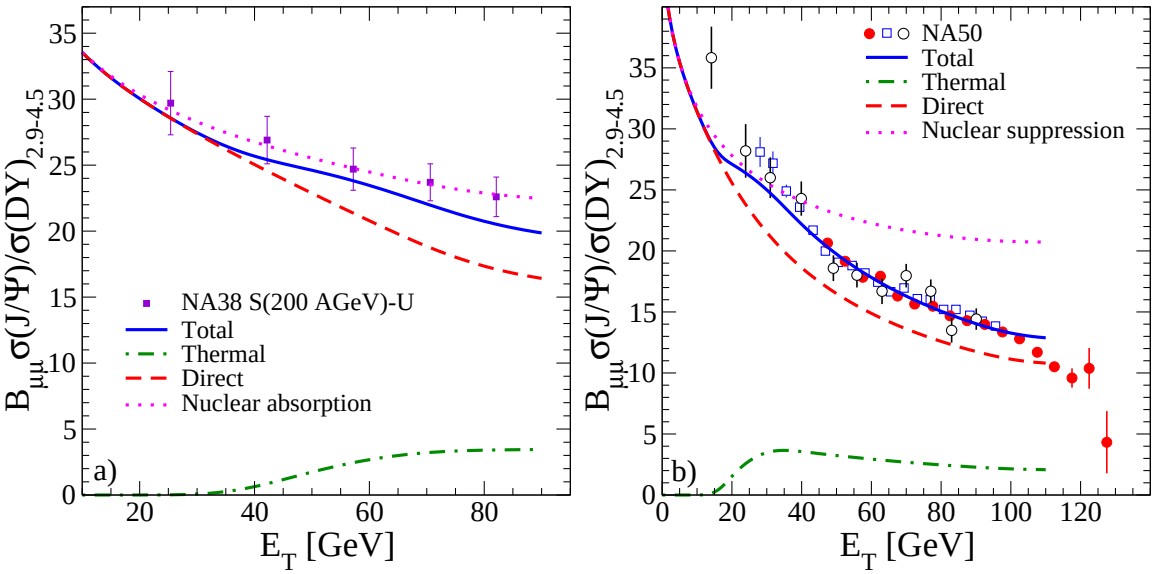

Figure 6.2: Results on J/ψ production within the two-component model as a function of centrality compared to NA38 [19] (left panel) and NA50 data [20] for S(200 AGeV)-U and Pb(158 AGeV)-Pb, respectively. Dotted lines: direct production with nuclear absorption alone; dashed lines: direct production subject to nuclear, QGP and hadronic absorption; dot-dashed lines: statistical (thermal) production from a hadronizing QGP including hadronic dissociation; solid lines: combined direct and statistical yield (sum of dashed and dot-dashed lines).

duction (dashed line) prevails over the thermal component (dot-dashed line). The latter

sets in once a QGP starts forming, which, in turn, requires a stronger QGP suppression of the direct component than without the thermal contribution. The adjustment of the only free parameter (strong coupling constant $g = 1.7$) to the most central *Pb-Pb* data allows for a satisfactory reproduction of the centrality dependence for this system. For *S-U* collisions, the results are somewhat on the low side. Note that in our approach the "drop" in the *Pb-Pb* data around $E_T \simeq 40$ GeV is a combination of a rather strong QGP suppression coupled with the onset of thermal production.

6.2.2 High E_T effects in the NA50 experiment

So far, our model does not capture the appearance of the "second drop" in the data for the most central *Pb-Pb* collisions at $E_T > 100$ GeV. In fact, the maximum transverse energy in our description is at $E_T^{max} = E_T(b = 0) = 100$ GeV, well below the experimental limit which extends up to $E_T \simeq 125$ GeV. It has been suggested that these features are associated with transverse energy fluctuations [21, 22, 23] and/or trigger energy losses [24], and are thus not necessarily related to a shortcoming in an underlying (microscopic) model description of J/ψ production (suppression).

Let us first address the E_T fluctuations. From the minimum bias (MB) event distribution of transverse energy, dN/dE_T, as measured in the NA50 apparatus [25], one finds a rapid falloff beyond $E_T = 100$ GeV, the so-called "knee" of the distribution. The tail of the latter, which reaches beyond $E_T = 100$ GeV, is associated with fluctuations in transverse energy at fixed geometry for $b = 0$. Events which fluctuate beyond $E_T > 100$ GeV contain a larger initial entropy and consequently have a hotter initial temperature and a longer plasma phase which implies additional J/ψ suppression (charm and J/ψ production being hard processes are not coupled to fluctuations in the "soft" sector). To account for this phenomenon [21], we replace in our calculations the total entropy at fixed impact parameter, $S_{tot}(b)$, by

$$S_{tot}(b) \to S_{tot}(b)\frac{E_T}{E_T(b)} \ . \tag{139}$$

This does not affect our results for $E_T \leq E_T(b = 0) \simeq 100$ GeV, but beyond the knee of the distribution, S_{tot} is enhanced by the factor $E_T/E_T(b = 0)$. The effect of this modification is shown in the left panel of Fig. 6.3, where we compare our calculations to data on J/ψ production normalized to the minimum bias E_T-distribution[1]. Obviously,

[1]This way of normalizing the data has the advantage of the much better statistics for dN/dE_T as

the description of the observed turnover for $E_T > 100$ GeV is improved by inclusion of E_T-fluctuations (cf. dashed versus dot-dashed curve), but does not suffice to quantitatively explain the data. Note that this effect relies on additional J/ψ suppression in both the direct component (due to stronger suppression) and the thermal component (due to a larger hadronization volume entailing a smaller value of γ_c at fixed $N_{c\bar{c}}$ and thus weakening the enhancement induced by the canonical-ensemble treatment).

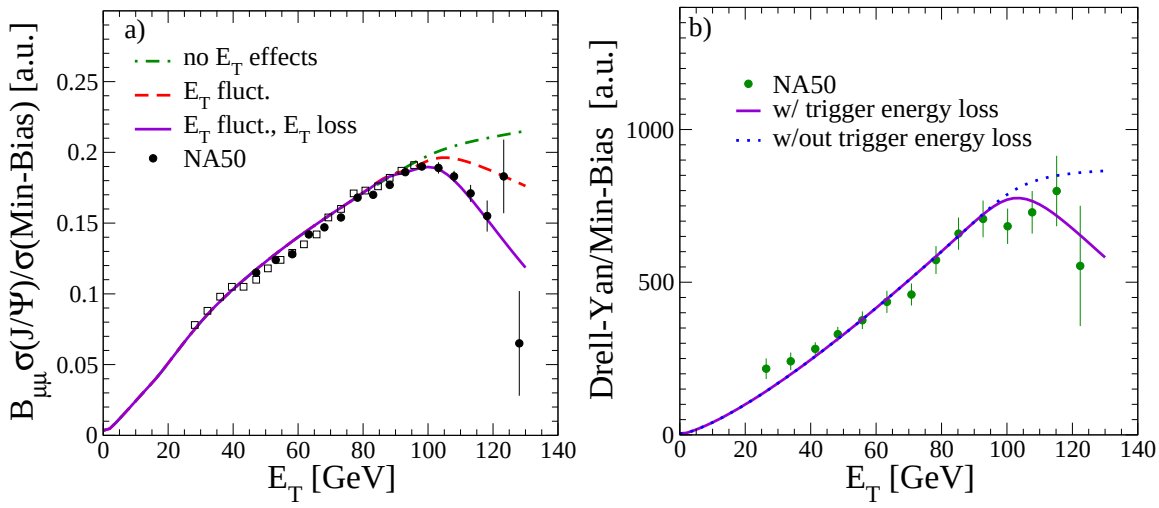

Figure 6.3: Left panel: J/ψ over Minimum Bias (MB) ratio compared to calculations within the two-component model (dot-dashed curve) with additional inclusion of effects due to E_T fluctuations (dashed curve) and trigger energy loss (solid curve). Right panel: impact of a model for trigger energy loss on the Drell-Yan (DY) over MB ratio. All data points are from NA50 for Pb(158 AGeV)-Pb [25].

However, as has been suggested by Capella *et al.* [24], there might be an additional feature in the large E_T-region unrelated to J/ψ physics, which can be gleaned from the Drell-Yan (DY) over minimum bias data, cf. right panel of Fig. 6.3. The theoretical ratio DY/MB (dotted line) computed by NA50 flattens out at large values of $E_T > 100$ GeV, whereas the data seem to indicate a slight turnover [25]. The argument [24] to explain this turnover (which equally applies to the J/ψ event sample) is that for DY-events the hadronic transverse energy deposited in the calorimeter is slightly reduced as compared to the corresponding MB-events due to triggering on the DY (or J/ψ) pair (2.9 GeV$< M_{DY} <$4.5 GeV). As elaborated in Ref. [24] a estimate of this effect is obtained by rescaling the amount of transverse energy in the J/ψ and DY events

compared to the Drell-Yan sample. On the other hand, since E_T production is governed by soft physics (which essentially scales with the number of participants rather than the number of N-N collisions), the characteristic features of J/ψ suppression are not readily discernible.

according to

$$E_T(b) \rightarrow E_T(b)\frac{N_{part}-2}{N_{part}} \ . \tag{140}$$

When incorporated into the E_T-b correlation, Eq. (37), this rather small loss in E_T entails a drop of up to ∼20-30% in the tail of the (DY/MB) distribution, cf. Fig. 6.3 (solid curve in the right panel).

Returning to the $(J/\psi)/MB$ ratio (left panel of Fig. 6.3), we see that the combined effect of E_T fluctuations and trigger energy loss, implemented within our microscopic model, gives a satisfactory description of the experimental findings. This also holds true for the more common representation of the data via the $J/\psi/DY$ ratio, cf. Fig. 6.4. Note that in this case the trigger energy-loss correction only applies to the "MB" data sets, which have been extracted using a theoretical expression for the MB/DY ratio according to

$$\left(\frac{J/\psi}{DY}\right)_{MB\ analysis} = \left(\frac{J/\psi}{MB}\right)_{exp}\left(\frac{MB}{DY}\right)_{th} \ , \tag{141}$$

where the theoretical DY/MB ratio is illustrated by the dotted line in the right panel of Fig. 6.3.

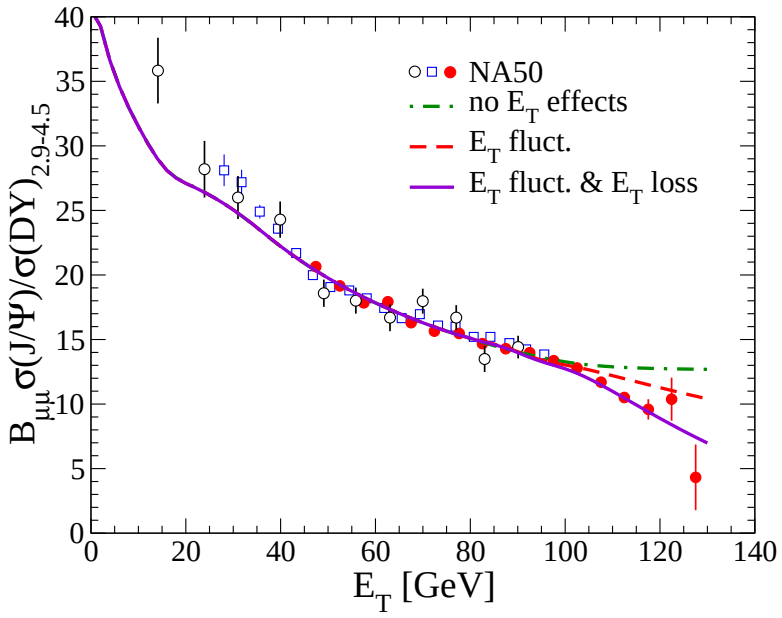

Figure 6.4: Results of the two-component model without (dot-dashed line) and with additional inclusion of transverse energy fluctuations (dashed line) and trigger energy loss (full line), for the centrality dependence of the $B_{\mu\mu}\sigma^{J/\psi}/\sigma^{DY}$ ratio in Pb(158 AGeV)-Pb collisions.

6.2.3 Ψ'/Ψ ratio

In p-p collisions in the SPS energy regime, the ratio of produced ψ' to J/ψ mesons amounts to a value of about 15%, which persists for p-A collisions as nuclear absorption affects both charmonium states in practically the same way, cf. Sec. 2.3. A marked deviation from this behavior has been observed in S(200 AGeV)-U and Pb(158 AGeV)-Pb collisions, with an onset at rather low centralities. For central collisions, the ψ'/ψ ratio does not seem to go to zero, but rather levels off at a value of around 3-4% (corresponding to the straight line in Fig. 6.5, which however includes the branching ratios of J/ψ and ψ' into dimuons). This is contrary to the expectation that ψ' mesons, due to their much smaller binding energy than the J/ψ states, would be almost completely suppressed. In Ref. [26] it has been suggested that, under the premise that all ψ' states are dissolved in the QGP, their abundance is regenerated in the hadronic phase from remaining Ψ states as a consequence of chiral symmetry restoration, via the process $\psi + \pi \to \psi' + \pi$. The interaction was assumed to be mediated through $\sigma(500)$ meson exchange, the mass of the latter approaching the pion mass thereby substantially enhancing ψ' formation. From another point of view, the fact that the value of 4% reflects the thermal ratio of ψ'/ψ at a temperature of $T = 170$ MeV (with little latitude), has been put forward in Ref. [3] as evidence for statistical charmonium production at the hadronization transition.

Within our two-component model as laid out above, the ψ'/ψ ratio follows without further assumptions. The results for both S-U and Pb-Pb systems are compared to NA38/50 data in Fig. 6.5. The discrepancy with experiment is rather significant, both for S(200 AGeV)-U and Pb(160 AGeV)-Pb. Since in the former reaction QGP effects are not expected to play a pronounced role, it seems that the deficiency in our description has to be assigned to the hadronic phase, *i.e.* an underestimation of the hadronic cross sections for the ψ'. Indeed, an artificial increase of this quantity by, *e.g.*, a factor of 5 clearly improves the agreement with the data. We have checked that such an increase in the ψ' hadronic cross sections has negligible impact on the ψ/DY ratio as plotted in Fig. 6.4 (the ψ' contributes maximally 8% to the observed J/ψ yield).

As mentioned before, recent lattice calculations indicate a large width of the ψ' in a static environment well below the phase transition temperature, due to the lowering of the $D\bar{D}$ continuum threshold below the in-medium ψ' mass. In a hadronic model framework, this can be implemented by an in-medium reduction of the D-meson masses,

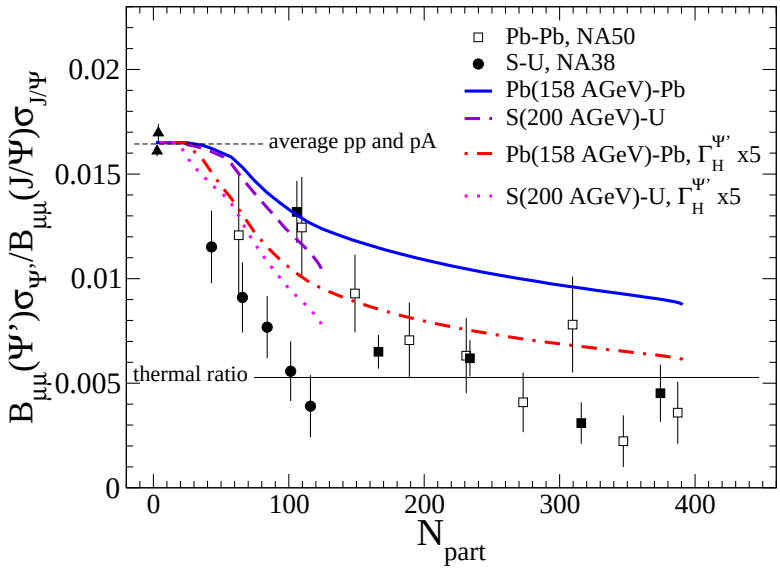

Figure 6.5: Our calculations for the centrality dependence of ψ'/ψ compared to data from NA38/50. The solid and dashed line are for S(200 AGeV)-U and Pb(158 AGeV)-Pb, respectively, using hadronic ψ' dissociation cross sections obtained by geometric scaling of the J/ψ one, cf. Fig. 4.12. The dashed and dotted lines are the corresponding results when artificially increasing the ψ' cross sections by another factor of 5.

which has been motivated in Ref. [27] by chiral restoration arguments inducing a lowering of the light-quark mass within the $c\bar{q}$ and $\bar{c}q$ states. We have investigated this possibility within the hadronic approach employed here, and found a strong sensitivity to the detailed modeling of the light-quark related portion of the D-meson masses. In fact, if the lifetimes of the charmonium states become comparable to duration of the fireball expansion, one needs to account for the reverse reaction of charmonium formation (as required by detailed balance), which is further investigated in Chapter 7[2].

6.2.4 Comparison to other model approaches at SPS

Alternative models to describe the J/ψ centrality dependence observed at SPS exist, which we review below. Two main mechanisms have been considered to explain the "anomalous" [28] J/ψ suppression (*i.e.* beyond normal nuclear matter absorption) reported by the NA50 collaboration, for Pb(158 AGeV)-Pb collisions. The extra suppression is either attributed to J/ψ destruction in the QGP [29, 30, 31] or to interactions with comoving hadrons [32, 33]. A third approach, recently developed, attributes the

[2]Note that with an increase by a factor of 5 for ψ' dissociation rate over the results shown in Fig. 4.12 (as applied in Fig. 6.5) the ψ' lifetimes in the vicinity of T_c are indeed close to the expansion time of the hadronic phase.

J/ψ yield in central *Pb-Pb* collisions to statistical production [3, 5, 4].

J/ψ suppression by Quark-Gluon Plasma formation

Blaizot and Ollitrault proposed in [29] a simple model in which J/ψ suppression is related to the local energy density of the matter created in the collision. They assume that above a critical energy density ε_c, *all* J/ψ's are destroyed. The magnitude of the suppression is then related to the size of the fireball region whose local energy density exceeds ε_c. Since the maximum energy densities reached in *S-U* and *Pb-Pb* collisions at SPS do not differ by more than 35% (according to Glauber type calculations), this indicates a strong sensitivity of the suppression mechanism to the local energy density, which is naturally attributed to Quark-Gluon Plasma formation. The critical energy density ε_c above which plasma suppression sets in is determined by comparing the density of participants in the transverse plane in *S-U* collisions (where no plasma is assumed to be formed) to the ones of *Pb-Pb* collisions [29]. The results of such a calculation are shown in Fig. 6.6. Such a model gives a very good description of

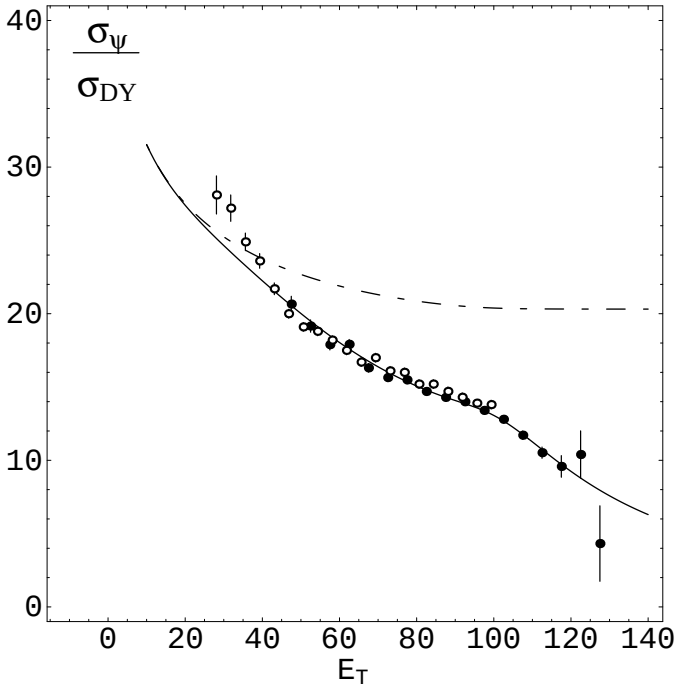

Figure 6.6: J/ψ centrality dependence, including transverse energy fluctuations at large E_T, in the model of Blaizot and Ollitrault [22].

the J/ψ centrality dependence observed at the SPS. Similar attempts to attribute the "anomalous" J/ψ suppression to Quark-Gluon Plasma formation differ by the criterion

determining when the J/ψ destruction occurs. *E.g.*, in [8], J/ψ's are destroyed above a critical temperature T_{crit} corresponding to the Debye temperature above which J/ψ formation is prevented by color screening of the $c\bar{c}$ potential in the plasma. We have considered a scenario of J/ψ suppression in the plasma based on [29, 22] which leads to a plasma suppression comparable to our quasifree mechanism, see Sec. 6.3.5. However, pictures relying on plasma suppression alone entail very different predictions for the J/ψ abundances at RHIC compared to our two-component approach.

J/ψ suppression by comoving hadrons

J/ψ suppression has also been interpreted in terms of J/ψ interactions with comoving hadrons [32, 33]. In such models, besides nuclear absorption, J/ψ is further suppressed by the comover interaction suppression factor $\mathcal{S}^{co}$ written as [34]

$$\mathcal{S}^{co}(b,s) = \exp\left[-\sigma^{co}\frac{3}{2}N^{co}(b,s)\ln\left(\frac{\frac{3}{2}N^{co}(b,s)}{N^{co}_{pp}}\right)\right] , \tag{142}$$

where $N^{co}(b,s)$ is the local density of charged comovers in the rapidity region of the dimuon trigger and N^{co}_{pp} the corresponding density in p-p collisions. The factor 3/2 accounts for neutral particles. The J/ψ-comover cross-section σ^{co}, assumed to be a constant, is left as a free parameter of the model, together with the absolute normalization. Comover models differ by the assumptions made for the local density of comovers, *e.g.* taken to be proportional to the density of participants in the transverse plane $N^{co}(b,s) \propto N_{part}(b,s)$ [31, 35], or calculated within the Dual Parton Model [36, 24]. Fig. 6.7 illustrates the results of the comover model which are also in good agreement with the NA50 data set. Comover models, upon reasonable assumptions on the ψ'-comover cross-section can describe the ψ'/ψ ratio at SPS [37]. Comover models are often presented as an *hadronic* alternative to explain J/ψ suppression without invoking Quark-Gluon Plasma formation. It should be noted, however, that the comover densities reached in the early stages of the collision, from which most of the suppression originates, correspond to energy densities well above critical ones obtained from Lattice QCD. This renders such models difficult to interpret as an exclusively *hadronic* scenario of J/ψ suppression. The comover scenario entails a stronger suppression at RHIC, compared to SPS, due to larger densities of comoving hadrons, albeit this may be compensated by smaller nuclear suppression at RHIC (charmonia forming outside the nuclei) as advocated in [34].

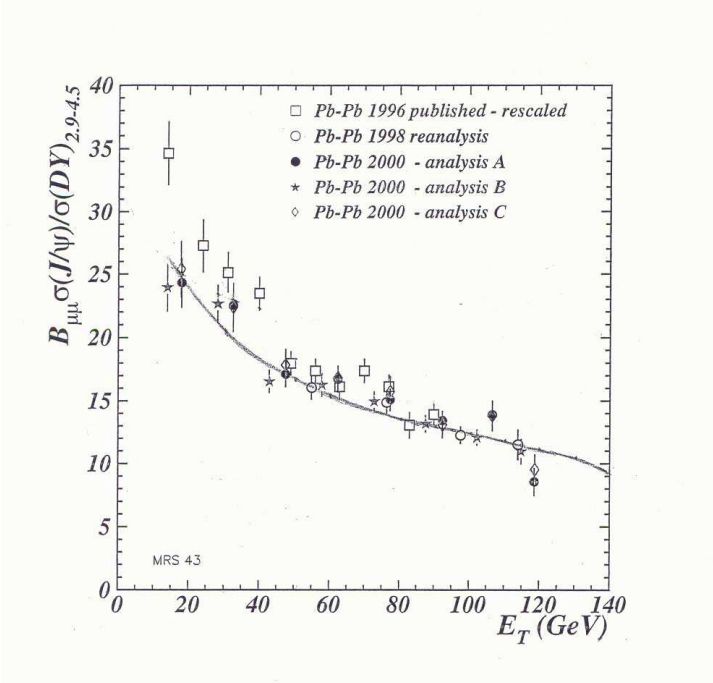

Figure 6.7: J/ψ centrality dependence in the comover model of Capella [34], including transverse energy fluctuations at large E_T.

Statistical J/ψ production at SPS

Before we developed our two-component model, Braun-Munzinger and Stachel [3, 4] and Gorenstein, Kostyuk, Stöcker and Greiner [5, 38] proposed to describe the J/ψ yield in central *Pb-Pb* collisions solely in terms of statistical coalescence of charm at the hadronization transition. Such approaches, as seen in Sec. 3.3.2, share the assumption that at the hadronization transition, no primordial J/ψ's remain in the system and the whole J/ψ yield stems from statistical coalescence. Fig. 6.8 displays the results of [39] (left panel) and [40] (right panel). The models [39, 40] have similar assumptions (modulo detailed prescription for $c\bar{c}$ production and the hadronization volume) and lead to similar conclusions: an open-charm enhancement factor of ~ 3 (in central collisions) from standard *p-p* extrapolation is needed to account for the data. This coincides (see dot-dashed curve in the left panel of Fig. 6.8) with the open-charm enhancement needed to explain the dimuon excess reported by NA50 [41] in the Intermediate Mass Region (IMR). Attempts have been made [42] to provide a mechanism for the open-charm enhancement which should be confirmed/ruled-out by the NA60 experiment. Let us recall that other mechanisms, such as thermal dimuon radiation [43, 44, 45], exist to explain the dimuon excess in the IMR. One marked feature of the statistical models of

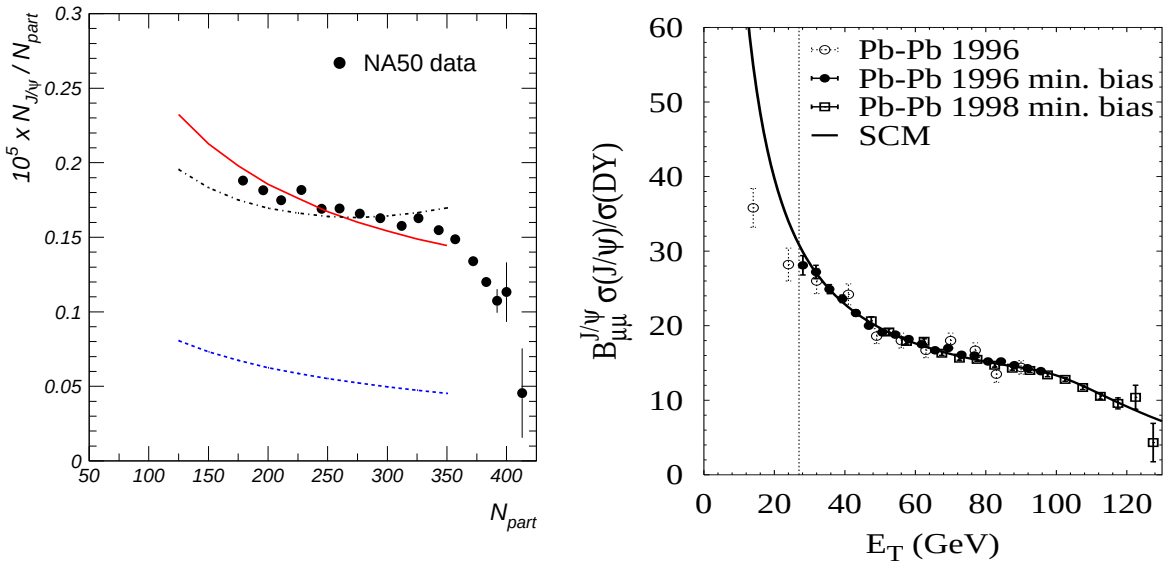

Figure 6.8: J/ψ centrality dependence at SPS given by statistical models of charmonium production. The figures are taken from [39] (left panel) and [40] (right panel).

J/ψ production is that their predictions for the J/ψ yield at RHIC are very different from the ones obtained in QGP and/or hadronic suppression scenarios. Due to the much more copious open-charm production expected at RHIC, statistical J/ψ production is much more abundant, see Secs. 6.3.2 and 6.3.3 for detailed results at RHIC.

6.3 Excitation function and predictions for RHIC

An essential part of the experimental program at RHIC is again on (penetrating) electromagnetic probes. The PHENIX detector will provide dilepton data via both the (forward) muon arms as well as electron identification in the central region. The results on charmonium should allow for valuable constraints on models. At full RHIC energy, standard extrapolations predict an open-charm production that is about two orders of magnitude larger than in the SPS regime, entailing a substantial increase in the statistical recombination mechanism for charmonia. At the same time, direct (hard) charmonium production, albeit also enhanced by presumably a similar factor as open charm, ought to be more strongly suppressed due to longer lived and initially hotter QGP phases.

6.3.1 From SPS to RHIC

A quantitative comparison between SPS and RHIC within our two-component model is performed in Fig. 6.9 where the final (observed) number of J/ψ's, normalized to the number J/ψ's remaining after nuclear absorption, $N^{nuc}_{J/\psi}$, is displayed for central collisions as a function of the fireball evolution time [46].

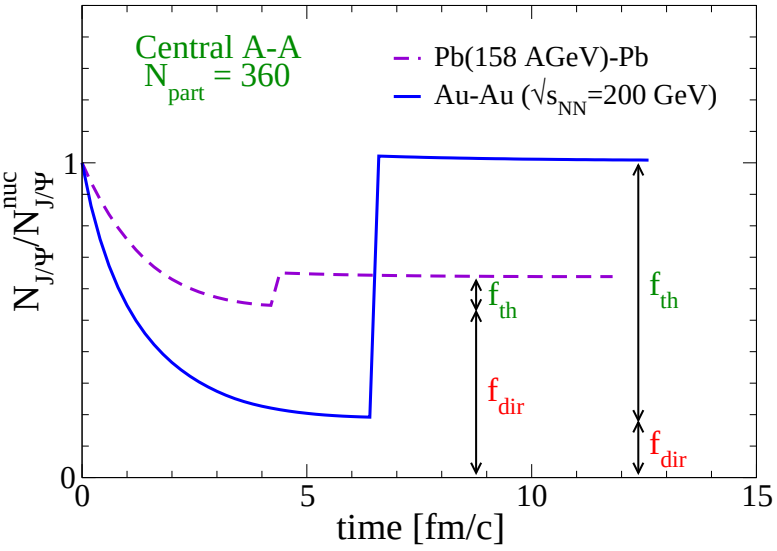

Figure 6.9: Time dependence of the ratio $N_{J/\psi}/N^{nuc}_{J/\psi}$ at SPS (dashed line) and RHIC (full line) for central collisions with $N_{part} = 360$, where $N^{nuc}_{J/\psi}$ is the number of J/ψ's remaining after nuclear absorption. The respective fractions of direct (f_{dir}) and thermal (f_{th}) yields are indicated by the arrows.

The freeze-out value for this ratio increases by about 50% going from SPS to RHIC (from 0.65 to about 1). In addition, the composition in terms of underlying sources is very different: whereas at SPS the (suppressed) direct yield dominates, J/ψ-mesons at RHIC originate to approximately 80% from thermal production (being proportional to $(N_{c\bar{c}})^2$). The upward jump of the two curves in Fig. 6.9 is located at the respective end of the mixed phase, τ_H, where in our approximation all thermal production is concentrated. As elucidated in Sec. 6.1.2, the final results are not sensitive to the exact production time within the mixed phase.

Since the phenomenological extrapolations for absolute numbers of primordial J/ψ and charm-quark production up to RHIC energies, which are input parameters to our calculations, are beset with appreciable uncertainties, it is desirable to define a quantity which reduces this sensitivity. Therefore, we show in Fig. 6.10 the predictions of our two-component approach for centrality dependencies of the ratio $N_{J/\psi}/N_{c\bar{c}}$, which, in

connection with open-charm measurements at RHIC, also has the virtue of being composed of experimental observables[3]. Whereas at SPS energies this quantity exhibits a

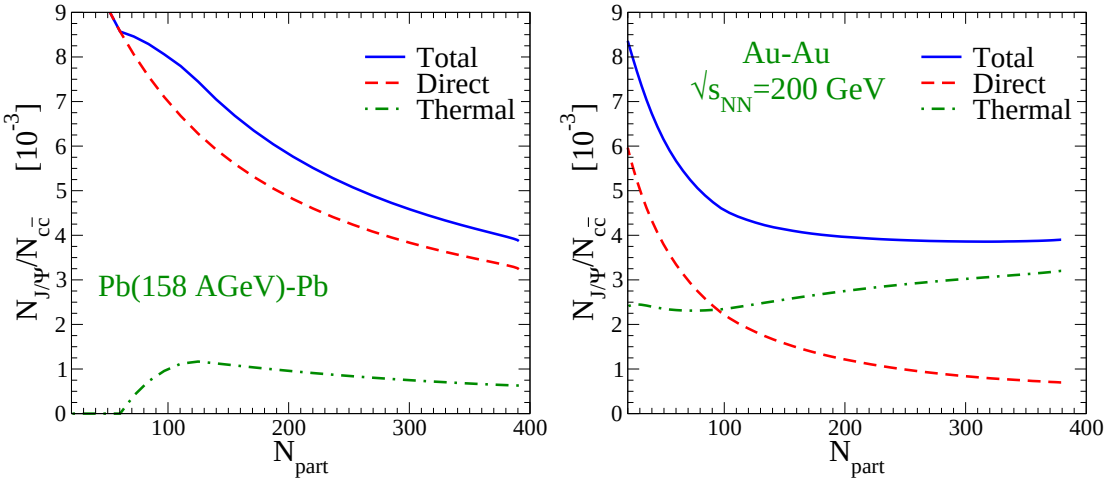

Figure 6.10: Comparison of the centrality dependence of the $N_{J/\psi}/N_{c\bar{c}}$ ratio at SPS and RHIC full energy (full line). The direct (thermal) contributions are shown separately, respectively in the dashed (dot-dashed) lines.

monotonous decrease with increasing number of participants (left panel of Fig. 6.10), it saturates already for rather peripheral collisions at full RHIC energy. Note that the decrease of the thermal component for $N_{part} \geq 100$ at SPS is caused by canonical ensemble effects, while at RHIC statistical production, for the most part, proceeds in the grand-canonical limit entailing a smooth increase with centrality. Thus, one may be able to discriminate between standard J/ψ suppression as opposed to thermal regeneration at full RHIC energy.

6.3.2 Two-component model predictions vs. PHENIX data

At the Quark Matter 2002 conference, the PHENIX collaboration reported preliminary measurements of the J/ψ centrality dependence at full RHIC energy [47]. Their results are presented as the number of J/ψ's per binary collision at midrapidity ($y = 0$) versus the number of participants. Since the open-charm production scales with the number of binary collisions, a comparison with our predictions [46] shown in the right panel of Fig. 6.10 is straightforward (by multiplying with a proportionality factor including the branching ratio, $\sigma_{c\bar{c}}^{pp}$ and the rapidity coverage of our fireball). Fig. 6.11

[3]However, this ratio may still be sensitive to, *e.g.* shadowing effects: since the J/ψ yield, being mostly thermal, goes as $N_{c\bar{c}}^2$ a modification of $c\bar{c}$ production due to nuclear shadowing does not cancel out in this ratio.

displays such a comparison [48]. The agreement of the two-component model *predic-*

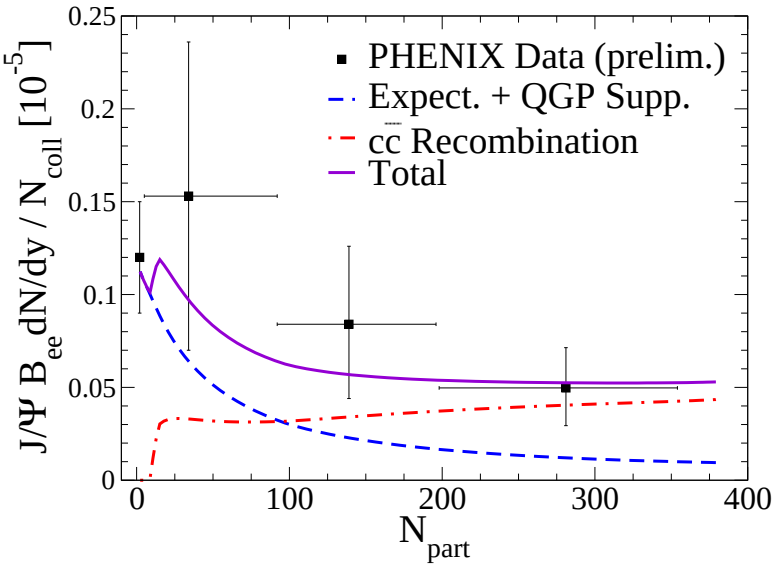

Figure 6.11: Centrality dependence of the $N_{J/\psi}/N_{coll}$ ratio at RHIC full energy (full line). The direct (thermal) contributions are shown separately, respectively in the dashed (dot-dashed) lines [48].

tions (full line) with the data is rather encouraging. Despite the large error bars which prevent from drawing definitive conclusions, we see that the substantial statistical regeneration (dot-dashed line) in central collisions compensates in our picture the strong direct suppression (dashed line). Models involving only J/ψ suppression whose results are similar to our direct contribution (dashed line) are disfavored by the data (unless nuclear absorption turns out to be much weaker at RHIC than at SPS [34]) as well as scenarios predicting large J/ψ enhancement [49, 50] (see also Fig. 6.13).

6.3.3 Other model approaches at RHIC

Let us confront calculations for RHIC energies from the other model approaches described in Sec. 6.2.4. The dot-dashed line in the left panel of Fig. 6.12 corresponds to calculations from Kostyuk *et al.* [51], for the J/ψ centrality dependence expected in the QGP suppression scenario of [29, 22]. Due to higher energy densities achieved in RHIC collisions, the J/ψ suppression is almost complete for central *Au-Au* collisions. Kostyuk *etal* [51], reached a similar conclusion within a comover model approach (dashed line, left panel of Fig. 6.12). In general, scenarios involving only the standard picture of J/ψ suppression from Matsui and Satz [1] (see also dashed line of Fig. 6.11), independently

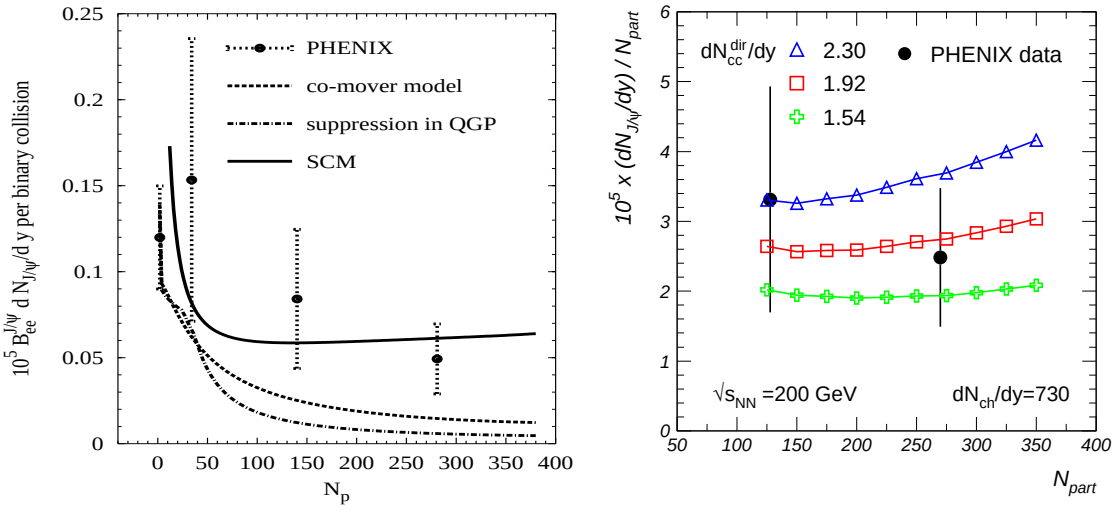

Figure 6.12: Comparison of models approaches for J/ψ suppression at RHIC. Left panel: QGP suppression, comover calculation and statistical coalescence model [51]. Right panel: statistical coalescence with sensitivity to the open-charm production per unit of rapidity [39].

of the details of the suppression mechanism (Debye screening in Quark-Gluon Plasma, dynamical quasifree destruction, or comover interactions) predict a very strong J/ψ suppression in central *Au-Au* collisions at RHIC [52].

On the other hand, J/ψ regeneration by statistical charm coalescence (full line - left panel - and right panel of Fig. 6.12), seems to account rather well for the observed data. Note, however, that the statistical model yields have inherent uncertainties, illustrated by the set of curves in the right panel of Fig. 6.12 reflecting the uncertainty of the open-charm yield. Further studies as well as more precise data are needed to make a definitive statement. In addition, nuclear absorption effects need to be experimentally clarified, since a reduced nuclear absorption together with a "suppression only" mechanism could be consistent with the data refraining from invoking any regeneration process.

More extreme scenarios of J/ψ recombination from $c\bar{c}$ coalescence have been put forward in [49, 50], where J/ψ formation in a pure plasma scenario was considered. In their approach, Rafelski and Thews solve the rate equations for J/ψ dissolution/formation in an expanding Quark-Gluon Plasma, using the gluo-dissociation process (Fig. 4.2) and its reverse reaction, without invoking medium effects. Their results are presented in Fig. 6.13. The strong J/ψ enhancement predicted by the simplest version of this model (diamonds) is disfavored by the data. However, (thermal) off-equilibrium corrections

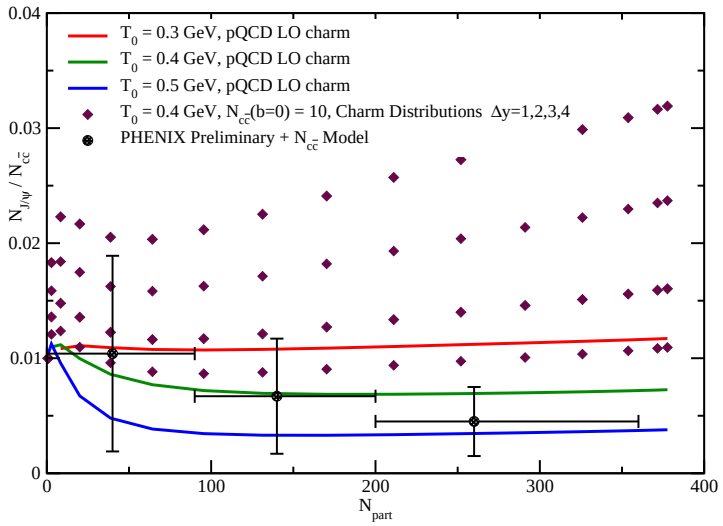

Figure 6.13: J/ψ centrality dependence at RHIC within the model of [49, 50]. The sets of lozenges corresponds to different rapidity windows in which J/ψ formation is considered. The full lines illustrates off-thermal equilibrium effects of the $c, \bar{c}$ momentum distributions on the J/ψ yield.

reduce the J/ψ formation rate and lead to a significantly better agreement with the data (full lines).

6.3.4 J/ψ excitation function

Within our two-component approach, we clearly predict a change from direct J/ψ production dominating the yield at SPS to mostly thermal production at RHIC. As we first pointed out in [6], it is therefore valuable (and experimentally feasible at RHIC) to map out the transition between the regimes of predominantly direct to thermal charmonium production as a function of cms energy $\sqrt{s_{NN}}$. In Fig. 6.14 we present a prediction of the excitation function for $N_{J/\psi}/N_{c\bar{c}}$ ratio[4] [46]. Although not strongly varying, the ratio exhibits a nontrivial minimum structure around $\sqrt{s_{NN}} \simeq 50$ GeV, which is a marked feature of the interplay between hard and thermal production (assuming no anomalies in open-charm production, cf. Ref. [53, 14]).

[4] As compared to our earlier results [6], we here also incorporate the corrections from feeddown of excited charmonia and from hadronic suppression. Within the uncertainty band quoted in Ref. [6], the results agree.

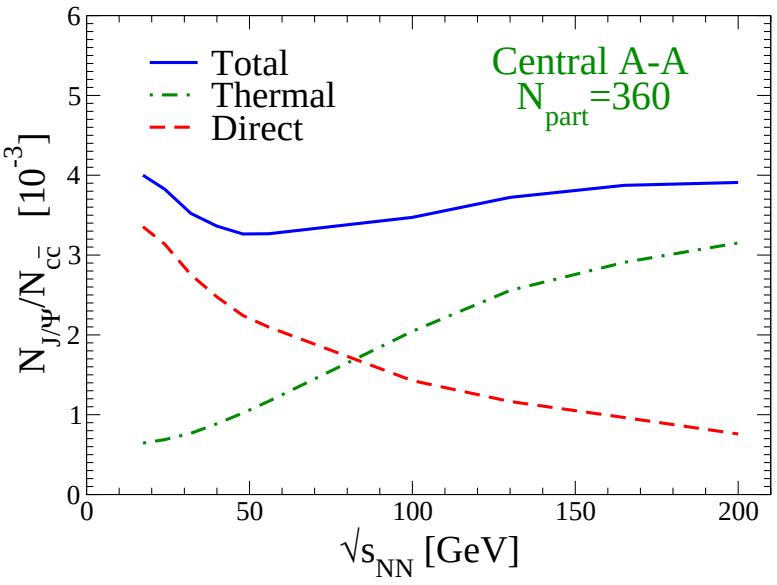

Figure 6.14: Excitation function of the $N_{J/\psi}/N_{c\bar{c}}$ ratio (full line). The interplay between the direct contribution (dashed line) and the thermal component (dot-dashed line) results in a minimum in the excitation function around $\sqrt{s_{NN}} \simeq 50$ GeV [6, 46].

6.3.5 Other QGP suppression mechanisms

Finally, we investigate the sensitivity of the minimum structure with respect to different QGP suppression mechanisms. Upon replacing the quasifree destruction process by the gluon photo-dissociation process shown in Fig. 4.5 (dashed line), we observe a slight overall increase in the yield without significant alteration of the shape. However, it seems difficult to reproduce the magnitude of the observed J/ψ suppression in central *Pb-Pb* collisions at SPS using the gluo-dissociation process (with vacuum binding energies). In a more extreme scenario based on Debye-screening, we assume J/ψ mesons to be entirely suppressed if they are formed in a region with initial energy density $\varepsilon_0(r) > \varepsilon_{Debye}$ (along the lines of Ref. [29, 22]). Within the Glauber model, the spatial distribution of primordial J/ψ's is inferred from the nuclear thickness function $T_{AB}(r)$ (characterizing the number of N-N collisions), whereas the energy-density profile is taken to be proportional to the density of participants in the transverse plane. We fix ε_{Debye} to obtain a suppression consistent with the NA50 data at $\sqrt{s} = 17.3$ GeV (translating into $T_{Debye} \simeq 220$ MeV). As expected, the pertinent excitation function exhibits a stronger suppression pattern with increasing $\sqrt{s}$, generating a more pronounced minimum structure (at similar position) in the $N_{J/\psi}/N_{c\bar{c}}$ ratio than found with dynamical dissociation processes, cf. Fig. 6.15.

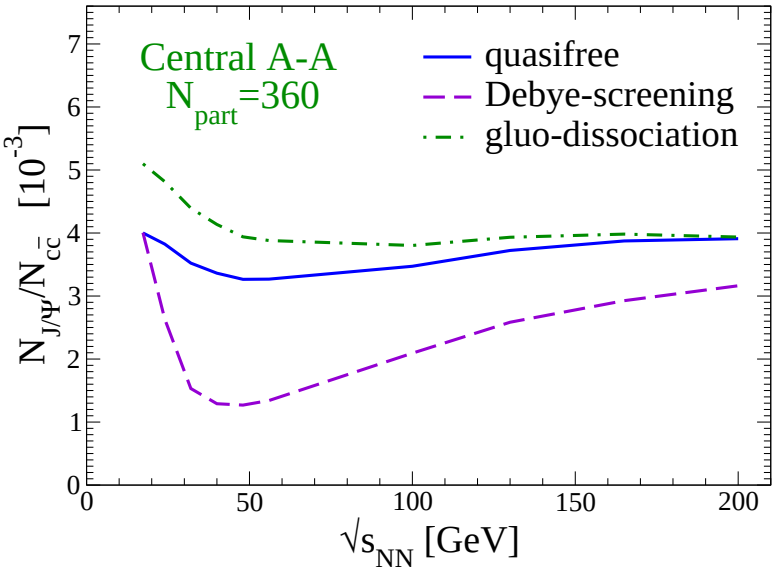

Figure 6.15: Comparison of Debye-screening (dashed curves), photo-dissociation (dotted curves) and quasifree dissociation (full curves) of J/ψ's in a thermalized QGP at various collision energies, combined with thermal production. Photo-dissociation (with vacuum J/ψ binding energy) gives results similar to quasifree suppression (with in-medium E_{diss}) whereas Debye screening induces stronger suppression reflected in a more pronounced minimum around $\sqrt{s} = 50$ GeV.

Bibliography

[1] T. Matsui and H. Satz, Phys. Lett. **B178**, 416 (1986).

[2] M. Gazdzicki and M. I. Gorenstein, Phys. Rev. Lett. **83**, 4009 (1999), hep-ph/9905515.

[3] P. Braun-Munzinger and J. Stachel, Phys. Lett. **B490**, 196 (2000), nucl-th/0007059.

[4] P. Braun-Munzinger and J. Stachel, Nucl. Phys. **A690**, 119 (2001), nucl-th/0012064.

[5] M. I. Gorenstein, A. P. Kostyuk, H. Stöcker, and W. Greiner, Phys. Lett. **B509**, 277 (2001), hep-ph/0010148.

[6] L. Grandchamp and R. Rapp, Phys. Lett. **B523**, 60 (2001), hep-ph/0103124.

[7] S. Digal, P. Petreczky, and H. Satz, Phys. Lett. **B514**, 57 (2001), hep-ph/0105234.

[8] S. Digal, P. Petreczky, and H. Satz, Phys. Rev. **D64**, 094015 (2001), hep-ph/0106017.

[9] PHENIX Collaboration, S. S. Adler *et al.*, (2003), hep-ex/0307019.

[10] C. Lourenco, Nucl. Phys. **A610**, 552c (1996), hep-ph/9612222.

[11] R. Gavai *et al.*, Int. J. Mod. Phys. **A10**, 3043 (1995), hep-ph/9502270.

[12] P. Braun-Munzinger, I. Heppe, and J. Stachel, Phys. Lett. **B465**, 15 (1999), nucl-th/9903010.

[13] P. Braun-Munzinger, K. Redlich, and J. Stachel, (2003), nucl-th/0304013.

[14] M. I. Gorenstein, A. P. Kostyuk, L. D. McLerran, H. Stoecker, and W. Greiner, (2000), hep-ph/0012292.

[15] PHENIX Collaboration, R. Averbeck *et al.*, Nucl. Phys. **A715**, 695 (2003), nucl-ex/0209016.

[16] P. Braun-Munzinger, D. Miskowiec, A. Drees, and C. Lourenco, Eur. Phys. J. **C1**, 123 (1998), nucl-ex/9704011.

[17] R. V. Gavai *et al.*, Int. J. Mod. Phys. **A10**, 2999 (1995), hep-ph/9411438.

[18] R. Vogt, (2002), hep-ph/0203151.

[19] NA38 Collaboration, M. C. Abreu *et al.*, Phys. Lett. **B449**, 128 (1999).

[20] NA50 Collaboration, M. C. Abreu *et al.*, Phys. Lett. **B477**, 28 (2000).

[21] A. Capella, E. G. Ferreiro, and A. B. Kaidalov, Phys. Rev. Lett. **85**, 2080 (2000), hep-ph/0002300.

[22] J.-P. Blaizot, M. Dinh, and J.-Y. Ollitrault, Phys. Rev. Lett. **85**, 4012 (2000), nucl-th/0007020.

[23] J. Hufner, B. Z. Kopeliovich, and A. Polleri, (2000), nucl-th/0012003.

[24] A. Capella, A. B. Kaidalov, and D. Sousa, Phys. Rev. **C65**, 054908 (2002), nucl-th/0105021.

[25] NA50 Collaboration, M. C. Abreu *et al.*, Phys. Lett. **B450**, 456 (1999).

[26] H. Sorge, E. V. Shuryak, and I. Zahed, Phys. Rev. Lett. **79**, 2775 (1997), hep-ph/9705329.

[27] A. Sibirtsev, K. Tsushima, K. Saito, and A. W. Thomas, Phys. Lett. **B484**, 23 (2000), nucl-th/9904015.

[28] NA50 Collaboration, M. C. Abreu *et al.*, Phys. Lett. **B410**, 337 (1997).

[29] J.-P. Blaizot and J.-Y. Ollitrault, Phys. Rev. Lett. **77**, 1703 (1996), hep-ph/9606289.

[30] M. Nardi and H. Satz, Phys. Lett. **B442**, 14 (1998), hep-ph/9805247.

[31] D. Kharzeev, C. Lourenco, M. Nardi, and H. Satz, Z. Phys. **C74**, 307 (1997), hep-ph/9612217.

[32] S. Gavin and R. Vogt, Phys. Rev. Lett. **78**, 1006 (1997), hep-ph/9606460.

[33] N. Armesto and A. Capella, Phys. Lett. **B430**, 23 (1998), hep-ph/9705275.

[34] A. Capella and D. Sousa, (2003), nucl-th/0303055.

[35] R. Vogt, Phys. Lett. **B430**, 15 (1998), hep-ph/9708294.

[36] A. Capella and D. Sousa, Phys. Lett. **B511**, 185 (2001), nucl-th/0101023.

[37] R. Vogt, Phys. Rept. **310**, 197 (1999).

[38] A. P. Kostyuk, M. I. Gorenstein, H. Stöcker, and W. Greiner, Phys. Lett. **B531**, 195 (2002), hep-ph/0110269.

[39] A. Andronic, P. Braun-Munzinger, K. Redlich, and J. Stachel, (2003), nucl-th/0303036.

[40] A. P. Kostyuk, M. I. Gorenstein, H. Stöcker, and W. Greiner, J. Phys. **G28**, 2297 (2002), hep-ph/0204180.

[41] NA38 Collaboration, M. C. Abreu *et al.*, Eur. Phys. J. **C14**, 443 (2000).

[42] A. P. Kostyuk, M. I. Gorenstein, and W. Greiner, Phys. Lett. **B519**, 207 (2001), hep-ph/0103057.

[43] R. Rapp and E. V. Shuryak, Phys. Lett. **B473**, 13 (2000), hep-ph/9909348.

[44] K. Gallmeister, B. Kampfer, and O. P. Pavlenko, Phys. Lett. **B473**, 20 (2000), hep-ph/9908269.

[45] I. Kvasnikova, C. Gale, and D. K. Srivastava, Phys. Rev. **C65**, 064903 (2002), hep-ph/0112139.

[46] L. Grandchamp and R. Rapp, Nucl. Phys. **A709**, 415 (2002), hep-ph/0205305.

[47] PHENIX Collaboration, A. D. Frawley *et al.*, Nucl. Phys. **A715**, 687 (2003), nucl-ex/0210013.

[48] L. Grandchamp and R. Rapp, Nucl. Phys. **A715**, 545 (2003), hep-ph/0209141.

[49] R. L. Thews, M. Schroedter, and J. Rafelski, Phys. Rev. **C63**, 054905 (2001), hep-ph/0007323.

[50] R. L. Thews, M. Schroedter, and J. Rafelski, J. Phys. **G27**, 715 (2001), hep-ph/0009090.

[51] A. P. Kostyuk, M. I. Gorenstein, H. Stöcker, and W. Greiner, (2003), hep-ph/0305277.

[52] R. Vogt, Nucl. Phys. **A661**, 205 (1999), nucl-th/9907090.

[53] M. I. Gorenstein, A. P. Kostyuk, H. Stöcker, and W. Greiner, Phys. Lett. **B524**, 265 (2002), hep-ph/0104071.

Chapter 7

In-Medium Effects on Charmonium Production in Heavy-Ion Collisions

The previously discussed two-component model approach gives a good description of the J/ψ centrality dependence observed at SPS and RHIC. However, the ψ' suppression seems to be underestimated. In addition, recent lattice data indicates that J/ψ survives as a resonance in the plasma. This has led us to subsequently improve the two-component approach along the following lines [1, 2]: *(i)* we adopt a more microscopic description of charmonium regeneration by solving rate equations within a kinetic approach and *(ii)* we take into account the recent lattice results presented in Chapter 3: First, the survival of lowest-lying charmonia in the plasma leads us to consider J/ψ recreation throughout the whole evolution (both in the QGP and hadronic phases) and not only at the hadronization transition. Secondly, we invoke a reduction of the open-charm threshold due to in-medium effects on open-charm states, which opens new decay channels, such as $\psi' \to D\bar{D}$ in hadronic matter, anticipated to help resolving the ψ'/ψ ratio issue. Let us start with the main elements of our improved approach.

7.1 Kinetic approach - rate equations

In the two-component model, charmonium regeneration was accounted for by simply adding a statistical component to the J/ψ yield at the hadronization transition. On a more microscopic level, one has to consider the reaction channels

$$\Psi + X_1 \underset{(G)}{\overset{(L)}{\rightleftharpoons}} X_2 + c + \bar{c}\ (D + \bar{D}) \tag{143}$$

If charm quark reinteractions are strong in the medium, it implies an approach toward thermalization and the backward channel in the charmonium dissociation equation (143) has to be included. Consequently, to model the time dependence, $N_\Psi(\tau)$, of charmonia in heavy-ion collisions, we solve the corresponding kinetic rate equation of Eq. (143), which applies as long as a well-defined Ψ state exists, *i.e.* $\tau_\Psi^{-1}(\tau) = \Gamma_\Psi(\tau) << m_\Psi$,

$$\frac{dN_\Psi}{d\tau} = -N_\Psi L(\tau) + G(\tau) \tag{144}$$

where $L(\tau)$ corresponds to the loss term (charmonium dissociation) and $G(\tau)$ denotes the gain term (charmonium regeneration). If we make the additional assumption that the surrounding light and open-charm constituents (either quarks or hadrons, depending on T) are in thermal equilibrium, Eq. (144) can be simplified to

$$\frac{dN_\Psi}{d\tau} = -\frac{1}{\tau_\Psi}\left[N_\Psi - N_\Psi^{eq}\right] \ , \tag{145}$$

where τ_Ψ is the equilibration time of the charmonium state under consideration and N_Ψ^{eq} is the corresponding thermal equilibrium abundance. This form of the rate equation clearly shows under which conditions the gain term can be neglected. Namely, when τ_Ψ is large compared to the typical fireball lifetimes and either *(i)* the initial abundances are large compared to the equilibrium ones (which is the case at SPS but not necessarily at RHIC) or *(ii)* no bound state exists.

The general solution of Eq. (145) is given by

$$N_\Psi(\tau) = \exp\left(-\int_0^\tau \frac{dt}{\tau_\Psi}\right)\left[N_\Psi^0 + \int_0^\tau \frac{N_\Psi^{eq}}{\tau_\Psi}\exp\left(\int_0^t \frac{dt'}{\tau_\Psi}\right)dt\right] \ . \tag{146}$$

Hence, the abundance of charmonium states Ψ in the system is fully characterized by τ_Ψ, N_Ψ^{eq} and the initial conditions N_Ψ^0, given the temperature profile of the reaction (*i.e.* the relation between the temperature T at a time t which we extract from the fireball model of Chapter 5).

7.1.1 In-medium equilibration times

In the plasma, the bare charm quark mass is modified due to a thermal charm quark correlation energy. We incorporate this modified charm quark mass $m_c^\star$ in our quasifree calculation of QGP charmonium dissociation exposed in Sec. 4.1.2, which induces small variations from the dissociation rates calculated with the vacuum value of m_c (see Fig.

4.5). Let us recall that the quasifree calculation includes in-medium reduced binding energies. As pointed out in Sec. 4.1.3, the J/ψ lifetimes we obtain are reminiscent of the J/ψ widths in the plasma observed in lattice calculations (within the large uncertainties of the lattice results, one has $\Gamma \sim 0.2$ GeV for $T = 1.1\ T_c$ [3] which corresponds to $T = 290$ MeV since the lattice calculations are quenched).

In the hadronic phase, medium effects increase the inelastic hadronic reactions, and with the reduction of the open-charm threshold, the process $\psi' \to D\bar{D}$ becomes possible. A detailed treatment of the in-medium effects in the hadron gas phase has been provided in Sec. 4.4 and the main results are summarized in Fig. 7.1 which shows the in-medium hadronic lifetimes of J/ψ, ψ' and χ. Note that the ψ' lifetime is well below the J/ψ

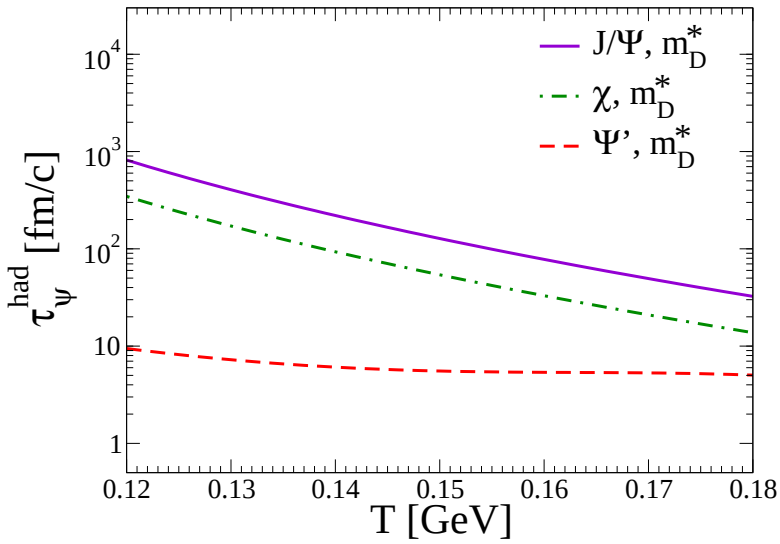

Figure 7.1: In-medium charmonia hadronic lifetimes. See Sec. 4.4 for details.

one, beyond geometric scaling. This is due to the direct decay $\psi' \to D\bar{D}$ which opens up in hadronic matter with the reduction of the open-charm threshold. Thus, as we will see in Sec. 7.2.2, in-medium effects inferred from lattice QCD lead to a stronger ψ' suppression, helping to resolve the discrepancies in the ψ'/ψ ratio identified in the previous chapter.

7.1.2 In-medium equilibrium abundances

The rate Eq. (145) also involves the equilibrium abundances of charmonia in the plasma and hadronic phases of the reaction, calculated as explained in Sec. 3.3.3. In principle, it is conceivable that also low-lying open-charm resonances ($D(1870)$ or

$D_s(1970)$) persist slightly above T_c [4, 5]. Such correlations are, however, at least partially encoded in the effective charm-quark mass, m_c^*, in the QGP. In fact, due to the very smooth decrease of the plateau of the heavy-quark free energy around T_c seen in lattice calculations, we assume a continuity of the open-charm states across the phase transition. Therefore, in what follows, we fix $m_c^*(T_c)$ such that the total open-charm multiplicity in the QGP at T_c matches the open-charm content of the hadronic phase at T_c. Fig. 7.2 displays the J/ψ equilibrium abundances at RHIC and SPS for the value of the charm quark mass $m_c^* \simeq 1.65$ GeV corresponding to a drop in the D-meson mass of $\Delta_m(T_c) = 140$ MeV, calculated within the NJL calculation detailed in Sec. 3.2.2. At

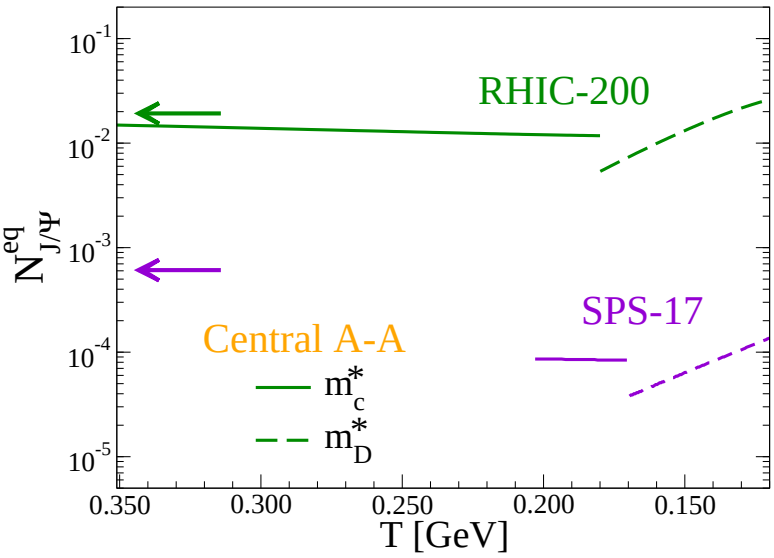

Figure 7.2: J/ψ abundances (with $m_\psi(T) \equiv m_\psi^{vac}$) in an isotropic, adiabatically expanding system at fixed $N_{c\bar{c}}$ for SPS and RHIC conditions for $m_c^* \simeq 1.65$ GeV smoothly matching the open-charm abundances on the hadronic side with in-medium reduced D-meson mass by $\Delta_m(T_c) = 140$ MeV. The arrows correspond the initial hard J/ψ production, after nuclear suppression.

T_c, the J/ψ equilibrium abundances are higher in the QGP than in the hadronic phase. This is a consequence of our hypothesis of continuity of the open-charm spectrum: at fixed $N_{c\bar{c}}$ and since at T_c the open-charm densities are equal in the plasma and hadronic phases, the larger volume of the hadronic phase leads to a smaller value of γ_c which entails a decrease in the equilibrium charmonium levels through T_c. On the contrary, in a full chemical equilibration scenario ($\gamma_c = 1$) without medium effects, N_ψ decouples from $N_{c\bar{c}}$ and increases proportionally to the volume expansion.

7.1.3 Initial conditions and off-equilibrium effects

The last quantity needed for an actual solution of the rate equations is the initial condition, N_Ψ^0, which we take from hard production systematics as in the two-component model. At RHIC, we use the recently reported value of

$$\sigma_{J/\psi}^{pp} = 3.99 \pm 0.61(stat) \pm 0.58(sys) \pm 0.40(abs)\ \mu\text{b}\ , \qquad \sqrt{s} = 200\ \text{GeV} \qquad (147)$$

by the PHENIX experiment. After taking into account the limited rapidity coverage of our fireball description and scaling the cross-section (Eq. (147)) with the number of binary collisions, the primordial charmonium yield is subjected to initial-state nuclear absorption (to account for "pre-equilibrium" dynamics) with a recently updated absorption cross-section $\sigma_{abs} = 4.4$ mb [6] which we keep constant from SPS to RHIC. The total charm number, $N_{c\bar{c}}$, in a A-A reaction at given centrality is determined by standard N-N cross-sections scaled by the number of primordial N-N collisions.

If the system is far from equilibrium, then the equilibrium term N_Ψ^{eq} is actually much smaller and our approach overestimates the charmonium regeneration. Thus, as in the two-component model, we relax the assumption of thermal equilibrium for the heavy-quarks by introducing a thermal relaxation time correction, $\mathcal{R} = 1 - \exp(-\int d\tau/\tau_c^{therm})$, which reduces N_Ψ^{eq} in the early phases of the reaction.

Another correction concerns the effective volume over which the charm quantum number is conserved (figuring into Eq. (132) via the argument of the Bessel functions). If only few $c\bar{c}$ pairs are present, their pointlike primordial production implies that they cannot explore the entire fireball volume in the early stages[1]. This problem is well-known from strange particle production at fixed target energies, where a phenomenological "correlation volume", V_0, has been introduced to *localize* strangeness conservation [7]. We adopt the same procedure here for local charm conservation by replacing $V_{FB}(\tau)$ in the argument of the Bessel functions in Eq. (132) with $V_0(\tau)=4\pi(r_0 + \langle v_c\rangle\tau)^3/3$. $r_0\simeq 1.2$ fm represents a minimal radius characterizing the range of strong interactions, and $\langle v_c\rangle\simeq 0.5c$ denotes the average relative speed of produced c and $\bar{c}$ quarks as inferred from experimental $p_\perp$-distributions of D-mesons [8]. We have checked that our results exhibit a very small sensitivity to the details of the correlation volume expansion.

[1] We thank U. Heinz for pointing this out to us, including useful discussions on the correlation volume.

7.2 Comparison to experiments at SPS

7.2.1 Centrality dependence

We first confront our improved approach to data obtained by the NA50/NA38 experiments in $\sqrt{s_{NN}}$=17.3 GeV *Pb-Pb* at CERN-SPS. Fig. 7.3 displays the ratio of $J/\psi \to \mu\mu$

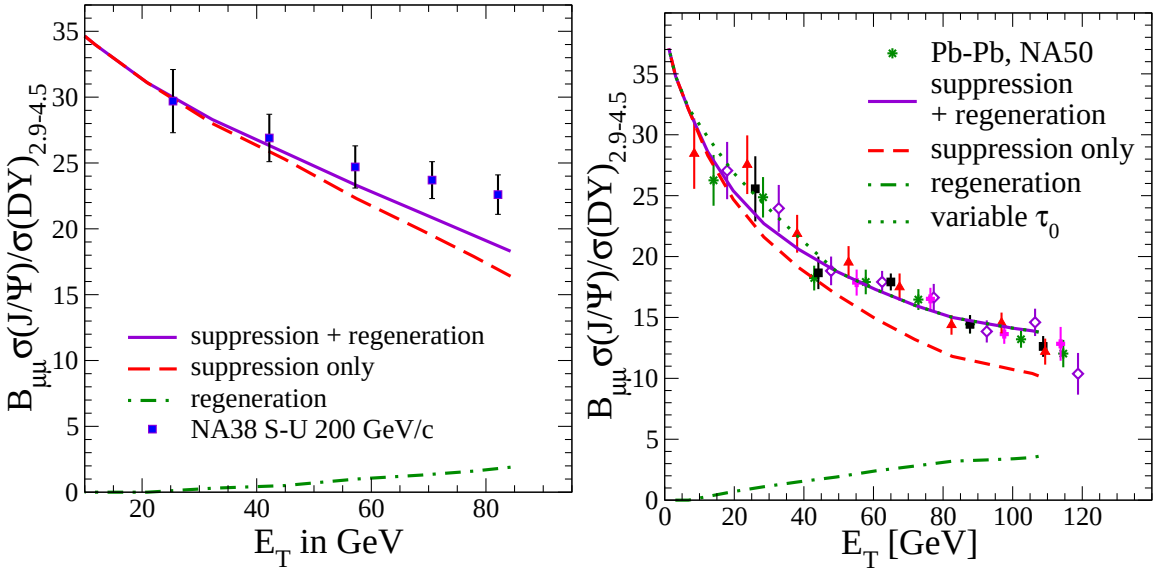

Figure 7.3: Centrality dependence of J/ψ/Drell-Yan dimuons at SPS; NA38 data [9] for the *S-U* system (left panel) and NA50 data [6] (*Pb-Pb*, right panel) are compared to our results with (solid line) and without (dashed line) charmonium regeneration (represented by the dot-dashed line). The dotted line includes longer thermalization times τ_0 in peripheral collisions.

to Drell-Yan dimuons as a function of centrality. The agreement between model (solid line) and data is fair for semi-/central collisions (at E_T>100 GeV, the data can be reproduced by accounting for transverse energy fluctuations and losses in the minimum bias analysis at impact parameters close to zero [10, 11, 12], cf. discussion in Sec. 6.2.2). Since the initial J/ψ number is well above the equilibrium level (cf. lower arrow in Fig. 7.2), J/ψ regeneration (the gain term in Eq. (144)) is very moderate (dot-dashed line). Therefore, in line with our previous findings [13], J/ψ *suppression* is the main effect at SPS energies.

In peripheral collisions, the suppression appears to be somewhat overestimated. We believe this discrepancy to reside in limitations of our fireball description. In particular, thermalization is expected to be delayed (and/or incomplete) at large impact parameters due to less energetic initial conditions. This is also borne out of hydrodynamic

calculations, which, *e.g.* , reproduce the observed elliptic flow for mid-central collisions, but overestimate it for peripheral ones. A suitable increase of the equilibration time would amount to up to a factor of ~ 3[2]. Such a scenario is indicated by the dotted line in Fig. 7.3, which obviously improves the agreement at small E_T.

7.2.2 Ψ'/Ψ ratio

Another important observable is the ψ'/ψ ratio. In the 2-component approach [13], the ψ' dissociation rates were too small by a factor of ~ 5 to account for NA50 data [14]. With in-medium D-meson masses, however, $\Gamma^{had}_{\psi'}$ increases substantially, primarily due to the opening of the $\psi' \to D\bar{D}$ decay channel. As a result, the ψ'/ψ data are reasonably well described, cf. Fig. 7.4.

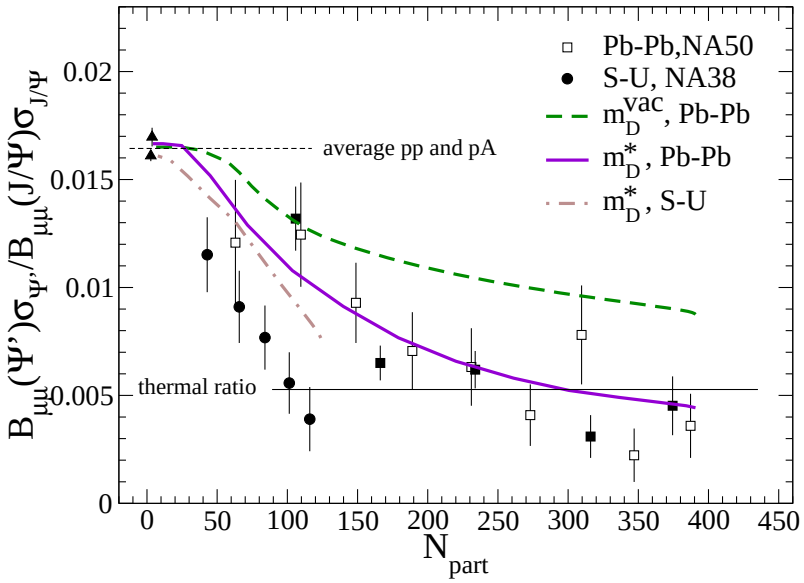

Figure 7.4: Centrality dependence of the ψ'/ψ data [14] at SPS compared to our results with (full line) and without (dashed line) in-medium reduced D-meson masses.

7.3 In-medium effects at RHIC

At RHIC, the initial hard production is quite similar in magnitude to the J/ψ equilibration abundances in the plasma. Consequently, one expects that regeneration will become much more important than at SPS. This is indeed the case, as shown in Fig. 7.5 where the J/ψ abundances are shown as a function of time for central *Pb-Pb* at

[2]P. Kolb, private communication

$\sqrt{s} = 17.3$ AGeV collisions (left panel) and *Au-Au* at $\sqrt{s} = 200$ AGeV for RHIC (right panel). At SPS, the J/ψ yield (full line) is always significantly above the J/ψ equilibrium

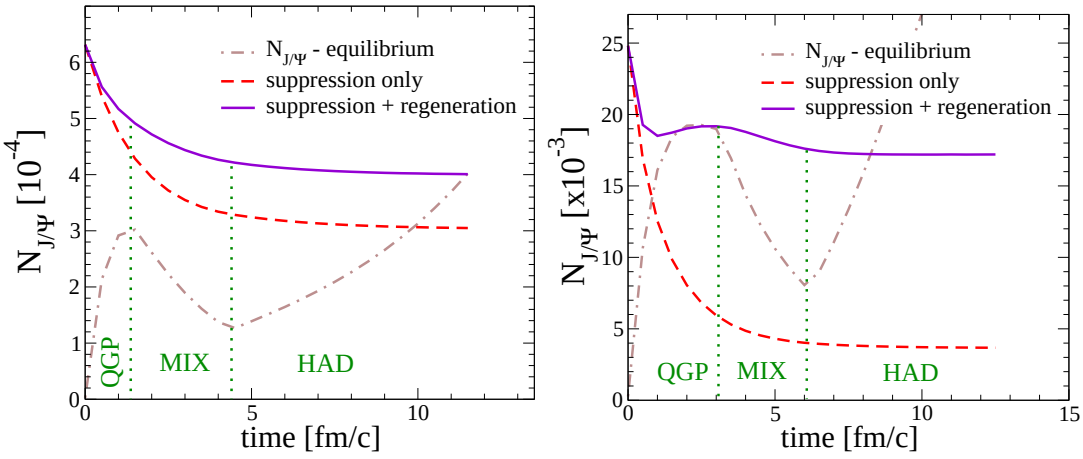

Figure 7.5: J/ψ abundance as a function of time for central ($N_p = 360$) *Pb-Pb* collisions at SPS (left panel), and *Au-Au* collisions at RHIC (right panel). The solid line indicates the results obtained by solving the full rate equation. The dashed line corresponds to the J/ψ when regeneration has been switched off. The difference, attributed to recreation is shown by the dot-dashed line.The dotted line depicts the J/ψ equilibrium number.

abundances (dot-dashed line) entailing a moderate regeneration (difference between full and dashed lines). This is no longer the case at RHIC where substantial regeneration occurs: The final J/ψ yield is close to the initial yield (after nuclear absorption), that is J/ψ regeneration and dissociation almost compensate eachother. Regeneration (difference between the full and the dashed lines in the right panel of Fig. 7.5) is shown to be preponderant at RHIC and occurs mostly in the plasma and the mixed phase of the reaction, delimited by the vertical lines in Fig. 7.5. Early in the hadronic phase, the J/ψ yield reaches its final value since the effect of the hadronic phase on the J/ψ is rather moderate.

We also studied the sensitivity of our predictions for RHIC [13, 15] to different in-medium modifications, cf. Fig. 7.6. Since reduced D-meson masses entail a lower J/ψ equilibrium level (cf. Fig. 3.11), the regeneration of J/ψ's is somewhat less pronounced than the statistical production with free hadron masses in the 2-component model [13]. Nevertheless, in central *Au-Au* collisions, regenerated J/ψ's still exceed the suppressed primordial contribution, with the total yield (solid curve) in line with published PHENIX data [17]. The uncertainty in the charm-hadron mass reduction is illustrated by the band in Fig. 7.6, corresponding to 80 MeV$<\Delta m_q(T_c)<$250 MeV with accordingly matched charm-quark masses in the QGP. Nuclear shadowing corrections, which could affect

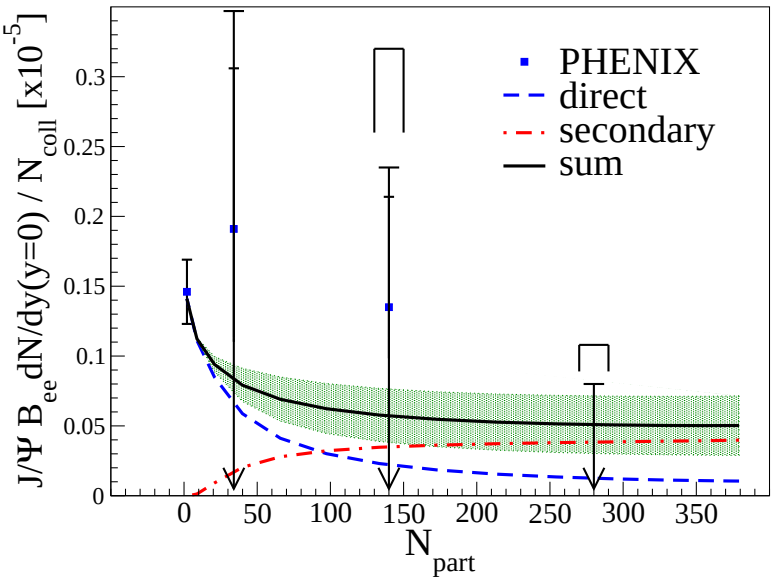

Figure 7.6: J/ψ yield per binary N-N collision versus participant number in $\sqrt{s_{NN}}$=200 GeV Au-Au collisions. Preliminary PHENIX data [16] are compared to our model calculations; band: total J/ψ yields with different values for in-medium open-charm masses; dot-dashed line: thermal regeneration; dashed line: suppressed primordial production.

both $N_{c\bar{c}}$ and J/ψ numbers, have been neglected. The main difference between our previous two-component model, besides in-medium effects, is that here J/ψ regeneration is considered throughout the entire evolution, including in the plasma phase, and not only at the hadronization transition.

We conclude this chapter by presenting a prediction of the ψ'/ψ ratio at RHIC. It is displayed in Fig. 7.7 as a function of the number of participants in the collision. Although the composition of the J/ψ and ψ' yields in terms of direct and secondary charmonia are rather different from SPS to RHIC, the centrality dependence of the ψ'/ψ ratio appears very similar going from SPS energies to RHIC energies.

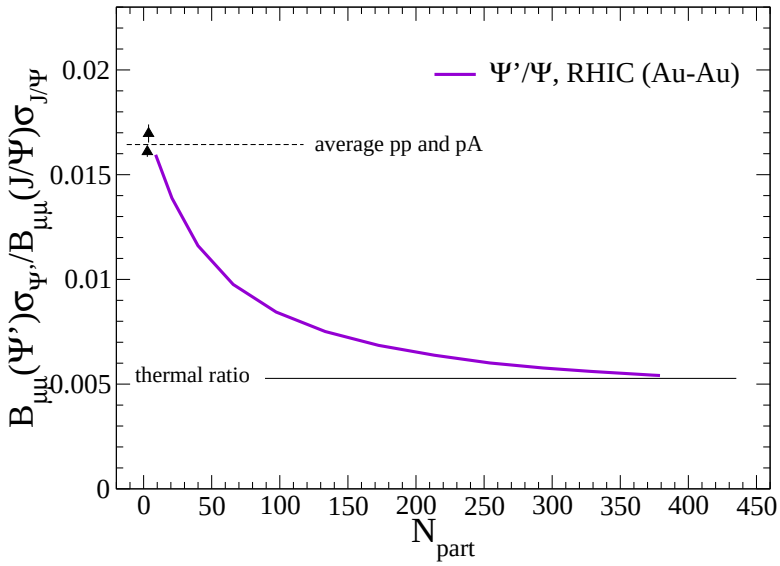

Figure 7.7: Prediction for the ψ'/ψ ratio at RHIC as a function of the centrality of the collision.

Bibliography

[1] R. Rapp and L. Grandchamp, (2003), hep-ph/0305143, proceedings of the 7th International Conference on Strangeness in Quark Matter (SQM 2003), Atlantic Beach, North Carolina, 12-17 March 2003, to appear in J. Phys. **G**.

[2] L. Grandchamp, R. Rapp, and G. E. Brown, (2003), submitted to Phys. Rev. Lett., hep-ph/0306077.

[3] T. Umeda, K. Nomura, and H. Matsufuru, (2002), hep-lat/0211003.

[4] D. Blaschke, G. Burau, T. Barnes, Y. Kalinovsky, and E. Swanson, (2002), hep-ph/0210265.

[5] T. H. Hansson, S. H. Lee, and I. Zahed, Phys. Rev. **D37**, 2672 (1988).

[6] NA50 Collaboration, B. Alessandro *et al.*, Nucl. Phys. **A715**, 243c (2003).

[7] S. Hamieh, K. Redlich, and A. Tounsi, Phys. Lett. **B486**, 61 (2000), hep-ph/0006024.

[8] BEATRICE Collaboration, M. Adamovich *et al.*, Nucl. Phys. **B495**, 3 (1997).

[9] NA38 Collaboration, M. C. Abreu *et al.*, Phys. Lett. **B449**, 128 (1999).

[10] A. Capella, E. G. Ferreiro, and A. B. Kaidalov, Phys. Rev. Lett. **85**, 2080 (2000), hep-ph/0002300.

[11] J.-P. Blaizot, M. Dinh, and J.-Y. Ollitrault, Phys. Rev. Lett. **85**, 4012 (2000), nucl-th/0007020.

[12] A. Capella, A. B. Kaidalov, and D. Sousa, Phys. Rev. **C65**, 054908 (2002), nucl-th/0105021.

[13] L. Grandchamp and R. Rapp, Nucl. Phys. **A709**, 415 (2002), hep-ph/0205305.

[14] NA50 Collaboration, M. C. Abreu *et al.*, Nucl. Phys. **A638**, 261 (1998).

[15] L. Grandchamp and R. Rapp, Nucl. Phys. **A715**, 545 (2003), hep-ph/0209141.

[16] PHENIX Collaboration, A. D. Frawley *et al.*, Nucl. Phys. **A715**, 687 (2003), nucl-ex/0210013.

[17] PHENIX Collaboration, S. S. Adler *et al.*, (2003), nucl-ex/0305030.

Chapter 8

Conclusions and Outlook

We have investigated the role of the J/ψ, ψ' and χ mesons in the studies the hot and/or dense QCD matter produced in collisions of heavy nuclei at ultra-relativistic energies.

In the original suggestion of J/ψ suppression by Matsui and Satz [1], the J/ψ yield measured in heavy-ion collisions stems from an initial hard production of ("direct") J/ψ's subsequently destroyed in nuclear, plasma and hadron gas interactions. Recently, other (soft) mechanisms of J/ψ production have been put forward [2, 3, 4, 5], in particular scenarios based on the coalescence of c and $\bar{c}$ quarks at the hadronization transition. To describe the J/ψ yield at SPS solely in terms of statistical recombination requires a large open-charm enhancement (up to a factor ~ 3) [4, 5]. Since *(i)* such a large open-charm enhancement lacks theoretical justification and *(ii)* these two mechanisms are not exclusive, we proposed to evaluate the J/ψ yield in heavy-ion collisions as the combination of the two sources aforementioned [6].

The first source amounts to the calculation of the number of direct J/ψ's and involves charmonium interactions with nuclear, partonic and hadronic matter. In the plasma phase, J/ψ properties are expected to be modified *both* by Debye screening of the heavy-quark potential and by dynamical dissociation with surrounding partons. We attempted to include both effects following a dynamical picture. However, the conventional gluo-dissociation process [7], widely used in the literature before, does not take into account the reduced binding energies of the charmonium states in the plasma and is hardly applicable for the ψ' and χ states. This has led us to propose a novel calculation of J/ψ interactions in the QGP [6] evaluating inelastic parton scattering in a quasifree approximation. This approach, which includes reduced charmonium binding energies

and can be aplied to the ψ' and χ mesons as well, has been found to dominate over the gluo-dissociation mechanism. For the J/ψ interactions in the hadronic phase, as a baseline calculation, we have reproduced the results of Haglin [8], Lin and Ko [9], Haglin and Gale [10] using a SU(4) symmetric effective theory. The ψ' and χ hadronic interactions were deduced from the J/ψ ones using geometric scaling [11].

As a second source, the statistical component of the J/ψ yield has been evaluated for a system in thermal equilibrium (but in chemical off-equilibrium) following the original suggestions of Braun-Munzinger and Stachel [3, 4] and Kostyuk, Gorenstein, Stöcker and Greiner [5]. We refrained, however, to invoke an open-charm enhancement. We included, in a simplified way, thermal off-equilibrium effects.

The two components of the J/ψ yield are then evaluated within a common thermal evolution scenario, including QGP formation when the initial conditions are energetic enough. The space-time description of the collision is modelled using a thermal fireball [12, 13] which captures the main properties of the reaction dynamics and provides a common framework to study hadro-chemistry [14, 15], dilepton production in the low- [12] and intermediate-mass [13] region, as well as direct photons [16].

Our findings have confirmed that at SPS energies, the main mechanism to interpret the NA50 data is *J/ψ suppression*. The total yield of J/ψ mesons is largely accounted for by primordial J/ψ's, subsequently destroyed by nuclear, plasma and hadronic interactions. In our approach, since the abundances of open-charm states are small at SPS, J/ψ regeneration by coalescence of c and $\bar{c}$ quarks is very moderate. In the absence of medium effects, the experimental ψ'/ψ ratio cannot be described, indicating an underestimation of the ψ' interactions in the hadron gas [11].

At RHIC energies, within our framework including J/ψ suppression and J/ψ regeneration, a picture of charmonium production has emerged which is very different from the originally proposed scenario of [1]. The stronger suppression, attributed to a hotter and longer plasma phase than at SPS, is essentially compensated by J/ψ regeneration, in line with purely statistical models [3, 5, 4]. The corresponding *prediction*, namely that the J/ψ yield at RHIC would not exhibit the strong suppression expected in the Matsui and Satz picture, is in line with first PHENIX measurements [17, 18], although it is fair to say that at this point the experimental accuracy does not suffice to draw definitive conclusions.

Our prediction [6] that the main underlying J/ψ production mechanism is very different at SPS (hard production coupled with suppression) and at RHIC (soft coalescence

production) suggests that the J/ψ excitation function (normalized to open-charm production) will exhibit a non-trivial structure and is a valuable tool to study the interplay between the two mechanisms of J/ψ production we have considered in this work.

Recent lattice calculations [19, 20, 21] have provided new information on open and hidden charm states at finite temperature. They seem to indicate that J/ψ states survive in the plasma up to temperatures $\sim 1.5\ T_c$ and that the open-charm threshold is reduced as the temperature of the medium increases [22]. Therefore, to improve on the two-component model, we have considered within a rate equation formalism J/ψ regeneration throughout the entire evolution of the system (including in the plasma phase) [23]. We have also shown that the lowering of the open-charm threshold, attributed to a partial restoration of chiral symmetry, opens new decay channels in the hadronic phase, most notably $\psi' \to D + \bar{D}$. In turns, this entails stronger ψ' hadronic interactions and provides a plausible explanation to the discrepancies observed in the ψ'/ψ ratio in the absence of medium effects [23].

With the gross features of charmonium production rather well reproduced within our approach, further experimental as well as theoretical scrutiny is needed. From the experimental side, we expect exciting measurements at RHIC to further test our approach. In addition, theoretical discrepancies in nuclear absorption have to be resolved. In that respect, it is crucial to have reliable experimental studies of nuclear absorption at RHIC energies, and the results of the recent *d-Au* run are eagerly awaited. Since the secondary J/ψ yield is (parametrically) proportional to $N_{c\bar{c}}^2$, tight constraints on open-charm production from experiments (*e.g.* direct measurements using D mesons reconstructed in the $K\pi$ invariant mass spectrum) will be very valuable to reduce theoretical uncertainties. The still standing issue of an open-charm enhancement at SPS − alternatively explained by thermal radiation [13] − has to be clarified (hopefully by NA60 [24]).

From the theoretical point of view, significant J/ψ regeneration at RHIC energies relies mostly on *(i)* an abundant open-charm production and *(ii)* thermal equilibration in the charm sector. These two points raise issues that we plan to address in the future. The first point involves nuclear shadowing effects [25, 26] which decrease the open-charm production and are expected to become even more important when extrapolating our approach to LHC energies. The second point, regarding thermalization in the charm sector, is part of the more general issue of thermalization. From thermal models of particle production and p_T spectra, we have evidence that the systems produced in

heavy-ion collisions at SPS and RHIC are in thermal equilibrium in the light sector. In the charm sector, the plausible assumption of thermal equilibrium [27] has to be further scrutinized and we intent to assess more precisely thermal off-equilibrium effects. One direction of investigation may be given by the elliptic flow of charmed particles [28, 29]. If charm quarks approach thermalization, they should participate in the collective expansion of matter which in turn would translate into a non-zero elliptic flow. The hadronic calculations of charmonium inelastic cross-sections also offer a good starting point to evaluate elastic D-meson scattering in the hadronic medium [30] and infer the corresponding equilibration time.

Another significant aspect of charmonium production which we have not addressed yet concerns transverse momentum spectra of charmonia. They are experimentally available and provide another interesting mean to delineate hard from soft production mechanisms, thus further testing our model. The coalescence mechanism should produce J/ψ's at small p_T but also implies an increase in the average p_T if J/ψ participate in the collective expansion of the system. At the other end of the spectrum, J/ψ's with large p_T are more likely to arise from the early stages, that is hard N-N collisions. Moreover, the suppression of fast J/ψ's is expected to be reduced since they are more likely to escape the system. Therefore, transverse momentum distributions should further exhibit the interplay between hard and soft J/ψ production and will be calculated within our model to be confronted with experimental results.

Two natural extensions of our model are in order: First, our studies can be extrapolated to LHC energies. There, we expect the hard production to be (almost) totally suppressed and the observed yield should be a direct reflection of J/ψ regeneration. The second extension is based on the analogy between charm and bottom physics. The analysis carried out for charmonium production throughout this work can be carried over to the upsilon family of bound states. The higher mass of the bottom quark should only "shift" the transition from direct production to statistical production to higher cms energies. It will be very interesting to evaluate the upsilon yield at LHC energies in terms of direct and secondary production to see which regime dominates.

Let us conclude here this thesis with these remarks on the exciting future of heavy-quarkonium production in heavy-ion collisions.

Bibliography

[1] T. Matsui and H. Satz, Phys. Lett. **B178**, 416 (1986).

[2] M. Gazdzicki and M. I. Gorenstein, Phys. Rev. Lett. **83**, 4009 (1999), hep-ph/9905515.

[3] P. Braun-Munzinger and J. Stachel, Phys. Lett. **B490**, 196 (2000), nucl-th/0007059.

[4] P. Braun-Munzinger and J. Stachel, Nucl. Phys. **A690**, 119 (2001), nucl-th/0012064.

[5] M. I. Gorenstein, A. P. Kostyuk, H. Stöcker, and W. Greiner, Phys. Lett. **B509**, 277 (2001), hep-ph/0010148.

[6] L. Grandchamp and R. Rapp, Phys. Lett. **B523**, 60 (2001), hep-ph/0103124.

[7] G. Bhanot and M. E. Peskin, Nucl. Phys. **B156**, 391 (1979).

[8] K. L. Haglin, Phys. Rev. **C61**, 031902 (2000), nucl-th/9907034.

[9] Z.-W. Lin and C. M. Ko, Phys. Rev. **C62**, 034903 (2000), nucl-th/9912046.

[10] K. L. Haglin and C. Gale, Phys. Rev. **C63**, 065201 (2001), nucl-th/0010017.

[11] L. Grandchamp and R. Rapp, Nucl. Phys. **A709**, 415 (2002), hep-ph/0205305.

[12] R. Rapp and J. Wambach, Eur. Phys. J. **A6**, 415 (1999), hep-ph/9907502.

[13] R. Rapp and E. V. Shuryak, Phys. Lett. **B473**, 13 (2000), hep-ph/9909348.

[14] P. Braun-Munzinger, J. Stachel, J. P. Wessels, and N. Xu, Phys. Lett. **B365**, 1 (1996), nucl-th/9508020.

[15] P. Braun-Munzinger, D. Magestro, K. Redlich, and J. Stachel, Phys. Lett. **B518**, 41 (2001), hep-ph/0105229.

[16] S. Turbide, R. Rapp, and C. Gale, (2003), hep-ph/0308085.

[17] PHENIX Collaboration, S. S. Adler *et al.*, (2003), nucl-ex/0305030.

[18] L. Grandchamp and R. Rapp, Nucl. Phys. **A715**, 545 (2003), hep-ph/0209141.

[19] F. Karsch, Lect. Notes Phys. **583**, 209 (2002), hep-lat/0106019.

[20] S. Datta, F. Karsch, P. Petreczky, and I. Wetzorke, (2002), hep-lat/0208012.

[21] T. Umeda, K. Nomura, and H. Matsufuru, (2002), hep-lat/0211003.

[22] R. Rapp and L. Grandchamp, (2003), hep-ph/0305143, proceedings of the 7th International Conference on Strangeness in Quark Matter (SQM 2003), Atlantic Beach, North Carolina, 12-17 March 2003, to appear in J. Phys. **G**.

[23] L. Grandchamp, R. Rapp, and G. E. Brown, (2003), submitted to Phys. Rev. Lett., hep-ph/0306077.

[24] NA60 Collaboration, B. Lenkeit *et al.*, (2001), nucl-ex/0108015.

[25] S. Liuti and R. Vogt, Phys. Rev. **C51**, 2244 (1995), hep-ph/9407272.

[26] K. J. Eskola, V. J. Kolhinen, P. V. Ruuskanen, and R. L. Thews, Int. J. Mod. Phys. **E12**, 197 (2003), hep-ph/0108093.

[27] B. Svetitsky, Phys. Rev. **D37**, 2484 (1988).

[28] S. Batsouli, S. Kelly, M. Gyulassy, and J. L. Nagle, Phys. Lett. **B557**, 26 (2003), nucl-th/0212068.

[29] Z.-W. Lin and D. Molnar, (2003), nucl-th/0304045.

[30] Z. W. Lin and X.-N. Wang, Phys. Lett. **B444**, 245 (1998), nucl-th/9808033.

Appendix A

The Nambu-Jona-Lasinio Model at Finite Temperature and Density

For two comprehensive reviews of the NJL model, including developments at finite temperature and density, see [1, 2]. Here we follow the original work of Bernard, Meissner and Zahed [3] to derive the set of coupled NJL gap-equations Eqs. (48)-(49).

The Lagrangian (45) contains scalar interactions $(\bar{\psi}\psi)^2$ and pseudo-scalar ones $(\bar{\psi}i\tau\gamma_5\psi)^2$. We work in the Hartree-Fock approximation illustrated by the corresponding graphs below,

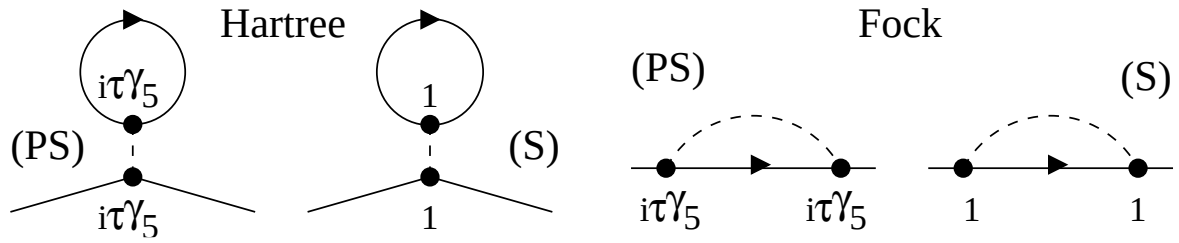

where we have given a finite range to the point-like NJL interaction for illustration purposes. The left graph corresponds to the Hartree term and its contribution to the self-energy associated with the scalar vertex is given by

$$\Sigma^s_{Hartree} = 2\,G\int\frac{d^4k}{(2\pi)^4}\mathrm{Tr}[S(k)]\;, \tag{148}$$

where $S(k)$ is the quark propagator in the medium $S^{-1}(k) = \not{k} - \Sigma(k) - m + i\varepsilon$. The Fock term reads (graph on the right)

$$\Sigma^s_{Fock} = -2\,G\int\frac{d^4k}{(2\pi)^4}S(k)\;. \tag{149}$$

Similarly, for the pseudo-scalar vertex, one has

$$\Sigma^{ps}_{Hartree} = 2\ G\ \int \frac{d^4k}{(2\pi)^4} i\tau\gamma_5 \mathrm{Tr}[i\tau\gamma_5 S(k)]\ , \tag{150}$$

and

$$\Sigma^{ps}_{Fock} = -2\ G\ \int \frac{d^4k}{(2\pi)^4} i\tau\gamma_5 S(k) i\tau\gamma_5\ . \tag{151}$$

The finite density case shifts the Hamiltonian of the system by a term $\mu\psi^\dagger\psi$ where μ is the chemical potential and $\psi^\dagger\psi$ the quark number density operator. Thus the density effects can be reabsorbed in the kinetic term of the Lagrangian as long as the self-energy Σ has the structure

$$\Sigma = \sigma_1 - \gamma^0\sigma_0\ . \tag{152}$$

The propagator can then be rewritten as

$$S(k) = \frac{\not{k}' + \sigma_1 + m}{k'^2 - (\sigma_1 + m)^2 + i\varepsilon}\ , \tag{153}$$

with $k' \equiv ({k'}_0, \vec{k}') = (k_0 + \sigma_0 + \mu, \vec{k})$. Upon performing the trace in Eq. (148), the scalar contribution to the self-energy in the Hartree approximation gives

$$\Sigma^{s}_{Hartree} = 2\ G\ 4N_cN_f \int \frac{d^3k}{(2\pi)^3} \int \frac{dk_0}{2\pi} \frac{\sigma_1 + m}{{k'}_0^2 - \omega_k^2}\ , \tag{154}$$

with $\omega_k^2 = \vec{k}^2 + (\sigma_1 + m)^2$. Similarly,

$$\Sigma^{s}_{Fock} = -2\ G\ \int \frac{d^3k}{(2\pi)^3} \int \frac{dk_0}{2\pi} \frac{{k'}_0\gamma^0 + \sigma_1 + m}{{k'}_0^2 - \omega_k^2} \tag{155}$$

$$\Sigma^{ps}_{Hartree} = 0 \tag{156}$$

$$\Sigma^{ps}_{Fock} = -2\ G\ 3\ \int \frac{d^3k}{(2\pi)^3} \int \frac{dk_0}{2\pi} \frac{-{k'}_0\gamma^0 + \sigma_1 + m}{{k'}_0^2 - \omega_k^2}\ . \tag{157}$$

At finite temperature, the integral over the energy is replaced by a sum over Matsubara frequencies $\omega_n = (2n+1)T$. With $\beta = 1/T$, the substitution reads

$$\int \frac{dk_0}{2\pi} \to \frac{1}{\beta} \sum_n\ . \tag{158}$$

Therefore, writing $k_n = \mu + \sigma_0 + i\omega_n$, we have

$$\Sigma = 2\ G\ \sum_n \frac{1}{\beta}\ \int \frac{d^3k}{(2\pi)^3} \frac{(4N_cN_f + 2)(m + \sigma_1) - 4k_n\gamma^0}{k_n^2 - \omega_k^2}\ . \tag{159}$$

Identifying with Eq. (152), we get the system of coupled equations

$$\sigma_0 = -8\,G\,\sum_n \frac{1}{\beta}\,\int \frac{d^3k}{(2\pi)^3}\frac{k_n}{k_n^2-\omega_k^2} \tag{160}$$

$$\sigma_1 = -4\,G\,(2N_cN_f+1)\sum_n \frac{1}{\beta}\,\int \frac{d^3k}{(2\pi)^3}\frac{m+\sigma_1}{k_n^2-\omega_k^2}\ . \tag{161}$$

Using the summation formula [4],

$$\sum_{-\infty}^{+\infty}\frac{1}{(n-x)(n-y)} = \frac{\pi(\cot\ \pi x - \cot\ \pi y)}{y-x}\ , \tag{162}$$

with, denoting $\omega_k^{\pm} = \omega_k \pm (\mu+\sigma_0)$,

$$\cot(\pi x) \equiv \cot\left(-\frac{\pi}{2}+i\frac{\beta\omega_k^+}{2}\right) = -i\tanh\left(\frac{\beta\omega_k^+}{2}\right) \tag{163}$$

$$\cot(\pi y) \equiv \cot\left(-\frac{\pi}{2}-i\frac{\beta\omega_k^-}{2}\right) = i\tanh\left(\frac{\beta\omega_k^-}{2}\right) \tag{164}$$

one arrives at Eqs. (48)-(49)

$$\sigma_1 = \frac{G}{2\pi^2}(2N_fN_c+1)(\sigma_1+m) \int_0^{\Lambda}\frac{k^2}{\omega_k}\left[\tanh\left(\frac{\beta\omega_k^-}{2}\right)+\tanh\left(\frac{\beta\omega_k^+}{2}\right)\right]dk\ , \tag{165}$$

$$\sigma_0 = \frac{2G}{\pi^2}\int_0^{\Lambda} k^2\left(n_k^+ - n_k^-\right)dk\ , \tag{166}$$

where $n_k^{\pm} = (1+e^{\beta\omega_k^{\pm}})^{-1}$.

Bibliography

[1] S. P. Klevansky, Rev. Mod. Phys. **64**, 649 (1992).

[2] U. Vogl and W. Weise, Prog. Part. Nucl. Phys. **27**, 195 (1991).

[3] V. Bernard, U. G. Meissner, and I. Zahed, Phys. Rev. **D36**, 819 (1987).

[4] J. I. Kapusta, *Finite-temperature field theory*, Cambridge University Press, Cambridge, USA (1999).

Appendix B

$SU(4)$ Effective Theory of J/ψ Hadronic Interactions

The first calculation of hadronic J/ψ interactions using a $SU(4)$ symmetric effective theory was performed by Matinian and Müller in [1]. This approach was later extended by Haglin [2] and Lin and Ko [3] to include contact graphs, necessary to satisfy gauge invariance. Here, following [3], we reproduce the calculations of the matrix elements of the graphs given in Fig. 4.8.

Interaction vertices

We are interested in the vertices involving the J/ψ, the light mesons π, ρ and the charmed mesons D, D^*. Inserting the $SU(4)$ pseudo-scalar and vector meson matrices Eqs. (97)-(98) in the Lagrangian (100), we obtain the following 3- and 4-points interaction vertices relevant for $\pi + J/\psi$ inelastic scattering

$$\mathcal{L}_{\pi DD^*} = ig_{\pi DD^*}\ D^{*\mu}\vec{\tau}\cdot\left(\bar{D}\partial_\mu\vec{\pi} - \partial_\mu\bar{D}\vec{\pi}\right) + \text{H.c.}\ , \tag{167}$$

$$\mathcal{L}_{\psi DD} = ig_{\psi DD}\ \psi^\mu\left(D\partial_\mu\bar{D} - \partial_\mu D\bar{D}\right)\ , \tag{168}$$

$$\begin{aligned}\mathcal{L}_{\psi D^*D^*} = {} & ig_{\psi D^*D^*}\ \left[\psi^\mu\left(\partial_\mu D^{*\nu}\bar{D}^*_\nu - D^{*\nu}\partial_\mu\bar{D}^*_\nu\right)\right. \\ & + \left(\partial_\mu\psi^\nu D^*_\nu - \psi^\nu\partial_\mu D^*_\nu\right)\bar{D^{*\mu}} \\ & \left. + D^{*\mu}\left(\psi^\nu\partial_\mu\bar{D}^*_\nu - \partial_\mu\psi^\nu\bar{D}^*_\nu\right)\right]\ ,\end{aligned} \tag{169}$$

$$\mathcal{L}_{\pi\psi DD^*} = -g_{\pi\psi DD^*}\ \psi^\mu\left(D^*_\mu\vec{\tau}\bar{D} + D\vec{\tau}\bar{D}^*_\mu\right)\cdot\vec{\pi}\ , \tag{170}$$

and for $\rho + J/\psi$ scattering,

$$\mathcal{L}_{\rho DD} = ig_{\rho DD}\ \left(D\vec{\tau}\partial_\mu \bar{D} - \partial_\mu D\vec{\tau}\bar{D}\right)\cdot\vec{\rho}^\mu\ , \tag{171}$$

$$\mathcal{L}_{\rho\psi DD} = g_{\rho\psi DD}\ \psi^\mu D\vec{\tau}\bar{D}\cdot\vec{\rho_\mu}\ , \tag{172}$$

$$\begin{aligned}\mathcal{L}_{\rho D^* D^*} = & ig_{\rho D^* D^*}\ \left[\left(\partial_\mu D^{*\nu}\vec{\tau}\bar{D}^*_\nu - D^{*\nu}\vec{\tau}\partial_\mu\bar{D}^*_\nu\right)\cdot\vec{\rho}^\mu\right. \\ & + \left(D^{*\nu}\vec{\tau}\cdot\partial_\mu\vec{\rho}_\nu - \partial_\mu D^{*\nu}\vec{\tau}\cdot\vec{\rho}_\nu\right)\bar{D^{*\mu}} \\ & \left. + D^{*\mu}\left(\vec{\tau}\cdot\vec{\rho}'\partial_\mu\bar{D}^*_\nu - \vec{\tau}\cdot\partial_\mu\vec{\rho}'\bar{D}^*_\nu\right)\right]\ ,\end{aligned} \tag{173}$$

$$\mathcal{L}_{\rho\psi D^* D^*} = g_{\rho\psi D^* D^*}\ \left(\psi^\nu D^*_\nu\vec{\tau}\bar{D}^*_\mu + \psi^\nu D^*_\mu\vec{\tau}\bar{D}^*_\nu - 2\psi_\mu D^{*\nu}\vec{\tau}\bar{D}^*_\nu\right)\cdot\vec{\rho}^\mu\ , \tag{174}$$

where $\vec{\tau}$ are the Pauli matrices and $\vec{\pi}$ ($\vec{\rho}$) corresponds to the pion (rho) meson isospin triplets.

$\mathbf{J/\psi + \pi \to \bar{D}D^*}$ process

The amplitude for the 3 graphs corresponding to $J/\psi + \pi$ inelastic scattering reads

$$\mathcal{M}_1 \equiv \mathcal{M}_1^{\nu\lambda}\ \varepsilon_{\psi\nu}\varepsilon_{D^*\lambda} = \left(\sum_{i=a,b,c}\mathcal{M}_{1i}^{\nu\lambda}\right)\varepsilon_{\psi\nu}\varepsilon_{D^*\lambda}, \tag{175}$$

where $\mathcal{M}_{1i}^{\nu\lambda}$ corresponds to each single process in the top row of Fig. 4.8, labelled a, b and c. The ε_j correspond to the polarization of external vector mesons. Isospin factors have been omitted and there is a remaining sum (average) over final (initial) spins. The matrix elements themselves are given by

$$\mathcal{M}_{1a}^{\nu\lambda} = -g_{\pi DD^*}g_{\psi DD}\ (-2p_\pi + p_{D^*})^\lambda\left(\frac{1}{t - m_D^2}\right)(p_\pi - p_{D^*} + p_{\bar{D}})^\nu, \tag{176}$$

$$\begin{aligned}\mathcal{M}_{1b}^{\nu\lambda} = & g_{\pi DD^*}g_{\psi D^* D^*}\ (-p_\pi - p_{\bar{D}})^\alpha \\ & \times\left(\frac{1}{u - m_{D^*}^2}\right)\left[g_{\alpha\beta} - \frac{(p_\pi - p_{\bar{D}})_\alpha(p_\pi - p_{\bar{D}})_\beta}{m_{D^*}^2}\right] \\ & \times\left[(-p_\psi - p_{D^*})^\beta g^{\nu\lambda} + (-p_\pi + p_\psi + p_{\bar{D}})^\lambda g^{\beta\nu} + (p_\pi + p_{D^*} - p_{\bar{D}})^\nu g^{\beta\lambda}\right],\end{aligned} \tag{177}$$

$$\mathcal{M}_{1c}^{\nu\lambda} = -g_{\pi\psi DD^*}\ g^{\nu\lambda}. \tag{178}$$

Averaging over initial spins and summing over final spins leads to the differential $J/\psi + \pi \to \bar{D}D^*$ cross-section, including isospin factors

$$\frac{d\sigma_{\pi\psi}}{dt} = \frac{1}{96\pi s p^{*2}}\mathcal{M}_1^{\nu\lambda}\mathcal{M}_1^{*\nu'\lambda'}\left(g_{\nu\nu'} - \frac{p_{\psi\nu}p_{\psi\nu'}}{m_\psi^2}\right)\left(g_{\lambda\lambda'} - \frac{p_{D^*\lambda}p_{D^*\lambda'}}{m_{D^*}^2}\right)\ , \tag{179}$$

s and t being the usual Mandelstam variables and p^{*2} the initial state meson 3-momentum in the center of mass frame. The remaining integration over t is easily performed numerically over the allowed kinematical domain.

$\mathbf{J}/\boldsymbol{\psi} + \boldsymbol{\rho} \to \mathbf{D}\bar{\mathbf{D}}$

Similarly, for the $J/\psi + \rho \to D\bar{D}$ process, depicted in the second row of Fig. 4.8, with the corresponding notations, the full amplitude reads

$$\mathcal{M}_2 \equiv \mathcal{M}_2^{\mu\nu}\varepsilon_{\rho\mu}\varepsilon_{\psi\nu} = \left(\sum_{i=a,b,c} \mathcal{M}_{2i}^{\mu\nu}\right)\ \varepsilon_{\rho\mu}\varepsilon_{\psi\nu}\ , \tag{180}$$

where

$$\mathcal{M}_{2a}^{\mu\nu} = -g_{\rho DD}g_{\psi DD}\ (p_\rho - 2p_D)^\mu \left(\frac{1}{t-m_D^2}\right)(p_\rho - p_D + p_{\bar{D}})^\nu\ , \tag{181}$$

$$\mathcal{M}_{2b}^{\mu\nu} = -g_{\rho DD}g_{\psi DD}\ (-p_\rho + 2p_{\bar{D}})^\mu \left(\frac{1}{u-m_D^2}\right)(-p_\rho - p_D + p_{\bar{D}})^\nu\ , \tag{182}$$

$$\mathcal{M}_{2c}^{\mu\nu} = g_{\rho\psi DD}\ g^{\mu\nu}\ . \tag{183}$$

The cross-section is then given by

$$\frac{d\sigma_{\rho\psi\to D\bar{D}}}{dt} = \frac{1}{288\pi s p^{*2}}\mathcal{M}_2^{\mu\nu}\mathcal{M}_2^{*\mu'\nu'}\left(g_{\mu\mu'} - \frac{p_{\rho\mu}p_{\rho\mu'}}{m_\rho^2}\right)\left(g_{\nu\nu'} - \frac{p_{\psi\nu}p_{\psi\nu'}}{m_\psi^2}\right)\ . \tag{184}$$

$\mathbf{J}/\boldsymbol{\psi} + \boldsymbol{\rho} \to \mathbf{D^*}\bar{\mathbf{D}}^*$

The last process we have considered is $J/\psi + \rho \to D^*\bar{D}^*$ (cf. last row of Fig. 4.8). Its full amplitude is

$$\mathcal{M}_3 \equiv \mathcal{M}_3^{\mu\nu\lambda\omega}\ \varepsilon_{1\mu}\varepsilon_{2\nu}\varepsilon_{3\lambda}\varepsilon_{4\omega} = \left(\sum_{i=a,b,c}\mathcal{M}_{3i}^{\mu\nu\lambda\omega}\right)\varepsilon_{1\mu}\varepsilon_{2\nu}\varepsilon_{3\lambda}\varepsilon_{4\omega}, \tag{185}$$

with the individual matrix elements

$$\begin{aligned}\mathcal{M}_{3a}^{\mu\nu\lambda\omega} &= g_{\rho D^*D^*}g_{\psi D^*D^*}\ \left[(-p_\rho - p_{D^*})^\alpha g^{\mu\lambda} + 2\ p_\rho^\lambda g^{\alpha\mu} + 2p_{D^*}^\mu g^{\alpha\lambda}\right] \\ &\quad\times\left(\frac{1}{t-m_{D^*}^2}\right)\left[g_{\alpha\beta} - \frac{(p_\rho - p_{D^*})_\alpha(p_\rho - p_{D^*})_\beta}{m_{D^*}^2}\right] \\ &\quad\times\left[-2p_\psi^\omega g^{\beta\nu} + (p_\psi + p_{\bar{D}^*})^\beta g^{\nu\omega} - 2p_{\bar{D}^*}^\nu g^{\beta\omega}\right], \end{aligned}\tag{186}$$

$$\begin{aligned}\mathcal{M}_{3b}^{\mu\nu\lambda\omega} &= g_{\rho D^*D^*}g_{\psi D^*D^*}\ \left[-2p_\rho^\omega g^{\alpha\mu} + (p_\rho + p_{\bar{D}^*})^\alpha g^{\mu\omega} - 2p_{\bar{D}^*}^\mu g^{\alpha\omega}\right] \\ &\quad\times\left(\frac{1}{u-m_{D^*}^2}\right)\left[g_{\alpha\beta} - \frac{(p_\rho - p_{\bar{D}^*})_\alpha(p_\rho - p_{\bar{D}^*})_\beta}{m_{D^*}^2}\right] \\ &\quad\times\left[(-p_\psi - p_{D^*})^\beta g^{\nu\lambda} + 2p_\psi^\lambda g^{\beta\nu} + 2p_{D^*}^\nu g^{\beta\lambda}\right], \end{aligned}\tag{187}$$

$$\mathcal{M}_{3c}^{\mu\nu\lambda\omega} = g_{\rho\psi D^*D^*}\ \left(g^{\mu\lambda}g^{\nu\omega} + g^{\mu\omega}g^{\nu\lambda} - 2g^{\mu\nu}g^{\lambda\omega}\right). \tag{188}$$

Finally, the differential cross-section is given by

$$\begin{aligned}\frac{d\sigma_{\rho\psi\to D\bar{D}}}{dt} &= \frac{1}{288\pi s p^{*2}}\mathcal{M}_3^{\mu\nu\lambda\omega}\mathcal{M}_3^{*\mu'\nu'\lambda'\omega'}\left(g_{\mu\mu'}-\frac{p_{\rho\mu}p_{\rho\mu'}}{m_\rho^2}\right)\left(g_{\nu\nu'}-\frac{p_{\psi\nu}p_{\psi\nu'}}{m_\psi^2}\right)\\ &\times \left(g_{\lambda\lambda'}-\frac{p_{D^*\lambda}p_{D^*\lambda'}}{m_{D^*}^2}\right)\left(g_{\omega\omega'}-\frac{p_{\bar{D}^*\omega}p_{\bar{D}^*\omega'}}{m_{\bar{D}^*}^2}\right). \qquad (189)\end{aligned}$$

The resulting cross-sections are indicated by the full lines in Fig. 4.9.

Bibliography

[1] S. G. Matinian and B. Müller, Phys. Rev. **C58**, 2994 (1998), nucl-th/9806027.

[2] K. L. Haglin, Phys. Rev. **C61**, 031902 (2000), nucl-th/9907034.

[3] Z.-W. Lin and C. M. Ko, Phys. Rev. **C62**, 034903 (2000), nucl-th/9912046.

Production des états liés charmés dans les collisions d'ions lourds

Résumé : Nous avons étudié la production des états liés charmés dans les collisons ultra-relativistes d'ions lourds. Nous proposons tout d'abord un modèle de la production des mésons J/ψ, à deux composantes, qui inclut : *(i)* une production primordiale des J/ψ dans les collisions dures couplée à l'absorption des J/ψ dans la matière nucléaire, le plasma de quarks et de gluons et la matière hadronique, et *(ii)* une production statistique des J/ψ résultant de la coalescence de quarks c et $\bar{c}$ lorsque le système hadronise. Les deux sources de J/ψ sont évaluées dans un scénario d'équilibre thermique et nôtre modèle permet de rendre compte de façon satisfaisante des données expérimentales obtenues au CERN-SPS et à RHIC. Nous étudions ensuite les conséquences des effets de milieux sur la production des hadrons charmés, en nous basant sur de récents résultats de la chromodynamique quantique sur réseau. Nous envisageons la régénération des J/ψ dans le plasma de quarks et de gluons et montrons que les effets de milieux dans la matière hadronique permettent d'expliquer la dépendance en centralité du rapport ψ'/ψ.

Charmonium production in heavy-ion collisions

Summary: We investigate the production of charmonia in ultra-relativistic heavy-ion collisions. We first construct a two-component model of charmonium production, which includes *(i)* early hard J/ψ production coupled with nuclear, Quark-Gluon Plasma and Hadron Gas suppression and *(ii)* statistical production of J/ψ's by coalescence of c and $\bar{c}$ at the hadronization transition. Both components are evaluated within a common thermal evolution scenario. Available data on J/ψ production at CERN-SPS and BNL-RHIC energies are reasonably well reproduced. We then improve our approach to account for in-medium effects on open and hidden charm states, inferred from recent lattice QCD results. Within a kinetic theory framework, we solve rate equations for charmonium abundances during the course of a heavy-ion collision. The survival of J/ψ states above the phase transition temperature T_c favors their recreation in the QGP. In-medium effects in the hadronic phase, possibly linked to the (partial) restoration of chiral symmetry, largely resolve earlier identified discrepancies in the ψ'/ψ ratio.

Mots-clés : J/Ψ, états liés charmés, collisions d'ions lourds, plasma de quarks et de gluons

Keywords: J/Ψ, charmonium, heavy-ion collisions, quark-gluon plasma

Institut de Physique Nucléaire de Lyon, IN2P3-CNRS et UCBL, Bâtiment Dirac, 43 Bd du 11 Novembre 1918, 69622 Villeurbanne cedex
Department of Physics and Astronomy, State University of New York at Stony Brook, Stony Brook, NY 11794-3800